Western Graduate&PostdoctoralStudies

Western University
Scholarship@Western

Electronic Thesis and Dissertation Repository

8-2-2017 2:00 PM

Fabrication and Characterization of Hybrid Nanocomposites by Matrix Assisted Pulsed Laser Evaporation

Songlin Yang
The University of Western Ontario

Supervisor
Dr. Jin Zhang
The University of Western Ontario

Graduate Program in Chemical and Biochemical Engineering
A thesis submitted in partial fulfillment of the requirements for the degree in Master of Engineering Science
© Songlin Yang 2017

Follow this and additional works at: https://ir.lib.uwo.ca/etd

 Part of the Biochemical and Biomolecular Engineering Commons, Biology and Biomimetic Materials Commons, Other Materials Science and Engineering Commons, and the Semiconductor and Optical Materials Commons

Recommended Citation

Yang, Songlin, "Fabrication and Characterization of Hybrid Nanocomposites by Matrix Assisted Pulsed Laser Evaporation" (2017). *Electronic Thesis and Dissertation Repository*. 4775.
https://ir.lib.uwo.ca/etd/4775

This Dissertation/Thesis is brought to you for free and open access by Scholarship@Western. It has been accepted for inclusion in Electronic Thesis and Dissertation Repository by an authorized administrator of Scholarship@Western. For more information, please contact wlswadmin@uwo.ca.

Abstract

Different methods have been applied to deposit hybrid nanocomposites which can be applied in various fields due to their light weight and multifunctional properties. Here, matrix assisted pulsed laser evaporation (MAPLE) equipment with 532 nm Nd:YAG laser is applied to fabricate three types of hybrid nanocomposites on different substrates.

Chemical synthesized FeCo nanoparticles were deposited on graphene sheets by MAPLE technique (laser fluence: 300 mJ/cm^2). The effects of deposition time (*t*) on particle amount, shape and size have been investigated. Yttrium barium copper oxide (YBCO) materials are one type of high-temperature superconductive materials and could be applied in transportation. To fabricate superconductive materials/graphene hybrid nanocomposites, YBCO nanoparticles were deposited on graphene sheets by MAPLE techniques with a laser fluence at 150 mJ/cm^2. The microstructures in terms of particle size, size distribution, and particle shape are studied as functions of the deposition time (*t*). In addition, up-conversion nanoparticles ($NaGdF_4$: Yb^{3+}, Er^{3+}) which are able to be excited by low energy photons (λ_{ex} = 980 nm) and emit high energy photons were deposited through MAPLE technique. Results indicate that 2 hours' deposition can result in high-quality samples in terms of particle size and particle amount. No toxic effect is imposed on the cells by the deposited up-conversion nanoparticles with/without protein modification.

Our results indicate that the MAPLE deposition technique demonstrates the good versatility of depositing different nanoparticles and preserving their chemical composition.

Key words

Graphene, YBCO nanoparticles, FeCo nanoparticles, hybrid nanocomposites, up-conversion nanoparticles, Bovine serum albumin (BSA), Immunoglobulin G (IgG), Surface coating, Matrix assisted pulsed laser evaporation (MAPLE)

Co-Authorship Statement

Chapter 1 (Introduction), Chapter 2 (Background and literature review) and Chapter 3 (Experiment Procedures) were written by Songlin Yang with some suggestions which were given by Dr. Jin Zhang. Songlin Yang, as the first author, written the Chapter 4, Chapter 5, Chapter 6 and Chapter 7. Chapter 4, Chapter 5, Chapter 6 includes the research data and characterization data of FeCo/graphene hybrid nanocomposites fabricated by MAPLE, YBCO/graphene hybrid nanocomposites fabricated by MAPLE and MAPLE deposition of the protein modified up-conversion nanoparticles, which have been published or under preparation. Invaluable assistance for this thesis is named in the acknowledge section.

Acknowledgments

This thesis would not have been written without the help and guidance from several people. I would like to gratefully acknowledge all of them.

I would like to thank my supervisor Dr. Jin Zhang for her guidance, support, trust and understanding throughout my program. The door of her office was always open whenever I ran into a trouble spot or had a question about my research. The support and encouragement from her have been and will continue to be fundamental for my development.

I would like to thank my examination committee: Dr. Lars Rehmann, Dr. Lyudmila Goncharova and Dr. Shahzad Barghi for their guidance and feedback throughout the course of my project. I would like to thank Dr. Richard Gardiner and Mrs. Karen Nygard of Biotron center for their help of using the facilities.

I would also like to thank all of my current and previous colleagues at Multifunctional Nanocomposite Lab, Andrew Tse, Longyi Chen, Dr. Longyan Chen, Vishnuvardhana Wuppaladhodi, Denghuang Zhan, Aditya Balaji, Deepthi Muraleedharan and Eugene Hwang for their continuous support, encouragement and nice time that we have had together. Finally, I would dearly like to thank my family for the support they provided me through my entire life. Without their love, encouragement, and assistance, I would not have finished this thesis.

This work has been supported by funding from Natural Science and Engineering Research Council of Canada (NSERC) through a Discovery Grant and Western Engineering Graduate Scholarship.

Table of Contents

List of Figures

List of Abbreviations

4-NP	——	4-nitrophenol
FRET	——	Fluorescence resonance energy transfer
CVD	——	Chemical vapor deposition
ALD	——	Atomic layer deposition
PVD	——	Physical vapor deposition
MAPLE	——	Matrix assisted pulsed laser evaporation
PLD	——	Pulse laser deposition
MRI	——	Magnetic resonance imaging
GO	——	Graphene oxide
ETPTA	——	Ethoxylated trimethylolpropane triacrylate
PDDA	——	Poly(diallydimethylammonium chloride)
PSS	——	Poly(sodium 4-styrenesulfonate)
GOx	——	Glucose oxidase
MPC	——	2-methacryloyloxyethyl phosphorylcholine
LED	——	Light-emitting diode
PEI	——	Polyethyleneimine
EDC	——	1-Ethyl-3-(3-dimethylaminopropyl) carbodimide
TEM	——	Transmission electron microscope

SEM	——	Scanning Electron Microscopy
EDS	——	Energy-dispersive X-ray spectroscopy
VSM	——	Vibrating sample magnetometer
FT-IR	——	Fourier transform infrared spectroscopy
UV-Vis	——	Ultraviolet–visible spectroscopy
HUVEC	——	Human umbilical vein endothelial cell
SPR	——	Surface plasmon resonance
YBCO	——	Yttrium barium copper oxide
XRD	——	X-ray diffraction
MTT	——	3-(4, 5-dimethylthiazolyl-2)-2,5-diphenyltetrazolium bromide
DMSO	——	Dimethyl sulfoxide
Ms	——	Saturation magnetisation
Hc	——	Coercivity
E.coli	——	Escherichia coli
BSA	——	Bovine serum albumin
IgG	——	Immunoglobulin G
ETU	——	Energy transfer up-conversion
ESA	——	Excited-state absorption
PA	——	Photon avalanche

NIR	——	Near-infrared
ROS	——	Reactive oxygen species
EDC	——	1-Ethyl-3-(3-dimethylaminopropyl) carbodiimide
BBS	——	Borate buffered saline
TCVD	——	Thermal chemical vapor deposition

Chapter 1

1 Introduction

1.1 Magnetic hybrid nanocomposites

Magnetism is the physical phenomenon which is triggered by the magnetic fields. Magnetic fields can be generated by the electric currents and magnetic moments which were created by electron spin. Due to the different conditions of electrons (paired and unpaired) and domain directions in the materials, different types of magnetism could be generated: ferromagnetism, paramagnetism, diamagnetism, antiferromagnetism, ferrimagnetism, and superparamagnetism. Magnetic materials have been applied in various fields of the modern technology, for instance, magnetic data storage, magnetic sensors, magnetic motors, medical instruments, energy storage, energy transfer, etc. In the past thirty years, nanostructured materials demonstrate great potentials in various applications because of their special magnetic properties. The magnetic nanomaterials with various structures and different magnetic properties were produced by different techniques. The magnetic nanomaterials hold advantages including large surface area, small particle size, and simple to manipulate. In addition, the superparamagnetism could be achieved by the magnetic nanomaterials if the size of the nanomaterials lower than the specific value and the temperature lower than the critical temperature.

Magnetic nanomaterials have been applied in various fields: catalysis, nanofluids, pollution treatment, data storage, magnetic detecting sensor, microorganism collection, cancer therapy, etc. Recent years, the magnetic hybrid nanocomposites have attracted the worldwide attention since they could combine the superiorities of magnetic nanomaterials with the advantages of the other nanostructures/nanomaterials. These magnetic hybrid nanocomposites can show enhanced and special multi-properties.

The magnetic nanocomposites with different structures have been developed for decades. The core-shell nanocomposites could achieve different properties of both two materials and core-shell nanostructure could protect the inside materials from oxidization. The

multilayer nanocomposites are produced to fabricate devices with different functions. The dumbbell nanocomposites are developed to fully display the feature of component materials. These nanocomposites are fabricated through growing other nanoparticles on the surface of the seeding nanoparticles. Unlike the core-shell nanocomposites and the dumbbell nanocomposites, dumbbell nanocomposites allow all the parts of the nanoparticle's surface exposing. These properties are crucial for the catalytic processes.

1.1.1 Core-shell nanocomposites

To expand the application fields of the conventional nanoparticles. Core-shell nanocomposites (Figure 1.1) are designed by the researchers. Core-shell structure is widely applied in the fabrication processes of different magnetic nanocomposites, especially the iron oxide based magnetic nanoparticles. Iron oxide based magnetic nanomaterials have been applied in various fields since these nanomaterials could achieve superparamagnetic properties. In addition, the iron-oxide based magnetic nanoparticles are biocompatible and easy to be degraded by the organisms. Some researchers coat iron-oxide nanoparticles and organic dye with silica shell to fabricate uniform size nanocomposites which could be applied for cell imaging and cell collection [1]. Iron oxide materials could be applied as the shell layer of the nanocomposites. Shevchenko et al. [2] fabricated gold/iron oxide core-shell nanocomposites which applied gold nanoparticles as the core part and hollow iron oxide nanoparticles as the shell part. Multicore magnetic nanocomposites are developed by the researchers to manipulate the magnetic properties of the core-shell nanocomposites. The magnetic properties of the multicore nanocomposites are decided by the number of the magnetic cores inside the particles [3]. By varying the materials of the core part and the shell part, the core-shell magnetic nanocomposites could resist the oxidation and grain other properties.

(a) Single core (b) Reverse core-shell (c) multicore

Figure 1.1 Schematic of the core-shell nanocomposites

1.1.2 Multilayer nanocomposites

Multilayer nanocomposites have been developed by the researchers to expand the application fields of the single layer nanocomposites. Generally, multilayer magnetic nanocomposites would have a magnetic core and multilayer shells with different functions. The researchers fabricated α-Fe_2O_3/Ag/SiO_2/SnO_2 multilayer magnetic nanocomposites through the adjusted Stöber method [4]. By varying the thickness of each layer, these nanocomposites could achieve different properties and could be applied as photo-catalysts under the UV light. Salazar-Alvarez et al. [5] produced maximum four layers uniform magnetic nanocomposites by depositing other materials on the surface of the magnetic core. In this experiment, the researchers deposited MnO layer on the surface of the magnetic core and MnO layer was passivated in the air. Multilayer magnetic nanocomposites have been developed by the researchers to overcome the drawbacks of single layer magnetic nanocomposites.

1.1.3 Dumbbell nanocomposites

Dumbbell nanocomposites normally contain two or more parts. The other nanoparticles are seeded on the surface of the magnetic nanoparticles. These nanocomposites allow the nanoparticles to fully unleash their physical and chemical properties since nanoparticles could direct contact with the external environment. The dumbbell magnetic nanocomposites possess the unique structure which could contribute to the catalytic process. The successful synthesis of the dumbbell magnetic nanocomposites needs to meet some critical requirements such as the matching of the lattice structure and critical synthesis conditions. In the past decades, the researchers developed various dumbbell magnetic nanocomposites and most of them combine noble metals with magnetic materials together. The Au-Fe_3O_4 dumbbell nanocomposites [6] are synthesized by adjusting and controlling the structure/size of the Au/Fe_3O_4 nanoparticles. The Pt-Fe_3O_4 [7], FePt-Fe_3O_4 [8] and Ag-Fe_3O_4 [9] dumbbell magnetic nanocomposites were synthesized by the researchers for different applications. The adding of noble metals in dumbbell magnetic nanocomposites could make magnetic nanomaterials grain optical properties and magnetic properties at the same time. This type of nanocomposites could be applied in the

multichannel image (magnetic/optical) for the medical applications. By varying materials type of dumbbell nanocomposites, these magnetic nanocomposites could be applied in different catalysis processes. The dumbbell nanocomposites could overcome the drawbacks of core-shell nanocomposites, but the synthesis requirements for these materials are strict.

Various nanomaterials have been incorporated with magnetic nanomaterials. For instance, silica nanoparticles, noble metal nanoparticles, quantum dots, graphene, proteins, etc. Different nanoparticles would graft magnetic nanomaterials different functions. Compared with the nanoparticles, the two-dimensional materials such as graphene could work as the matrix of the hybrid nanocomposites. There are various methods to incorporate the magnetic nanomaterials with the two-dimensional materials, both chemical methods and physical methods. All of these methods are not hard to perform since the two-dimensional nanomaterials have large superficial area and a lot of functional groups on their surface. In addition, it is possible to combine two or more nanomaterials with two-dimensional materials to fabricate nano-size devices which could be applied in various fields.

1.2 Two-dimensional materials

Two-dimensional materials, also known as the 2D materials or single layer materials. These materials possess the unique structure which only consists one single layer of atoms. This unique structure makes the two-dimensional materials grain various superior physical and chemical properties. Andre Geim and Konstantin Novoselov [10] found a simple method to fabricate graphene. They separated graphene from the graphite with scotch tape. After the successful preparation of the single layer graphene, a series of two-dimensional materials were fabricated by the researchers such as borophene[11], germanene[12], silicene[13] and phosphorene[14]. These two-dimensional materials have been applied in different fields such as semiconductors, high-performance batteries, optical electronic devices, therapy, etc. Since the two-materials hold superb mechanical, electrical and optical properties, these materials have attracted the attention of the researchers from all over the world.

1.2.1 Graphene

Graphene is a typical two-dimensional carbon nanomaterial. Since graphene possesses unique structure, it offers remarkable mechanical, electrical, thermal and optical properties. These properties which measured by the researchers surpassed such properties of the normal materials. Some of them even reached the limit of the theoretical calculation. Such as, Young's modulus of graphene is around 1 TPa and the intrinsic strength of graphene is 130 GPa [15]. The room temperature electron mobility of graphene is 2.5×10^5 cm^2 V^{-1} s^{-1} [16]. The thermal conductivity of the graphene is > 3000 W mK^{-1}.

Since graphene sheets possess these excel properties, various applications have been developed by researchers, such as energy-storage devices, polymer composite materials, 'paper-like' materials, mechanical resonators, sensors [17], etc. Graphene was used to fabricate flexible electronics [18, 19], high-frequency transistors [20] and logic transistor [21]. Because the optical energy of low layer graphene is smaller than double of the Fermi level value, the single layer and double layer graphene could become transparent [22]. Graphene sensors can be applied to detect the gas molecules [23] and biomolecules [24]. New high-performance clear energy batteries can be fabricated by using graphene as the electrode materials [25].

1.3 Fabrication of graphene based hybrid nanocomposites

Compared with other two-dimensional materials, the synthesis processes of graphene nanosheets are not complicated and easy to perform both at lab or factory. Because graphene possesses various outstanding physical and chemical properties, the fabrication of graphene based magnetic hybrid nanocomposites attracts the attention of the researchers. The superficial area of the graphene is higher than the other nanomaterials due to the nature of the two-dimensional materials. There are various applications of the graphene hybrid nanocomposites in different fields such as: electronic sensors [26], biosensors [27], therapy/medical imaging [28], catalysts [29], filling materials, photochemical sensors [30], solar cells [31], electrodes [32], supercapacitors [33], etc.

1.3.1 Graphene based hybrid nanocomposites

Among various graphene or graphene derivatives based materials, graphene hybrid nanocomposites can effectively integrate the advantages of graphene and nanoparticles. Graphene hybrid nanocomposites can provide good catalytic properties and adsorption abilities. In recent years, the researchers developed various types of graphene hybrid nanocomposites base on the different materials. For example, the researchers developed a graphene nanocomposites which could provide magnetic properties and catalytic properties used for 4-nitrophenol (4-NP) reduction. These nanocomposites were fabricated by decorating magnetic/catalytic nanoparticles on graphene [34]. Another application of the graphene hybrid nanocomposites is growing Pt-on-Pd bimetallic nano-dendrites on graphene nanosheets to fabricate an advanced graphene/metal heterostructure which could work as nano-electro-catalyst for methanol oxidation [35]. Graphene hybrid nanocomposites could be applied as biological devices. The researchers conjugated graphene nanosheets with up-conversion nanoparticles to form a bio-sensing platform to detect glucose through Fluorescence Resonance Energy Transfer (FRET) process [36]. There were many other graphene hybrid nanocomposites which were investigated with enhanced performance and novel chemical physical properties for bio-applications [37], supercapacitor [38], photovoltaic, electrodes, sensors [39], etc.

Graphene magnetic hybrid nanocomposites were fabricated through different methods which include solution methods [40], chemical vapor deposition [41] and physical deposition [42]. Ren et al. [43] grafted Fe_3O_4 and ZnO on the surface of graphene nanosheets and fabricated graphene magnetic hybrid nanocomposites. Researchers found these graphene magnetic hybrid nanocomposites are good electronic magnetic wave absorption materials. Liang et al. [44] fabricated Fe_3O_4/graphene magnetic and conductive paper by filtrating the Fe_3O_4/graphene oxide solution and reducing through hydrazine. They assembled a magnetic controlling switch with these graphene hybrid magnetic materials. Su et al. [45] prepared graphene/Fe_3O_4 magnetic hybrid nanocomposites to fabricate high-performance lithium batteries. The fabricated high-performance lithium batteries show highly reversible capacity and high cycle performance.

For combining particles with graphene and graphene derivatives, the graphene hybrid nanocomposites provide a good design model for various applications and functions. By changing the particles on the surface of graphene nanosheets, such as metal nanoparticles, metal oxide nanoparticles, semiconductor nanoparticles, inorganic or organic nanoparticles, noble Au/Ag nanoparticles, polymer nanoparticles, up-conversion nanoparticles, bio-micelles, DNA nanoribbon, etc., various graphene nanocomposites with different applications and functions could be achieved.

1.3.2 Fabrication methods of graphene based hybrid nanocomposites

To fabricate organic graphene nanocomposites, the graphene is first well dispersed in the polymer matrix [46], then use the methods like solution mixing, melt blending and in situ polymerization to synthesize. Among these methods, the in situ polymerization could achieve preferable dispersion of the graphene filler [47]. Other methods use emulsion polymerization to graft the polymer microspheres on the surface of graphene oxide's surface by covalent bonds [48]. The synthesis methods of inorganic graphene nanocomposites shared the similar concept with their organic counterparts. By fixing the inorganic nanoparticles on the graphene sheets, various functions are grafted to graphene nanocomposites. Some researchers used the seed and grow methods to form ZnO nanorods [49] array on the surface of graphene sheets. There are alternate methods which use hydrothermal methods to graft nanoparticles such as ZnO [50], TiO_2 [51] onto the graphene nanosheets. Same as the organic graphene nanocomposites, covalent bonds are applied to fix the inorganic nanoparticles on the surface of graphene [52].

But the major drawback of these methods it's that the chemical conjugation could change the surface structure of the graphene and interfere the function of graphene. Another problem is that some particles are hard to fabricate by conventional methods. For example, some ceramic materials need to be synthesized under high temperature and can't be fabricated by the methods which use the solution as a matrix. It is hard to synthesize

nanoparticles by these materials and difficult to fabricate nanocomposites by these materials through normal bottom up methods.

1.4 Surface modification methods

The concept of surface modification methods is the modification of the materials' surface and grafting various functions. Meanwhile, the bulk properties of the materials would be preserved. Various surface modification methods were developed by the researchers to improve the reactivity [53], biocompatibility [54], cytocompatibility [55], corrosion resistivity [56] and hydrophilicity [57] of the substrate materials' surface.

There are two main types of these surface modification methods: chemical methods and physical methods. Representative two of the chemical surface modification methods are wet chemical method [58] and chemical vapor deposition (CVD) [59]. The chemical methods modify the substrate by processing chemical reaction between the import materials and surface molecules and creating a covalent bond between them. To meet the reaction criteria, the modification processes must be carried out under extreme conditions, such as high temperature, toxic or corrosive reactants, and highly flammable gas sphere. For example, atomic layer deposition (ALD) which is a subclass of CVD, normally use Trimethylaluminium [60], Diethylzinc [61] and Titanium isopropoxide [11] as the precursors or reactants. These chemicals are highly reactive, flammable and not eco-friendly. These chemicals could cause the irreversible decomposition or damage to the molecules of biomaterials [62]. In addition, it is essential for the chemical modification methods to use these molecules involved in specific reactions. That means these techniques are hard to be employed with biological/organic materials [63].

The physical surface modification methods involve physical vapor deposition (PVD) [64], dip coating [65] and spin coating [66]. Compared with the chemical methods, most of the physical methods don't require harsh conditions. It is hard for some conventional physical deposition methods to control the thickness of the films. In contrast with these methods, it is simple for PVD methods to control the thickness of the films. By controlling the deposition time, the thickness of the films could be controlled in nanoscale. PVD methods

include cathodic arc deposition, electron beam physical vapor deposition, evaporative deposition, pulsed laser deposition (PLD) and sputter deposition, etc. But the disadvantages of the normal PVD methods are obvious: to deposit the target material on the surface of substrates, it needs input energy (high energy laser beam, high-power electric arc, and extremely high temperature) onto the target materials, which could damage the structure of the delicate materials. To overcome these drawbacks and expand the application fields of the PVD method, researchers developed a new technique: matrix assisted pulsed laser evaporation (MAPLE).

1.5 Matrix assisted pulsed laser evaporation (MAPLE) technique

The MAPLE method was developed from pulse laser deposition (PLD) by the Naval Research Laboratories. The researchers tried to study a new physical method to deposit organic materials and they tried to protect the target materials from the damage of high energy flow. Since MAPLE method derived from the PLD method, it inherits the advantages of the PLD method, such as thickness controlling and thin and uniform film fabricating. It overcomes the drawbacks of the traditional PLD deposition methods and could deposit inorganic materials, organic materials and biomaterial with delicate structures on the substrate surface.

Similar with the PLD methods, the high energy laser beam is applied as the energy source. In the MAPLE process, the target material is dissolved in a solvent (matrix) with a weight concentration lower than 5 % (w/v). This target solution is frozen by the liquid nitrogen which flows through the tube between the sidewalls of the holder. As Figure 1.2 shows, during the deposition process, most of the laser energy is absorbed by the solvent and the target materials are protected. Among the photo thermal process, the frozen solvent molecules absorb the energy of photons and convert that to thermal energy. In this process, target molecules are heated and the solvent is allowed to vaporize [67]. The target molecules absorb enough energy through collisions with solvent molecules among the evaporation process. The substrate is placed in the same direction of the molecular

movement to make the target molecules reach it easily. For the same reason, the process is carried out under high vacuum to improve the average travel distance of the molecules and reduce the collision times with other molecules when the target solution is vaporized. During the MAPLE process, the target molecules start fabricating the thin film on the surface of the substrate. At the meantime, the solvent molecules are pumped away by the pumps because their adhesion coefficient of them are low [68].

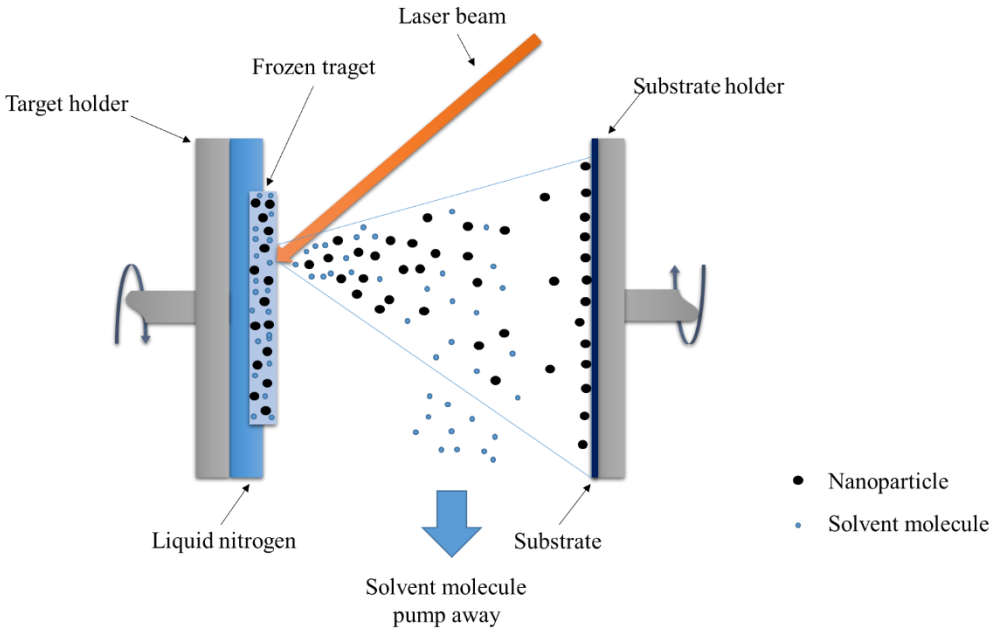

Figure 1.2 Mechanism of MAPLE method

1.6 Fabricate hybrid nanocomposites by MAPLE method

It is possible to fabricate nanocomposites and deposit hybrid nanocomposites on the surface of the substrate through MAPLE technique. The hybrid nanocomposites can obtain various functions based on the deposited materials. Meanwhile, MAPLE technique could protect target materials and maintain its functions. The researchers has already deposited TiO_2 [69], CdSe [70], SnO_2 [71], carbon nanotubes [72], graphene oxide [73], graphene-iron oxide nanocomposites [74] by the MAPLE technique. The former works of our group deposited Ag-PVP nanocomposites [48] and ZnO-PEG nanocomposites [49] on the surface of the silicone hydrogel to solve the biofouling problems of the silicone hydrogel. These experiments proved that MAPLE method can deposit nanomaterials on the surface of the

substrate and preserve the chemical/physical structure of the nanomaterials. By switching the deposition materials and the substrates, the hybrid nanocomposites could obtain various properties: such as electronical[74], optical[75] and biological[76] properties.

1.7 Motivations and thesis objectives

Two-dimensional hybrid nanocomposites have demonstrated the extensive applications in fabricating various electronic and magnetic devices. In particular, they bring promising future for miniaturized medical devices. However, it is a challenge to have the suitable surface modification and efficient manufacturing process for hybrid nanocomposites fabrication. As compared to other modify methods, the MAPLE method could be applied in different fields. Various materials could be deposited through MAPLE method. The primary objective of MAPLE technique is depositing target materials and minimizing the effect of the process. It is possible to overcome the drawbacks of the normal physical and chemical deposition methods and deposit ultra-thin nanocomposites films uniformly through MAPLE technique. In addition, there are few reports on incorporating magnetic nanocomposites onto two-dimensional materials by the MAPLE technique. The studies about the deposition of the protein incorporated nanomaterials through MAPLE technique are less for past decades.

The main objective of this thesis is to deposit different magnetic nanoparticles on two-dimensional materials to form hybrid nanocomposites. In addition, the protein incorporated nanomaterials are deposited through MAPLE technique in this study. The effect of MAPLE process on different nanoparticles is studied to make a full-scale understand of the MAPLE process mechanism and the influence of different parameters on the target materials.

(1) To design and fabricate different two-dimensional hybrid nanocomposites by using MAPLE method.
(2) To thoroughly investigate the effect of the different parameters of the matrix assisted pulsed laser evaporation (MAPLE) on nanoparticles with different magnetic properties.

(3) To understand the inherent mechanism of MAPLE method by characterizing the particles before deposition process and after the deposition process. The hybrid nanocomposites before and after MAPLE deposition are thoroughly characterized.

(4) To study the special physical and chemical properties of the hybrid nanocomposites made by MAPLE, and to explore the developed materials in different applications.

1.8 Thesis overview

The overview of the following is presented here.

Chapter 2 Literature review

This chapter reviews the applications/properties of magnetic nanoparticles and magnetic hybrid nanocomposites. Different methods which are used to produce magnetic nanoparticles and magnetic hybrid nanocomposites are mentioned in this chapter. The applications and properties of particles which are used for fabricating hybrid nanocomposites by MAPLE process are mentioned in this chapter. In addition, the history, developments, applications and the full mechanism of Matrix Assisted Pulsed Laser Evaporation (MAPLE) would be reviewed in this chapter.

Chapter 3 Experimental methods

This chapter presents the experimental procedures of the chemical synthesis processes of the FeCo nanoparticles, up-conversion nanoparticles (UCNPs) and protein modified up-conversion nanoparticles. The deposition processes of FeCo, YBCO and up-conversion particles are described in this chapter. The factors of the MAPLE deposition processes are showed in this chapter. The characterization techniques and test procedures which are applied in this study are described in this chapter.

Chapter 4 Fabricating FeCo/graphene hybrid nanocomposites by MAPLE

This chapter mainly focuses on fabricating FeCo/graphene hybrid nanocomposites through MAPLE technique. The chemical synthesis processes of the FeCo nanoparticles are described in this chapter. The specific parameters of the MAPLE deposition process are

presented in this chapter. The graphene nanosheets were coated on the surface of the glass plate as the substrates of the deposition. Ultraviolet–visible spectroscopy (UV-Vis) was applied to characterize the synthesis results of the graphene. Deposition products of this experiment were characterized through the techniques such as transmission electron microscope (TEM), energy-dispersive X-ray spectroscopy (TEM-EDS) and vibrating sample magnetometer (VSM). The relationships between deposition time (*t*) with the morphology of the FeCo/graphene hybrid nanocomposites were investigated.

Chapter 5 Fabricating YBCO/graphene hybrid nanocomposites by MAPLE

In this chapter, the fabrication process and results of the YBCO/graphene hybrid nanocomposites by MAPLE technique are discussed. Various characterization techniques were applied to investigate the deposition products and the raw materials: transmission electron microscope (TEM), energy-dispersive X-ray spectroscopy (TEM-EDS), X-ray Diffraction (XRD) and vibrating sample magnetometer (VSM). These techniques were applied to characterize the fabrication of the YBCO/graphene hybrid nanocomposites. The relationships between size/shape of the YBCO nanoparticles and deposition time (*t*) were characterized by these techniques.

Chapter 6 Deposition of protein modified up-conversion nanoparticles by MAPLE technique

In this chapter, the up-conversion nanoparticles and protein (Bovine serum albumin and Immunoglobulin G) modified up-conversion nanoparticles were deposited through MAPLE technique. The chemical synthesized up-conversion nanoparticles and protein modified up-conversion nanoparticles were investigated with Fourier transform infrared spectroscopy (FT-IR), fluorometer and transmission electron microscope (TEM). The up-conversion properties and the protein modification results were observed. The deposition products of up-conversion nanoparticles and protein modified nanoparticles were investigated by TEM and FT-IR spectrum. The shift and the presence of the specific peaks indicate the successful deposition of the target nanoparticles. Furthermore, the influence of the up-conversion nanoparticles/Immunoglobulin G (IgG) modified up-conversion

nanoparticles on the Human umbilical vein endothelial cells (HUVECs) were studied. The results of MTT test and confocal microscopy characterization indicate that IgG modified up-conversion nanoparticles show the minimum effect on the cells and could help cells grow on its surface.

Chapter 7 Summary and future work

This chapter mainly focuses on the summaries and conclusions of this study. The further experiments, structure changes of the equipment and procedure's modifications of this study are discussed in this chapter.

1.9 Reference

[1] C.-S. Lee, H.H. Chang, P.-K. Bae, J. Jung, B.H. Chung, Bifunctional Nanoparticles Constructed Using One-Pot Encapsulation of a Fluorescent Polymer and Magnetic (Fe3O4) Nanoparticles in a Silica Shell, Macromol. Biosci. 13 (2013) 321-331.

[2] E.V. Shevchenko, M.I. Bodnarchuk, M.V. Kovalenko, D.V. Talapin, R.K. Smith, S. Aloni, W. Heiss, A.P. Alivisatos, Gold/Iron Oxide Core/Hollow-Shell Nanoparticles, Adv. Mater. 20 (2008) 4323-4329.

[3] C. Yang, G. Wang, Z. Lu, J. Sun, J. Zhuang, W. Yang, Effect of ultrasonic treatment on dispersibility of Fe_3O_4 nanoparticles and synthesis of multi-core Fe_3O_4/SiO_2 core/shell nanoparticles, J. Mater. Chem. 15 (2005) 4252-4257.

[4] L. Sun, W. Wu, S. Yang, J. Zhou, M. Hong, X. Xiao, F. Ren, C. Jiang, Template and Silica Interlayer Tailorable Synthesis of Spindle-like Multilayer α-Fe2O3/Ag/SnO2 Ternary Hybrid Architectures and Their Enhanced Photocatalytic Activity, ACS Appl. Mater. Interfaces 6 (2014) 1113-1124.

[5] G. Salazar-Alvarez, H. Lidbaum, A. López-Ortega, M. Estrader, K. Leifer, J. Sort, S. Suriñach, M.D. Baró, J. Nogués, Two-, Three-, and Four-Component Magnetic Multilayer Onion Nanoparticles Based on Iron Oxides and Manganese Oxides, J. Am. Chem. Soc. 133 (2011) 16738-16741.

[6] H. Yu, M. Chen, P.M. Rice, S.X. Wang, R.L. White, S. Sun, Dumbbell-like Bifunctional Au−Fe3O4 Nanoparticles, Nano Lett. 5 (2005) 379-382.

[7] C. Wang, H. Daimon, S. Sun, Dumbbell-like Pt−Fe_3O_4 Nanoparticles and Their Enhanced Catalysis for Oxygen Reduction Reaction, Nano Lett. 9 (2009) 1493-1496.
[8] Q. Li, L. Wu, G. Wu, D. Su, H. Lv, S. Zhang, W. Zhu, A. Casimir, H. Zhu, A. Mendoza-Garcia, S. Sun, New Approach to Fully Ordered fct-FePt Nanoparticles for Much Enhanced Electrocatalysis in Acid, Nano Lett. 15 (2015) 2468-2473.
[9] C. Wang, H. Yin, S. Dai, S. Sun, A General Approach to Noble Metal−Metal Oxide Dumbbell Nanoparticles and Their Catalytic Application for CO Oxidation, Chem. Mater. 22 (2010) 3277-3282.
[10] K.S. Novoselov, A.K. Geim, S.V. Morozov, D. Jiang, Y. Zhang, S.V. Dubonos, I.V. Grigorieva, A.A. Firsov, Electric Field Effect in Atomically Thin Carbon Films, Science 306 (2004) 666-669.
[11] M.T. McDowell, M.F. Lichterman, A.I. Carim, R. Liu, S. Hu, B.S. Brunschwig, N.S. Lewis, The Influence of Structure and Processing on the Behavior of TiO_2 Protective Layers for Stabilization of n-Si/TiO_2/Ni Photoanodes for Water Oxidation, ACS Appl. Mater. Interfaces 7 (2015) 15189-15199.
[12] Z. Ni, Q. Liu, K. Tang, J. Zheng, J. Zhou, R. Qin, Z. Gao, D. Yu, J. Lu, Tunable Bandgap in Silicene and Germanene, Nano Lett. 12 (2012) 113-118.
[13] P. Vogt, P. De Padova, C. Quaresima, J. Avila, E. Frantzeskakis, M.C. Asensio, A. Resta, B. Ealet, G. Le Lay, Silicene: Compelling Experimental Evidence for Graphenelike Two-Dimensional Silicon, Phys. Rev. Lett. 108 (2012) 155501.
[14] H. Liu, A.T. Neal, Z. Zhu, Z. Luo, X. Xu, D. Tománek, P.D. Ye, Phosphorene: An Unexplored 2D Semiconductor with a High Hole Mobility, ACS Nano 8 (2014) 4033-4041.
[15] F. Liu, P. Ming, J. Li, Calculation of ideal strength and phonon instability of graphene under tension, Phys. Rev. B 76 (2007) 064120.
[16] A.S. Mayorov, R.V. Gorbachev, S.V. Morozov, L. Britnell, R. Jalil, L.A. Ponomarenko, P. Blake, K.S. Novoselov, K. Watanabe, T. Taniguchi, A.K. Geim, Micrometer-Scale Ballistic Transport in Encapsulated Graphene at Room Temperature, Nano Lett. 11 (2011) 2396-2399.
[17] S. Park, R.S. Ruoff, Chemical methods for the production of graphenes, Nat Nano 4 (2009) 217-224.

[18] R.R. Nair, P. Blake, A.N. Grigorenko, K.S. Novoselov, T.J. Booth, T. Stauber, N.M.R. Peres, A.K. Geim, Fine Structure Constant Defines Visual Transparency of Graphene, Science 320 (2008) 1308-1308.

[19] S. Bae, H. Kim, Y. Lee, X. Xu, J.-S. Park, Y. Zheng, J. Balakrishnan, T. Lei, H. Ri Kim, Y.I. Song, Y.-J. Kim, K.S. Kim, B. Ozyilmaz, J.-H. Ahn, B.H. Hong, S. Iijima, Roll-to-roll production of 30-inch graphene films for transparent electrodes, Nat Nano 5 (2010) 574-578.

[20] Y.-M. Lin, C. Dimitrakopoulos, K.A. Jenkins, D.B. Farmer, H.-Y. Chiu, A. Grill, P. Avouris, 100-GHz Transistors from Wafer-Scale Epitaxial Graphene, Science 327 (2010) 662-662.

[21] L. Britnell, R.V. Gorbachev, R. Jalil, B.D. Belle, F. Schedin, A. Mishchenko, T. Georgiou, M.I. Katsnelson, L. Eaves, S.V. Morozov, N.M.R. Peres, J. Leist, A.K. Geim, K.S. Novoselov, L.A. Ponomarenko, Field-Effect Tunneling Transistor Based on Vertical Graphene Heterostructures, Science 335 (2012) 947-950.

[22] Z.Q. Li, E.A. Henriksen, Z. Jiang, Z. Hao, M.C. Martin, P. Kim, H.L. Stormer, D.N. Basov, Dirac charge dynamics in graphene by infrared spectroscopy, Nat Phys 4 (2008) 532-535.

[23] Y. Dan, Y. Lu, N.J. Kybert, Z. Luo, A.T.C. Johnson, Intrinsic Response of Graphene Vapor Sensors, Nano Lett. 9 (2009) 1472-1475.

[24] Y. Ohno, K. Maehashi, Y. Yamashiro, K. Matsumoto, Electrolyte-Gated Graphene Field-Effect Transistors for Detecting pH and Protein Adsorption, Nano Lett. 9 (2009) 3318-3322.

[25] E. Yoo, J. Kim, E. Hosono, H.-s. Zhou, T. Kudo, I. Honma, Large Reversible Li Storage of Graphene Nanosheet Families for Use in Rechargeable Lithium Ion Batteries, Nano Lett. 8 (2008) 2277-2282.

[26] S. Guo, D. Wen, Y. Zhai, S. Dong, E. Wang, Platinum Nanoparticle Ensemble-on-Graphene Hybrid Nanosheet: One-Pot, Rapid Synthesis, and Used as New Electrode Material for Electrochemical Sensing, ACS Nano 4 (2010) 3959-3968.

[27] V. Mani, B. Devadas, S.-M. Chen, Direct electrochemistry of glucose oxidase at electrochemically reduced graphene oxide-multiwalled carbon nanotubes hybrid material modified electrode for glucose biosensor, Biosens. Bioelectron. 41 (2013) 309-315.

[28] X. Ma, H. Tao, K. Yang, L. Feng, L. Cheng, X. Shi, Y. Li, L. Guo, Z. Liu, A functionalized graphene oxide-iron oxide nanocomposite for magnetically targeted drug delivery, photothermal therapy, and magnetic resonance imaging, Nano Research 5 (2012) 199-212.

[29] Y. Liang, Y. Li, H. Wang, J. Zhou, J. Wang, T. Regier, H. Dai, Co3O4 nanocrystals on graphene as a synergistic catalyst for oxygen reduction reaction, Nat Mater 10 (2011) 780-786.

[30] Y. Liu, X. Dong, P. Chen, Biological and chemical sensors based on graphene materials, Chem. Soc. Rev. 41 (2012) 2283-2307.

[31] Z. Yin, S. Wu, X. Zhou, X. Huang, Q. Zhang, F. Boey, H. Zhang, Electrochemical Deposition of ZnO Nanorods on Transparent Reduced Graphene Oxide Electrodes for Hybrid Solar Cells, Small 6 (2010) 307-312.

[32] H. Wang, L.-F. Cui, Y. Yang, H. Sanchez Casalongue, J.T. Robinson, Y. Liang, Y. Cui, H. Dai, Mn3O4−Graphene Hybrid as a High-Capacity Anode Material for Lithium Ion Batteries, J. Am. Chem. Soc. 132 (2010) 13978-13980.

[33] X. Yu, B. Lu, Z. Xu, Super Long-Life Supercapacitors Based on the Construction of Nanohoneycomb-Like Strongly Coupled $CoMoO_4$–3D Graphene Hybrid Electrodes, Adv. Mater. 26 (2014) 1044-1051.

[34] S. Bai, X. Shen, G. Zhu, M. Li, H. Xi, K. Chen, In situ Growth of NixCo100–x Nanoparticles on Reduced Graphene Oxide Nanosheets and Their Magnetic and Catalytic Properties, ACS Appl. Mater. Interfaces 4 (2012) 2378-2386.

[35] S. Guo, S. Dong, E. Wang, Three-Dimensional Pt-on-Pd Bimetallic Nanodendrites Supported on Graphene Nanosheet: Facile Synthesis and Used as an Advanced Nanoelectrocatalyst for Methanol Oxidation, ACS Nano 4 (2010) 547-555.

[36] C. Zhang, Y. Yuan, S. Zhang, Y. Wang, Z. Liu, Biosensing Platform Based on Fluorescence Resonance Energy Transfer from Upconverting Nanocrystals to Graphene Oxide, Angew. Chem. Int. Ed. 50 (2011) 6851-6854.

[37] P.T. Yin, S. Shah, M. Chhowalla, K.-B. Lee, Design, Synthesis, and Characterization of Graphene–Nanoparticle Hybrid Materials for Bioapplications, Chem. Rev. 115 (2015) 2483-2531.

[38] D. Wang, R. Kou, D. Choi, Z. Yang, Z. Nie, J. Li, L.V. Saraf, D. Hu, J. Zhang, G.L. Graff, J. Liu, M.A. Pope, I.A. Aksay, Ternary Self-Assembly of Ordered Metal Oxide−Graphene Nanocomposites for Electrochemical Energy Storage, ACS Nano 4 (2010) 1587-1595.

[39] X. Huang, Z. Yin, S. Wu, X. Qi, Q. He, Q. Zhang, Q. Yan, F. Boey, H. Zhang, Graphene-Based Materials: Synthesis, Characterization, Properties, and Applications, Small 7 (2011) 1876-1902.

[40] Q. Han, Z. Wang, J. Xia, S. Chen, X. Zhang, M. Ding, Facile and tunable fabrication of Fe_3O_4/graphene oxide nanocomposites and their application in the magnetic solid-phase extraction of polycyclic aromatic hydrocarbons from environmental water samples, Talanta 101 (2012) 388-395.

[41] J. Luo, J. Liu, Z. Zeng, C.F. Ng, L. Ma, H. Zhang, J. Lin, Z. Shen, H.J. Fan, Three-Dimensional Graphene Foam Supported Fe3O4 Lithium Battery Anodes with Long Cycle Life and High Rate Capability, Nano Lett. 13 (2013) 6136-6143.

[42] G. Wang, Z. Gao, G. Wan, S. Lin, P. Yang, Y. Qin, High densities of magnetic nanoparticles supported on graphene fabricated by atomic layer deposition and their use as efficient synergistic microwave absorbers, Nano Research 7 (2014) 704-716.

[43] Y.-L. Ren, H.-Y. Wu, M.-M. Lu, Y.-J. Chen, C.-L. Zhu, P. Gao, M.-S. Cao, C.-Y. Li, Q.-Y. Ouyang, Quaternary Nanocomposites Consisting of Graphene, Fe_3O_4@Fe Core@Shell, and ZnO Nanoparticles: Synthesis and Excellent Electromagnetic Absorption Properties, ACS Appl. Mater. Interfaces 4 (2012) 6436-6442.

[44] J. Liang, Y. Xu, D. Sui, L. Zhang, Y. Huang, Y. Ma, F. Li, Y. Chen, Flexible, Magnetic, and Electrically Conductive Graphene/Fe3O4 Paper and Its Application for Magnetic-Controlled Switches, J. Phys. Chem. C 114 (2010) 17465-17471.

[45] J. Su, M. Cao, L. Ren, C. Hu, Fe_3O_4–Graphene Nanocomposites with Improved Lithium Storage and Magnetism Properties, J. Phys. Chem. C 115 (2011) 14469-14477.

[46] E.T. Thostenson, C. Li, T.-W. Chou, Nanocomposites in context, Compos. Sci. Technol. 65 (2005) 491-516.

[47] K. Kalaitzidou, H. Fukushima, L.T. Drzal, A new compounding method for exfoliated graphite–polypropylene nanocomposites with enhanced flexural properties and lower percolation threshold, Compos. Sci. Technol. 67 (2007) 2045-2051.

[48] H. Hu, X. Wang, J. Wang, L. Wan, F. Liu, H. Zheng, R. Chen, C. Xu, Preparation and properties of graphene nanosheets–polystyrene nanocomposites via in situ emulsion polymerization, Chem. Phys. Lett. 484 (2010) 247-253.

[49] J.M. Lee, Y.B. Pyun, J. Yi, J.W. Choung, W.I. Park, ZnO Nanorod−Graphene Hybrid Architectures for Multifunctional Conductors, J. Phys. Chem. C 113 (2009) 19134-19138.

[50] G. Williams, P.V. Kamat, Graphene−Semiconductor Nanocomposites: Excited-State Interactions between ZnO Nanoparticles and Graphene Oxide, Langmuir 25 (2009) 13869-13873.

[51] G. Williams, B. Seger, P.V. Kamat, TiO_2-Graphene Nanocomposites. UV-Assisted Photocatalytic Reduction of Graphene Oxide, ACS Nano 2 (2008) 1487-1491.

[52] D.I. Son, B.W. Kwon, D.H. Park, W.-S. Seo, Y. Yi, B. Angadi, C.-L. Lee, W.K. Choi, Emissive ZnO-graphene quantum dots for white-light-emitting diodes, Nat Nano 7 (2012) 465-471.

[53] G. London, K.-Y. Chen, G.T. Carroll, B.L. Feringa, Towards Dynamic Control of Wettability by Using Functionalized Altitudinal Molecular Motors on Solid Surfaces, Chem. Eur. J. 19 (2013) 10690-10697.

[54] S. Bertazzo, W.F. Zambuzzi, H.A. Da Silva, C.V. Ferreira, C.A. Bertran, Bioactivation of alumina by surface modification: a possibility for improving the applicability of alumina in bone and oral repair, COIR 20 (2009) 288-293.

[55] M. Guo, M. Li, X. Liu, M. Zhao, D. Li, D. Geng, X. Sun, H. Gu, N-containing functional groups induced superior cytocompatible and hemocompatible graphene by NH_2 ion implantation, JMSMM 24 (2013) 2741-2748.

[56] R.A. Buchanan, I.-S. Lee, J.M. Williams, Surface modification of biomaterials through noble metal ion implantation, J. Biomed. Mater. Res. 24 (1990) 309-318.

[57] A.P. Alekhin, G.M. Boleiko, S.A. Gudkova, A.M. Markeev, A.A. Sigarev, V.F. Toknova, A.G. Kirilenko, R.V. Lapshin, E.N. Kozlov, D.V. Tetyukhin, Synthesis of biocompatible surfaces by nanotechnology methods, Nanotechnol Russ 5 (2010) 696-708.

[58] R. Fan, X. Deng, L. Zhou, X. Gao, M. Fan, Y. Wang, G. Guo, Injectable thermosensitive hydrogel composite with surface-functionalized calcium phosphate as raw materials, Int J Nanomedicine 9 (2014) 615-626.

[59] Y. Zhang, L. Zhang, C. Zhou, Review of Chemical Vapor Deposition of Graphene and Related Applications, Acc. Chem. Res. 46 (2013) 2329-2339.

[60] R. Bankras, J. Holleman, J. Schmitz, M. Sturm, A. Zinine, H. Wormeester, B. Poelsema, In Situ Reflective High-Energy Electron Diffraction Analysis During the Initial Stage of a Trimethylaluminum/Water ALD Process, Chem. Vap. Deposition 12 (2006) 275-279.

[61] C.-H. Lin, S. Polisetty, L. O'Brien, A. Baruth, M.A. Hillmyer, C. Leighton, W.L. Gladfelter, Size-Tuned ZnO Nanocrucible Arrays for Magnetic Nanodot Synthesis via Atomic Layer Deposition-Assisted Block Polymer Lithography, ACS Nano 9 (2015) 1379-1387.

[62] K.L. Choy, Chemical vapour deposition of coatings, Prog. Mater Sci. 48 (2003) 57-170.

[63] D.Y. Ryu, K. Shin, E. Drockenmuller, C.J. Hawker, T.P. Russell, A Generalized Approach to the Modification of Solid Surfaces, Science 308 (2005) 236-239.

[64] P.M. Sirimanne, M. Rusop, T. Shirata, T. Soga, T. Jimbo, Characterization of transparent conducting CuI thin films prepared by pulse laser deposition technique, Chem. Phys. Lett. 366 (2002) 485-489.

[65] P.S. Hume, C.N. Bowman, K.S. Anseth, Functionalized PEG hydrogels through reactive dip-coating for the formation of immunoactive barriers, Biomaterials 32 (2011) 6204-6212.

[66] M.E. Nash, W.M. Carroll, P.J. Foley, G. Maguire, C.O. Connell, A.V. Gorelov, S. Beloshapkin, Y.A. Rochev, Ultra-thin spin coated crosslinkable hydrogels for use in cell sheet recovery-synthesis, characterisation to application, Soft Matter 8 (2012) 3889-3899.

[67] A.P. Caricato, S. Capone, M. Epifani, M. Lomascolo, A. Luches, M. Martino, F. Romano, R. Rella, P. Siciliano, J. Spadavecchia, A. Taurino, T. Tunno, D. Valerini, Nanoparticle thin films deposited by MAPLE for sensor applications, in, 2008, pp. 69850H-69850H-69813.

[68] A. Piqué, R.A. McGill, D.B. Chrisey, D. Leonhardt, T.E. Mslna, B.J. Spargo, J.H. Callahan, R.W. Vachet, R. Chung, M.A. Bucaro, Growth of organic thin films by the matrix assisted pulsed laser evaporation (MAPLE) technique, Thin Solid Films 355–356 (1999) 536-541.

[69] A.P. Caricato, V. Arima, M. Catalano, M. Cesaria, P.D. Cozzoli, M. Martino, A. Taurino, R. Rella, R. Scarfiello, T. Tunno, A. Zacheo, MAPLE deposition of nanomaterials, Appl. Surf. Sci. 302 (2014) 92-98.

[70] E. György, A.P.d. Pino, J. Roqueta, B. Ballesteros, A.S. Miguel, C.D. Maycock, A.G. Oliva, Synthesis and Laser Immobilization onto Solid Substrates of CdSe/ZnS Core–Shell Quantum Dots, J. Phys. Chem. C 115 (2011) 15210-15216.

[71] A.P. Caricato, M. Epifani, M. Martino, F. Romano, R. Rella, A. Taurino, T. Tunno, D. Valerini, MAPLE deposition and characterization of SnO_2 colloidal nanoparticle thin films, J. Phys. D: Appl. Phys. 42 (2009) 095105.

[72] Á. Pérez del Pino, E. György, L. Cabana, B. Ballesteros, G. Tobias, Deposition of functionalized single wall carbon nanotubes through matrix assisted pulsed laser evaporation, Carbon 50 (2012) 4450-4458.

[73] P. Ángel Pérez del, G. Enikö, L. Constantin, D. Anca, Study of the deposition of graphene oxide by matrix-assisted pulsed laser evaporation, J. Phys. D: Appl. Phys. 46 (2013) 505309.

[74] A. Pérez del Pino, E. György, C. Logofatu, J. Puigmartí-Luis, W. Gao, Laser-induced chemical transformation of graphene oxide–iron oxide nanoparticles composites deposited on polymer substrates, Carbon 93 (2015) 373-383.

[75] S.M. O'Malley, J. Tomko, A.P.d. Pino, C. Logofatu, E. György, Resonant Infrared and Ultraviolet Matrix-Assisted Pulsed Laser Evaporation of Titanium Oxide/Graphene Oxide Composites: A Comparative Study, J. Phys. Chem. C 118 (2014) 27911-27919.

[76] G. Huang, W.H. Tse, J. Zhang, Deposition of a hydrophilic nanocomposite-based coating on silicone hydrogel through a laser process to minimize UV exposure and bacterial contamination, RSC Adv. 6 (2016) 67166-67172.

Chapter 2

2 Literature review

The magnetic hybrid materials are applied in various fields such as sensors, electronic devices, drug delivery, implant materials, coating materials, etc. The topic which about the fabrication of magnetic hybrid nanocomposite has attracted the interest of researchers in recent years. The magnetic hybrid nanocomposite has been applied in different fields and the methods to form the hybrid nanocomposites on the substrate surface are various. Compared with other methods, it is simple for Matrix Assisted Pulsed Laser Evaporation (MAPLE) method to control the thickness of the nanocomposites film. On the other hand, the MAPLE method can provide protection for the target materials during the deposition process compared with the conventional PLD methods. To fabricate hybrid nanocomposites, the MAPLE method is applied in this study, to overcome the disadvantages of the conventional PLD and other surface modification methods such as spin coating and dip coating. In this study, different nanoparticles were deposited through MAPLE method to fabricate nanocomposites base on the substrates which were applied in this study.

2.1 Magnetic hybrid nanocomposites

Magnetic hybrid nanocomposites or magnetic hybrid nanocomposites are part of hybrid nanocomposites which combine the magnetic nanomaterials with other nanocomposites. The magnetic nanoparticles have been developed by the researchers for decades. This type of nanoparticles has been applied in various fields, such as magnetic resonance imaging (MRI), magnetic data storage, pollution treatment, therapy, biomedicine [1, 2], etc. As the investigations proceeding, some problems of the magnetic nanoparticles emerged. Some of the problems related to the nature of the nanoparticles. The first problem is the long period aggregation which is caused by the high affinity between magnetic nanoparticles. The aggregation problem cause decrease of the superficial area of the nanoparticles which influence the performance of magnetic nanoparticles. In addition, the magnetic

nanoparticles face oxidation problem which could cause degradation or lose magnetism. A series of magnetic hybrid nanocomposites are fabricated to protect the magnetic nanoparticles from aggregation and oxidation. For instance, the magnetic nanoparticles are incorporated with silica nanostructure with different methods and structures such as: embedding magnetic nanoparticles in silica sphere, coating magnetic core with silica shells and grafting magnetic nanoparticles on silica nanochannels [3]. Another type of magnetic hybrid nanocomposites was developed by the researchers to expand the application fields of the magnetic nanoparticles. The magnetic dumbbell nanocomposites and surface modified magnetic nanocomposites are developed to be applied in catalysis, medical imaging, and electronic industry. Compared with other materials which are applied as a matrix of the magnetic hybrid nanocomposites, the two-dimensional nanomaterials hold more superiorities in hybrid materials fabrication. The two-dimensional nanomaterials, especially graphene, possess a lot of functional groups on its surface and the large surface area which are suitable for the nanoparticles to connect with both physical and chemical methods. In addition, as the graphene nanosheets possess excellent mechanical, physical and chemical properties, graphene could protect the magnetic nanoparticles and improve the properties of the magnetic hybrid nanocomposites

2.2 Graphene-based magnetic hybrid nanocomposites

In recent years, graphene nanocomposites have been applied in various fields. There are two main streams of the graphene nanocomposites: organic graphene nanocomposites and inorganic graphene nanocomposites. The organic graphene nanocomposites normally are fabricated by modifying graphene with polymers [4]. Some researchers used graphene to graft polymer conductive properties. Compared with the carbon black and carbon nanofibers, graphene achieves high conduction rate with significant low loading [4]. In addition, the graphene filling materials could give polymer matrix unique mechanical and thermal properties. The mechanical properties of the polymer/graphene composites are remarkable and this type of nanocomposite materials could be applied in various fields [5]. Inorganic graphene nanocomposites normal fabricate through modifying the graphene sheets by inorganic nanoparticles such as ZnO, Fe_2O_3, TiO_2, ZnS and CdS nanoparticles.

The ZnS is known as early studied semiconductors, the ZnS modified graphene nanosheets could have both two advantages of UV-properties and large surface area. The ZnS/graphene nanocomposites could be applied as UV sensors [6].

Magnetic nanomaterials have been applied in the different area of the modern technology: medical treatment [7], multi-model medical imaging [8], pollution control, biomedicine, etc. The properties and advantages of graphene-based magnetic hybrid nanocomposites attracted attention from various fields. Pan et al. [9] fabricated Fe_3O_4/TiO_2/graphene nanocomposites for high-rate lithium storage. The researchers assembled Fe_3O_4 nanoparticles and TiO_2 nanorods on the surface of the graphene nanosheets to increase the conductivity of TiO_2 nanorods. Gu et al. [10] prepared graphene/Fe_3O_4@Au nanocomposites to fabricate magnetic-controlled biosensor. The Au luminescence nanoparticles were deposited on graphene sheets together with magnetic nanoparticles to fabricate high-performance electrochemiluminescence biosensor. Li et al. [11] prepared 3D ordered Fe_3O_4/graphene nanocomposites which could be applied to improve the capacity of the Lithium battery and this nanomaterial could be used as the drug delivery carriers. Lin et al. [12] fabricated graphene-TiO_2-Fe_3O_4 nanomaterials to increase the durability of the photocatalysts. This high stability photo-catalysts is mainly applied on organic dyes decomposition. By varying the nanoparticles which are anchored on the surface of the graphene sheets, these hybrid nanocomposites could achieve different functions and properties.

2.2.1 Graphene

The two-dimensional sp^2-hybridized carbon nanosheets were named graphene. These honeycomb structure nanosheets can act as the building block of other allotropes of carbon. The graphene can be stacked up to form graphite, rolled to make carbon nanotubes and wrapped to become the fullerenes. It became a new exciting research area for the researchers and scientists since Andre Geim and Konstantin Novoselov discovered the single layer graphene nanosheet at 2004 [13]. The honeycomb structure and the long-range π-conjugation give graphene unique electrical [14], thermal [15], optical [16] and mechanical [17] properties. Another unique property is the quantum hall effect. It can be

observed in two-dimensional structure materials. Researchers observed high carrier mobility on graphene at the room temperature [18]. Since graphene holds these extraordinary properties, there are various applications of this material. In medical applications fields, graphene was applied in different processes since it has excellent biocompatibility and mechanical properties. Graphene could be applied as reinforce material for the implant device to increase the mechanical properties [19]. Graphene solution could be used as MRI contrast agents [20]. In electronic field, graphene is an appropriate material for field-effect transistors. Because graphene has high carrier mobility and low noise [21]. Since it possesses transparency and electrical conductivity, graphene can be used to fabricate transparent electrodes which are the critical part of the flexible display devices, organic photovoltaic cells and organic light-emitting diodes [22]. In energy generation [23] and storage field, graphene is a promised material for solar cell fabrication because of the high transparency and high conductivity of graphene. Graphene's large surface area can be used for building high-performance supercapacitor [24] and high-performance batteries which base on graphene electrode [25]. Graphene could be used to fabricate pressure sensors [26], adsorption sensors [27], body sensors [28] and magnetic sensors. As a material with the promising future, graphene could be applied in various areas and different fields. Since it possesses remarkable thermal, mechanical, optical and electronic properties. Graphene materials and graphene devices could reshape the daily life of us.

2.2.2 Synthesis method of graphene

The single layer graphene was obtained by mechanical exfoliation at 2004 [13]. Compared with the solution methods, mechanical exfoliation methods may be simple but inefficiency. Ruoff's group discovered solution method to produce the single layer graphene [29]. In this method, graphene oxide (GO) was first produced by the Hummers' method and the graphene oxide transfer to graphene after a reduction process. Another method is called thermal chemical vapor deposition technique (TCVD). In 2006, Prakash and his coworkers, fabricate few layer graphene through TCVD method on Ni substrate [30]. Another thermal decomposition method fabricates graphene by decomposed the SiC crystal plate on the

surface of Si plate [31]. Some researchers un-zipping the carbon nanotubes to fabricate graphene sheets. The carbon nanotubes were treated by with oxidizers such as (H_2SO_4, $KMnO_4$, and H_2O_2) and reduced by NH_4OH and hydrazine monohydrate ($N_2H_4 \cdot H_2O$) solution [32]. Kim and his coworkers use aluminum sulfide (Al_2S_3) to reduce GO under high-temperature environment [33, 34].

Compared with other methods, chemical synthesis methods is simple for the normal lab to accomplish. The chemical synthesis methods could achieve higher production rate and it is not necessary to introduce the special equipment. Although the mechanical exfoliation is not complicated for a lab without specific equipment to carry out. But the production rate of this method could be low which only enough for fundamental study [35]. In summary, the chemical synthesis methods are easy to perform and hold high production rate, compared with other methods.

2.3 Magnetic nanoparticles

The magnetic nanoparticle is an important type of the nanomaterials. The magnetic nanoparticles have been developed for decades and they have been applied in various fields such as sensors, cancer treatment, drug delivery, solar cells, high-performance batteries, data storage materials, etc. Because magnetic nanoparticles normally are active and easy to aggregate, the modification of the nanoparticles surface or fabrication of hybrid nanocomposites is necessary to improve the stability of the magnetic nanoparticles. The general strategy to protect the magnetic nanoparticles from oxidation and aggregation is coating a non-reactivity layer on the surface of the magnetic core. By fabricating core-shell structure, the magnetic core could be isolated from the corrosive environment. The materials which applied as the shell include to two major types: organic materials (polymer) [36] and inorganic materials (silica) [37]. Another strategy is embedded magnetic nanoparticles in matrix materials such as silica nanorods, silica nanospheres, carbon nanotubes, graphene, etc. The synthesis methods of the magnetic nanoparticles could be divided into different types: co-precipitation, thermal decomposition, and hydrothermal synthesis. For the iron oxides magnetic nanoparticles, the co-precipitation methods are convenient techniques to be applied. The thermal decomposition methods are developed

from the synthesis methods of the oxide semiconductors. Similar methods are used by the researchers to fabricate Fe, Mn, Co, Ni, Cr based nanomaterials with small size and different shapes. The hydrothermal process is one of the most general techniques which are applied in the nanomaterials syntheses. Some researchers fabricated Fe_3O_4 and $CoFe_2O_4$ through the methods based on this mechanism [38]. All of these synthesis methods are developed by the researchers to precisely control the size and shape of synthesized magnetic nanomaterials. The size and shape control of the magnetic nanoparticles are crucial for improving various properties.

2.3.1 The influence of particle size and surface conditions on chemical and physical properties

Magnetism is a normal physical phenomenon which is controlled by the magnetic fields. Magnetism is generated by two different sources: electronic currents and the magnetic moments from the single electron spin. Because the directions of the magnetic fields which are created by the electrons in the materials may not face the same direction, different types of the magnetic properties are generated, such as diamagnetism, paramagnetism, ferromagnetism, antiferromagnetism, ferrimagnetism, and superparamagnetism. Some of the magnetic nanoparticles could achieve superparamagnetism when the diameter of these particles less than 10-20 nm. These nanoparticles would become single magnetic domain and achieve superparamagnetism when the temperature is lower than a critical temperature called blocking temperature.

The two curial parts which influence the chemical and physical properties of the magnetic nanoparticles are particle size and surface conditions. The size of the magnetic nanoparticles is a key factor which influences the physical properties especially magnetic properties. The domain limit and superparamagnetic limit are two most investigated topics in this area. In the large size magnetic nanoparticles, the domain walls separate the uniform magnetization area called domains. There is a critical volume of energy for the domain wall to stay at single-domain state when the size of the nanoparticles reduce. This lead to a critical diameter limit of the nanoparticles to keep single-domain state. The superparamagnetic limit could be reached by overcoming the energy barrier when the

temperature exceeds some critical limits called blocking temperature and the size of the nanoparticles reduced to the critical level. The small size nanoparticles hold large superficial area. This feather could contribute to the chemical process especially catalytic process which occurs on nanoparticles. The surface properties of the magnetic nanoparticles become more important as the surface area of the nanoparticles increasing. In addition, the electron spin from the surface would contribute more to the total magnetic properties of the nanoparticles as the particle size decreasing. For example, the uncoated antiferromagnetic nanoparticles which are influenced by the electron spin from the surface would show weak ferromagnetism at low temperature [39]. The organic and inorganic coatings could influence the nanoparticles magnetic properties since they influence the surface properties.

2.3.2 FeCo nanoparticles

FeCo alloy is famous as it possesses the highest magnetic moment among the magnetic materials. The magnetic moment of FeCo alloy could reach 245 emu/g. Since FeCo alloy possesses these outstanding magnetic properties, FeCo nanoparticles are extremely suitable for applications which high magnetic moment are required. FeCo is a suitable material for fabricating magnetic film which could be used as recording media for data storage devices [40]. FeCo nanoparticles could be applied in the biomedical field. It is a suitable material for magnetic carriers in cells or microorganism separation process [41]. It could be used as magnetic resonance imaging (MRI) contrast agent [42]. However, it is difficult to control the size and composition of the FeCo nanoparticles. Compared with the formation process of the single component nanoparticles, the two components of FeCo nanoparticles have different growth and nucleation mechanism [43]. A lot of researchers try to solve this problem by varying the synthesis methods [44].

2.3.3 YBCO nanoparticles

Yttrium barium copper oxide (YBCO) is a large series of crystalline chemical compounds which display the high-temperature superconductivity properties. YBCO compounds include the first material which was discovered to display superconductivity under a temperature above 77 K (liquid nitrogen boiling temperature). Since April 1986, Yttrium barium copper oxide (YBCO) has been one of the most important fields of the superconductor research [45]. The application of YBCO has two main aspects: first, the YBCO superconductors can be applied in devices of transportation vehicles in the future. The second aspect is the coated conductor application. Since YBCO possess a great potential to be used as the high temperature superconducting coated conductors, it could be applied to fabricate the high magnetic parts including transformers and cables [46]. But it holds a low current density while maintaining superconductivity, the application area is limited. The grain boundary angle of the YBCO is the reason of this problem and this problem could be solved by using the method such as chemical vapor deposition (CVD) [47] or physical vapor deposition (PVD) to produce films [48]. Another method is combining YBCO with another material to align the crystal plane [49].

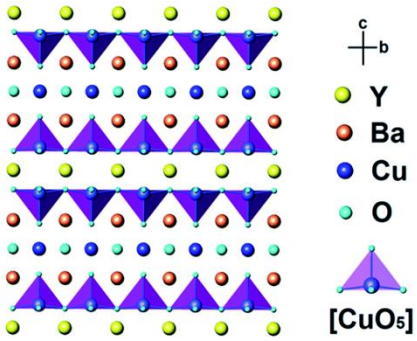

Figure 2.1 Structure of the YBCO [50] Copyright 2017, Royal Society of Chemistry

2.3.4 up-conversion nanoparticles

Up-conversion nanoparticles doped by lanthanide elements possess anti-Stokes emission property. For these nanoparticles, the required pump intensity is lower compared with normal nonlinear optical devices [51]. The word up-conversion stands for a nonlinear optical phenomenon which called anti-Stokes emission process. In this process, a particle

absorbs low-energy photons and emit high-energy photons [52, 53]. For past fifty years, the researchers made enormous progress on developing the application of up-conversion nanoparticles, especially in the bio-application fields. Up-conversion nanoparticles have been widely used in bio-imaging techniques, such as In vitro cell and tissue imaging [54], fluorescence diffuse optical tomography [55] and multimodal imaging [56]. Up-conversion nanoparticles are applied in drug delivery [57] and treatment fields, especially cancer treatments [57]. In normal application field, display devices and energy transfer devices could be fabricated by the up-conversion nanoparticles. In display technique fields, up-conversion could be used to fabricate RGB and white-light output [58]. Similar to other particles which possess optical properties, up-conversion could be applied as fundamental parts of the solar cells [59] and photocatalysts [60].

2.4 Fabrication methods for magnetic hybrid nanocomposites

The magnetic hybrid nanocomposites are developed by the researchers to solve the aggregation and oxidation problem. Some of the magnetic hybrid nanocomposites are produced to combine the magnetic nanoparticles with other nanomaterials. There are two main types of the magnetic hybrid nanocomposites. One is modifying the surface of the magnetic cores such as core-shell nanocomposites and dumbbell nanocomposites. Another one is embedded or anchored the magnetic nanoparticles on the matrices such as silica nanotube or graphene nanosheets. The researchers normally used chemical synthesis methods to fabricate the first type nanostructures. Wu et al. [61] first time fabricated silica shell Fe_3O_4 nanocomposites by depositing silica on the surface of the magnetic nanoparticles. After this, Ying et al. [62] developed the reverse-microemulsion methods to synthesize $Fe_2O_3@SiO_2$ nanoparticles. Su et al. [63] modified the graphene nanosheets with magnetic nanoparticles through hydrothermal methods. Instead of traditional chemical synthesis methods, some of the researchers fabricated magnetic hybrid nanocomposites through surface modification methods. Wu et al. [64] coated Fe_3O_4 the surface of the carbon nanotube and fabricated magnetic hybrid nanocomposites through the sputtering technique. Seo et al. [65] produced FeCo/graphitic shell nanocrystals which could be applied as magnetic-resonance-imaging(MRI) agents through chemical vapor deposition(CVD) technique. Liu et al. prepared FeCo-codoped ZnO nanowires by the CVD

method. These studies proved the possibility to fabricate magnetic hybrid nanocomposites with surface modification techniques.

2.5 Surface modification methods

Surface modification means to modify the surface of the substrate and provide different physical, chemical and biological functions. Using surface modification methods, the properties such as reactivity, surface energy, biocompatibility, and hydrophobicity could be grafted to the substrates' surface. A series of chemical and physical techniques have been developed by the scientists to deposit various materials on the surface of the substrates. There are two main streams of the surface modification method, chemical methods, and physical methods. In physical fields, the methods include dip coating, spin coating, plasma treatment, and physical vapor deposition, etc. In chemical field, the most important method is the layer by layer deposition, surface grafting, and chemical vapor deposition.

2.5.1 Normal deposition methods

Spin coating and dip coating are two important methods which have been widely applied in various fields. Since the procedures of these two methods are simple to perform and these two methods possess advantages such as low-cost and high reproducibility. Spin coating is a method which mainly bases on centrifugal force. The flat substrate is placed in the center on of a rotating plate and the coating materials which could be high viscous liquid are added to the center of the substrate. Due to its requirements for the coating materials, spin coating is widely used in polymer film deposition. Peng and his group member deposited colloidal crystal-polymer nanocomposite film(ETPTA and silica microspheres) on the surface of silicon wafer [66]. These results indicate that high-quality, large area and uniform colloidal crystals macroporous polymers could be fabricated through this method. Chang, et al. [67] deposited Poly(3-hexylthiophene) on the surface of heavily n-doped silicon which is the gate part to fabricate the high mobility transistor. Gang [68] and his lab mate fabricated polymer photovoltaic cells by spin coating technique. Dean et al. [69] investigated the relationships between the spin-coating speed with polymer microstructure and hole mobility. However, the study shows that only 2-5 % of the

materials deposited on the surface of the substrate by spin coating. Meanwhile, around 95 % of the coating materials can't be effectively deposited on the substrate. Most of them are flung off the coating bowl [70].

Dip coating is a low cost, simple surface modification method [71]. The specific procedure of this method is putting the substrate into the liquid form coating materials. After a period of time, the substrate is removed from the liquid and air dried. Lu et al. [72] developed supported cubic and hexagonal mesoporous films through dip-coating method. Duc et al.[73] fabricated graphene-based sponges by sample dip-coating method. The graphene sponges obtained superhydrophobic and superoleophilic properties, after dip-coating treatment. Dong et al. [74] prepared the TiO_2 films by sol-gel dip coating method. The researchers found the particle size and calcination temperature would influence the structural and optical properties. G.G. Valle et al. [75] deposited ZnO: Al films which possess transparency and electric conductivity. These aluminum doped zinc oxide polycrystalline films could be applied as part of the optical electronic devices.

Plasma treatment is a method that normally used for modified the surface properties of hydrogel through oxidation of the materials' surface. After oxidation treatment, the reactive functional groups are grafted on the substrate surface to get hydrophilic properties. The oxidation process could be achieved by glow discharges, radio frequencies [76] and gas arcs. Normal plasma sources are gases such as oxygen, argon, nitrogen, and hydrogen. K.S. Kim et al. [77] modified the polysulfone ultrafiltration membrane surface by oxygen through plasma treatments. The polysulfone ultrafiltration membranes are changed from hydrophobic to hydrophilic after plasma treatments since the new polar functional group introduced. T. Ihara et al. [78] treated the anatase TiO_2 with hydrogen plasma to reduce the TiO_2 and fabricate visible-light-active TiO_2 photo-catalyst which displayed remarkable visible-light activities in the oxidation process for isopropanol and benzoic acid. However, the functional groups which could be added by plasma treatments highly depend on the chemical composition of precursors. This method could cause the aging problem, especially for the target materials which are not stable for long-time treatment [79].

Layer by layer deposition is a wet chemical deposition method which mainly based on the electrostatic interaction between the two layers of materials. Stephan T. Dubas et al. [80] deposited silver nanoparticles on the surface of the silk and nylon fibers. The treated fiber displayed the antimicrobial activity and could be applied to treat waste water and fabricate antimicrobial fabrics. Wei Zhao et al. [81] fabricated multilayer membranes through the layer-by-layer method to fabricate a multilayer glucose biosensor. In this experiment, the researchers deposited poly (diallyl dimethyl ammonium chloride) (PDDA) and poly (sodium 4-styrene sulfonate) (PSS) on the surface of Au electrodes. Following with the deposition of the organic protected Prussian blue nanoparticles and glucose oxidase (GOx) which was negatively charged.

Surface grafting is an approved method to modify the surface of the polymer materials. For the solid materials which fabricated by polymerization, the modification for the end of the polymer chains is necessary [82]. Toru Moro et al. [83] modified the surface of the artificial joints through the surface grafting. By modifying the polyethylene surface with 2-methacryloyloxyethyl phosphorylcholine (MPC), the artificial joints could be protected from periprosthetic osteolysis while this modification reduces the decreasing amount of the materials which were caused by friction and wear. Masahide Taniguchi et al. [84] modified the surface of synthetic membranes to reduce the protein biofouling by UV-assisted surface grafting. By varying the monomer types, the researchers got different hydraulic resistance and wettability due to the different functional groups. Kai Zhang et al. [85] fabricated silica core and polymer shell microspheres through surface grafting and emulsion polymerization. Xiaodong Cao et al. [86] fabricated waterborne polyurethane-cellulose nanocrystal nanocomposites through surface grafting and polymerization. The researchers found that the cellulose nanocrystal obtained a strong interfacial adhesion with waterborne polyurethane. The dispersion, thermal stability, and mechanical properties were strongly improved after surface grafting treatment.

2.5.2 Chemical vapor deposition (CVD)

Chemical vapor deposition (CVD) is a popular chemical process to deposit high-quality solid material films. It is the common method to produce films for the semiconductor

industry. In this technique, normally the substrate materials required to be exposed to the volatile chemical (known as precursors). The precursors would react and deposit on the surface of the substrate to form uniform films. Meanwhile, some volatile by-products would be removed from the reaction chamber by the pumps. Rong Yang et al. [87] fabricated zwitterionic antifouling films with surface-tethered properties through chemical vapor deposition. After this treatment, 30 to 100 nm thickness surface-attached zwitterionic anti-biofouling films could be deposited on the surface of delicate substrates (such as membranes). Hennrik Schmidt et al. [88] explored the electronic transport properties of the MoS_2 film produced by CVD technique. The researchers found this film could obtain low-temperature mobilities and a clear sign of metallic conduction when it reached the high doping densities. Wen Liao et al. [89] prepared Ruthenium films on the surface of the SiO_2 plate through low-temperature chemical vapor deposition. The researchers studied the influence of CO on the nucleation process of Ru. The influence which depends on the different adding time point of CO could be reversed. The CO compounds could help to fabricate uniform and smooth film. Another popular technique which developed from the CVD is atomic layer deposition (ALD). The difference between the CVD and ALD is input sequence of precursors. In ALD process, the precursors are injected into the reaction chamber in separate rounds which are different with CVD process [90]. Chun Haolin et al. [91] prepared size-tuned ZnO nanocrucible arrays through ALD method and block polymer lithography technique. This highly ordered nanocrucible arrays could be applied in various fields. Mato Knez et al. [92] used biological macromolecules as the template for ALD deposition and successfully fabricate metal oxide nanotubes by using tobacco mosaic virus as the template of the ALD deposition. Chih-Yu Chang et al. [93] fabricated high-performance solar cells through low-temperature ALD technique. The resulting devices could gain both air-stability and semi-transparency. However, the disadvantages of CVD and ALD techniques are obvious. CVD and ALD techniques are based on the chemical reaction between the precursor and substrate surface. These processes could be harmful to the structure of the substrate surface. Both CVD and ALD require the precursors to be volatile, good saturation properties and highly reactive. These drawbacks limit the application of CVD and ALD in various fields since not all the target materials could meet these requirements and the highly reactive precursors could harm the environment.

2.5.3 Matrix-assisted pulsed laser evaporation (MAPLE)

The early developed laser assisted surface modification method is pulsed laser deposition (PLD). This method use focusing pulse laser beam to input the energy to the target material inside the vacuum chamber. The molecules of the target material are lifted (vaporized) and transferred to plasma plume. Finally, the target molecules would be deposited on the surface of the substrates and form uniform films. This technique has been used for various materials depositions, such as metals [94], alloys [95] and semiconductors [96]. The basic parts of PLD deposition technique are similar to other deposition technique. But the physical phenomena which happened on the surface of the target are quite complex when the high energy laser beam heats the surface of the target material. The target materials would absorb energy from the laser beam. Because the electronic excitation of the target material, this energy is transferred to thermal energy. Meanwhile, the evaporation and ablation occur and transfer the target materials to plasma. The major disadvantage of the PLD method and some other deposition methods which use high energy source is that the high energy laser beam could destroy the structure of delicate materials such as polymers or organic materials [97]. To overcome this problem, the researchers from the US naval research laboratory invent a new technique called matrix assist pulse laser deposition (MAPLE). The key difference between MAPLE and PLD is that in the PLD method the target materials are direct ablated by the high energy laser but in MAPLE method the target materials are protected by the matrix. The target materials are dissolved in a solvent which is highly volatile and this solution would be frozen by the liquid nitrogen. Most of the laser energy would be absorbed by this matrix and the target material could be protected.

In the MAPLE deposition process, the target material concentration which is dissolved by the solvent normally less than 5 wt. %. The target materials and the substrates are placed in the vacuum chamber and the high energy laser come through the CaF_2 window. There is a special double side wall target holder to place the frozen target solution and maintain target frozen by liquid nitrogen. When the laser heat the surface of the target materials, there is a photo thermal process initiated. The frozen target sublimates and releases the delicate materials into the vacuum chamber [98]. The solvent molecule and delicate

materials could gain momentum through this process and move to the surface of the substrate. Mechanical pumps are applied to remove the solvent molecules which have lower molecular weight and higher vapor pressure compared with target materials' molecules meanwhile the target materials forming the film on substrate's surface. Most of the laser energy transfer to the solvent molecules when the target materials stay intact [99]. In addition, MAPLE provides a better method to control the morphology, homogeneity, and roughness of the film. The thickness of the film could be controlled precisely by alternating the laser fluence and the laser pulse number/frequency. In conclusion, the MAPLE process provides an alternate method to deposit delicate material and protect the chemical structure of that material. By choosing solvent matrix, solution concentration and laser wavelength properly, this method can deposit delicate materials (polymeric, organic and biological materials) on the substrate uniformly and minimize the thermal decomposition.

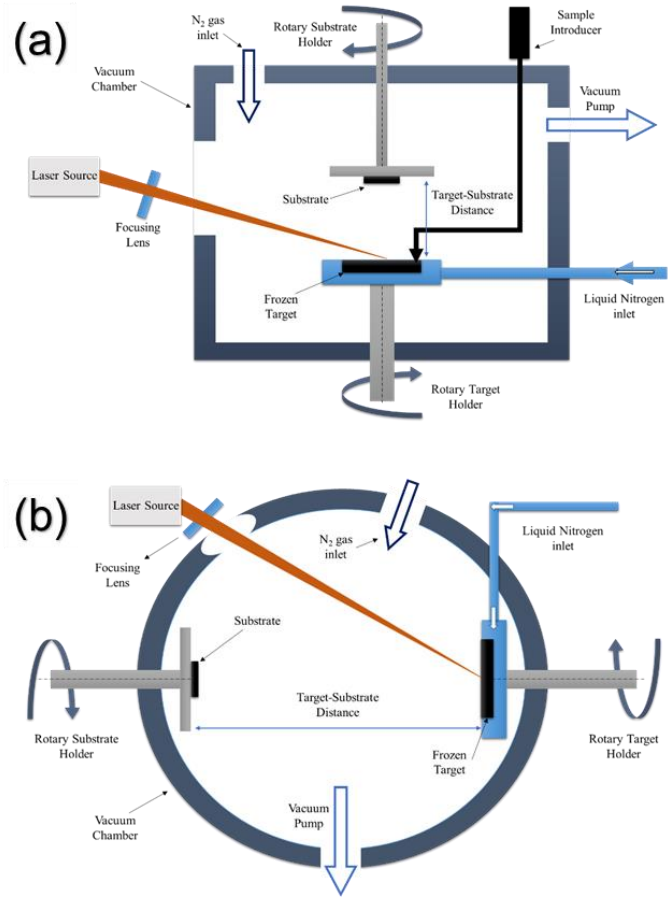

Figure 2.2 Schematic of MAPLE equipment (a) vertical configuration, (b) horizontal configuration

2.6 Our contribution

MAPLE provide a new method to deposit vulnerable material and fabricate uniform films on the surface of the substrate. Various materials have been deposited by the MAPLE process to improve the surface properties and overcome the problems and disadvantages of the substrate materials.

The former researchers have shown that particles and nanoparticles could be deposited by MAPLE method without cause damage and decomposition. Previous studies show that various type of nanoparticles could be fabricated by MAPLE technique. The former works of our group have already demonstrated that it is possible to deposited Ag/PVP nanoparticles and ZnO/PEG nanoparticles on the surface of silicone hydrogels to change the hydrophobicity and graft anti-microbial properties to the substrate.

In this study, FeCo nanoparticles were fabricated by chemical methods and deposited on the substrates (graphene) by MAPLE process and the size of the nanoparticles was dramatically reduced. The YBCO nanoparticles could fabricate through MAPLE process and YBCO/graphene hybrid nanocomposites could be fabricated by this technique. In addition, the up-conversion nanoparticles and protein modified up-conversion nanoparticles were deposited by MAPLE method to study the influence of the MAPLE process on biological materials.

2.7 Summary

Hybrid composites, particularly, two-dimensional hybrid nanocomposites, have been widely applied in various materials and different fields such as electronic devices, solar cells, biological devices, semiconductor devices, LED devices, etc. In the past decade, various techniques were developed to deposit uniform films. Each of them has their own advantages and disadvantages. The CVD methods are not complex for the mass production and industry. However, the precursor properties such as high reactivity and high vaporability limit the application fields of these techniques. Some physical methods like dip coating and spin coating are simple to carry out and could get uniform films. But it is

hard for these methods to control the thickness of the film. The physical vapor deposition techniques could control the thickness of the films properly by varying the energy input and the deposition time. The limitation of these methods is that these methods can't deposit the materials with delicate structure since the direct high energy input leads to the chemical decomposition of the target materials. To overcome these obstructions, MAPLE technique was developed by the researchers to deposit delicate materials such as polymers, organic materials, biological materials, and nanoparticles. There are various factors (solution concentration, substrate-target distance, holder rotate frequency, solvent types, the temperature of substrates, deposition time, laser wavelength, laser energy and laser pulse frequency could be controlled in MAPLE process to achieve better morphological properties and avoid damages to the target materials. MAPLE technique is an appropriate method to deposit delicate materials and fabricate films which need to preserve the structure of the target materials.

2.8 Reference

[1] A.-H. Lu, E.L. Salabas, F. Schüth, Magnetic Nanoparticles: Synthesis, Protection, Functionalization, and Application, Angew. Chem. Int. Ed. 46 (2007) 1222-1244.

[2] A.K. Gupta, M. Gupta, Synthesis and surface engineering of iron oxide nanoparticles for biomedical applications, Biomaterials 26 (2005) 3995-4021.

[3] J. Liu, S.Z. Qiao, Q.H. Hu, G.Q. Lu, Magnetic Nanocomposites with Mesoporous Structures: Synthesis and Applications, Small 7 (2011) 425-443.

[4] P. Steurer, R. Wissert, R. Thomann, R. Mülhaupt, Functionalized Graphenes and Thermoplastic Nanocomposites Based upon Expanded Graphite Oxide, Macromol. Rapid Commun. 30 (2009) 316-327.

[5] Y. Xu, W. Hong, H. Bai, C. Li, G. Shi, Strong and ductile poly(vinyl alcohol)/graphene oxide composite films with a layered structure, Carbon 47 (2009) 3538-3543.

[6] C. Li, D. Jiang, L. Zhang, J. Xia, Q. Li, Controlled Synthesis of ZnS Quantum Dots and ZnS Quantum Flakes with Graphene as a Template, Langmuir 28 (2012) 9729-9734.

[7] S.-W. Cao, Y.-J. Zhu, M.-Y. Ma, L. Li, L. Zhang, Hierarchically Nanostructured Magnetic Hollow Spheres of Fe_3O_4 and γ-Fe_2O_3: Preparation and Potential Application in Drug Delivery, J. Phys. Chem. C 112 (2008) 1851-1856.

[8] K. Park, S. Lee, E. Kang, K. Kim, K. Choi, I.C. Kwon, New Generation of Multifunctional Nanoparticles for Cancer Imaging and Therapy, Adv. Funct. Mater. 19 (2009) 1553-1566.

[9] L. Pan, X.-D. Zhu, X.-M. Xie, Y.-T. Liu, Smart Hybridization of TiO_2 Nanorods and Fe_3O_4 Nanoparticles with Pristine Graphene Nanosheets: Hierarchically Nanoengineered Ternary Heterostructures for High-Rate Lithium Storage, Adv. Funct. Mater. 25 (2015) 3341-3350.

[10] W. Gu, X. Deng, X. Gu, X. Jia, B. Lou, X. Zhang, J. Li, E. Wang, Stabilized, Superparamagnetic Functionalized Graphene/Fe3O4@Au Nanocomposites for a Magnetically-Controlled Solid-State Electrochemiluminescence Biosensing Application, Anal. Chem. 87 (2015) 1876-1881.

[11] X. Li, X. Huang, D. Liu, X. Wang, S. Song, L. Zhou, H. Zhang, Synthesis of 3D Hierarchical Fe_3O_4/Graphene Composites with High Lithium Storage Capacity and for Controlled Drug Delivery, J. Phys. Chem. C 115 (2011) 21567-21573.

[12] Y. Lin, Z. Geng, H. Cai, L. Ma, J. Chen, J. Zeng, N. Pan, X. Wang, Ternary Graphene–TiO_2–Fe_3O_4 Nanocomposite as a Recollectable Photocatalyst with Enhanced Durability, Eur. J. Inorg. Chem. 2012 (2012) 4439-4444.

[13] K.S. Novoselov, A.K. Geim, S.V. Morozov, D. Jiang, Y. Zhang, S.V. Dubonos, I.V. Grigorieva, A.A. Firsov, Electric Field Effect in Atomically Thin Carbon Films, Science 306 (2004) 666-669.

[14] A.H. Castro Neto, F. Guinea, N.M.R. Peres, K.S. Novoselov, A.K. Geim, The electronic properties of graphene, RvMP 81 (2009) 109-162.

[15] C. Yu, L. Shi, Z. Yao, D. Li, A. Majumdar, Thermal Conductance and Thermopower of an Individual Single-Wall Carbon Nanotube, Nano Lett. 5 (2005) 1842-1846.

[16] F. Wang, Y. Zhang, C. Tian, C. Girit, A. Zettl, M. Crommie, Y.R. Shen, Gate-Variable Optical Transitions in Graphene, Science 320 (2008) 206-209.

[17] C. Lee, X. Wei, J.W. Kysar, J. Hone, Measurement of the Elastic Properties and Intrinsic Strength of Monolayer Graphene, Science 321 (2008) 385-388.

[18] K.S. Novoselov, A.K. Geim, S.V. Morozov, D. Jiang, M.I. Katsnelson, I.V. Grigorieva, S.V. Dubonos, A.A. Firsov, Two-dimensional gas of massless Dirac fermions in graphene, Nature 438 (2005) 197-200.

[19] G. Lalwani, A.M. Henslee, B. Farshid, L. Lin, F.K. Kasper, Y.-X. Qin, A.G. Mikos, B. Sitharaman, Two-Dimensional Nanostructure-Reinforced Biodegradable Polymeric Nanocomposites for Bone Tissue Engineering, Biomacromolecules 14 (2013) 900-909.

[20] S. Kanakia, J.D. Toussaint, S.M. Chowdhury, G. Lalwani, T. Tembulkar, T. Button, K.R. Shroyer, W. Moore, B. Sitharaman, Physicochemical characterization of a novel graphene-based magnetic resonance imaging contrast agent, Int J Nanomedicine 8 (2013) 2821-2833.

[21] J.H. Chen, M. Ishigami, C. Jang, D.R. Hines, M.S. Fuhrer, E.D. Williams, Printed Graphene Circuits, Adv. Mater. 19 (2007) 3623-3627.

[22] Large area, continuous, few-layered graphene as anodes in organic photovoltaic devices, Appl. Phys. Lett. 95 (2009) 063302.

[23] R.R. Nair, H.A. Wu, P.N. Jayaram, I.V. Grigorieva, A.K. Geim, Unimpeded Permeation of Water Through Helium-Leak–Tight Graphene-Based Membranes, Science 335 (2012) 442-444.

[24] M.D. Stoller, S. Park, Y. Zhu, J. An, R.S. Ruoff, Graphene-Based Ultracapacitors, Nano Lett. 8 (2008) 3498-3502.

[25] L. David, R. Bhandavat, G. Kulkarni, S. Pahwa, Z. Zhong, G. Singh, Synthesis of Graphene Films by Rapid Heating and Quenching at Ambient Pressures and Their Electrochemical Characterization, ACS Appl. Mater. Interfaces 5 (2013) 546-552.

[26] In-plane and tunneling pressure sensors based on graphene/hexagonal boron nitride heterostructures, Appl. Phys. Lett. 99 (2011) 133109.

[27] Y. Dan, Y. Lu, N.J. Kybert, Z. Luo, A.T.C. Johnson, Intrinsic Response of Graphene Vapor Sensors, Nano Lett. 9 (2009) 1472-1475.

[28] X. Li, T. Yang, Y. Yang, J. Zhu, L. Li, F.E. Alam, X. Li, K. Wang, H. Cheng, C.-T. Lin, Y. Fang, H. Zhu, Large-Area Ultrathin Graphene Films by Single-Step Marangoni Self-Assembly for Highly Sensitive Strain Sensing Application, Adv. Funct. Mater. 26 (2016) 1322-1329.

[29] S. Stankovich, D.A. Dikin, G.H.B. Dommett, K.M. Kohlhaas, E.J. Zimney, E.A. Stach, R.D. Piner, S.T. Nguyen, R.S. Ruoff, Graphene-based composite materials, Nature 442 (2006) 282-286.

[30] P.R. Somani, S.P. Somani, M. Umeno, Planer nano-graphenes from camphor by CVD, Chem. Phys. Lett. 430 (2006) 56-59.
[31] Z.-S. Wu, W. Ren, L. Gao, B. Liu, C. Jiang, H.-M. Cheng, Synthesis of high-quality graphene with a pre-determined number of layers, Carbon 47 (2009) 493-499.
[32] D.V. Kosynkin, A.L. Higginbotham, A. Sinitskii, J.R. Lomeda, A. Dimiev, B.K. Price, J.M. Tour, Longitudinal unzipping of carbon nanotubes to form graphene nanoribbons, Nature 458 (2009) 872-876.
[33] C.-D. Kim, B.-K. Min, W.-S. Jung, Preparation of graphene sheets by the reduction of carbon monoxide, Carbon 47 (2009) 1610-1612.
[34] J. Liang, Y. Huang, L. Zhang, Y. Wang, Y. Ma, T. Guo, Y. Chen, Molecular-Level Dispersion of Graphene into Poly(vinyl alcohol) and Effective Reinforcement of their Nanocomposites, Adv. Funct. Mater. 19 (2009) 2297-2302.
[35] S. Park, R.S. Ruoff, Chemical methods for the production of graphenes, Nat Nano 4 (2009) 217-224.
[36] L.E. Euliss, S.G. Grancharov, S. O'Brien, T.J. Deming, G.D. Stucky, C.B. Murray, G.A. Held, Cooperative Assembly of Magnetic Nanoparticles and Block Copolypeptides in Aqueous Media, Nano Lett. 3 (2003) 1489-1493.
[37] Y. Kobayashi, M. Horie, M. Konno, B. Rodríguez-González, L.M. Liz-Marzán, Preparation and Properties of Silica-Coated Cobalt Nanoparticles, J. Phys. Chem. B 107 (2003) 7420-7425.
[38] X. Wang, J. Zhuang, Q. Peng, Y. Li, A general strategy for nanocrystal synthesis, Nature 437 (2005) 121-124.
[39] W.S. Seo, H.H. Jo, K. Lee, B. Kim, S.J. Oh, J.T. Park, Size-Dependent Magnetic Properties of Colloidal Mn3O4 and MnO Nanoparticles, Angew. Chem. Int. Ed. 43 (2004) 1115-1117.
[40] R.S. Sundar, S.C. Deevi, Soft magnetic FeCo alloys: alloy development, processing, and properties, Int. Mater. Rev. 50 (2005) 157-192.
[41] A. Hütten, D. Sudfeld, I. Ennen, G. Reiss, K. Wojczykowski, P. Jutzi, Ferromagnetic FeCo nanoparticles for biotechnology, J. Magn. Magn. Mater. 293 (2005) 93-101.
[42] B. Silke, B. Helmut, M. Nina, G. Angelika, D. Eckhard, H. Wilhelm, B. Jens, Z. Svetlana, P. Natalie, H. Josef, M. Hartwig, B. Stephan, K. Volker, Surface engineering of

Co and FeCo nanoparticles for biomedical application, J. Phys.: Condens. Matter 18 (2006) S2543.

[43] N.O. Núñez, P. Tartaj, M.P. Morales, P. Bonville, C.J. Serna, Yttria-Coated FeCo Magnetic Nanoneedles, Chem. Mater. 16 (2004) 3119-3124.

[44] C. Desvaux, C. Amiens, P. Fejes, P. Renaud, M. Respaud, P. Lecante, E. Snoeck, B. Chaudret, Multimillimetre-large superlattices of air-stable iron-cobalt nanoparticles, Nat Mater 4 (2005) 750-753.

[45] M.K. Wu, J.R. Ashburn, C.J. Torng, P.H. Hor, R.L. Meng, L. Gao, Z.J. Huang, Y.Q. Wang, C.W. Chu, Superconductivity at 93 K in a new mixed-phase Y-Ba-Cu-O compound system at ambient pressure, Phys. Rev. Lett. 58 (1987) 908-910.

[46] V. Narayanan, I. Van Driessche, Aqueous chemical solution deposition of lanthanum zirconate and related lattice-matched single buffer layers suitable for YBCO coated conductors: A review, Prog. Solid State Chem. 40 (2012) 57-77.

[47] L. Montero, G. Gabriel, A. Guimerà, R. Villa, K.K. Gleason, S. Borrós, Increasing biosensor response through hydrogel thin film deposition: Influence of hydrogel thickness, Vacuum 86 (2012) 2102-2104.

[48] Pulsed laser deposition of thick $YBa_2Cu_3O_{7-\delta}$ films with $J_c \geq 1$ MA/cm^2, Appl. Phys. Lett. 63 (1993) 1848-1850.

[49] H.-S. Shin, K.-H. Kim, J.R.C. Dizon, T.-Y. Kim, R.-K. Ko, S.-S. Oh, The strain effect on critical current in YBCO coated conductors with different stabilizing layers, Supercond. Sci. Technol. 18 (2005) S364.

[50] C.S. Lim, L. Wang, C.K. Chua, Z. Sofer, O. Jankovsky, M. Pumera, High temperature superconducting materials as bi-functional catalysts for hydrogen evolution and oxygen reduction, J. Mater. Chem. A 3 (2015) 8346-8352.

[51] B. Zhou, B. Shi, D. Jin, X. Liu, Controlling upconversion nanocrystals for emerging applications, Nat Nano 10 (2015) 924-936.

[52] F. Auzel, Upconversion and Anti-Stokes Processes with f and d Ions in Solids, Chem. Rev. 104 (2004) 139-174.

[53] M. Haase, H. Schäfer, Upconverting Nanoparticles, Angew. Chem. Int. Ed. 50 (2011) 5808-5829.

[54] H.J.M.A.A. Zijlmans, J. Bonnet, J. Burton, K. Kardos, T. Vail, R.S. Niedbala, H.J. Tanke, Detection of Cell and Tissue Surface Antigens Using Up-Converting Phosphors: A New Reporter Technology, Anal. Biochem. 267 (1999) 30-36.

[55] D.J. Gargas, E.M. Chan, A.D. Ostrowski, S. Aloni, M.V.P. Altoe, E.S. Barnard, B. Sanii, J.J. Urban, D.J. Milliron, B.E. Cohen, P.J. Schuck, Engineering bright sub-10-nm upconverting nanocrystals for single-molecule imaging, Nat Nano 9 (2014) 300-305.

[56] Y. Yang, Y. Sun, T. Cao, J. Peng, Y. Liu, Y. Wu, W. Feng, Y. Zhang, F. Li, Hydrothermal synthesis of $NaLuF_4$:153Sm,Yb,Tm nanoparticles and their application in dual-modality upconversion luminescence and SPECT bioimaging, Biomaterials 34 (2013) 774-783.

[57] Y. Yang, B. Velmurugan, X. Liu, B. Xing, NIR Photoresponsive Crosslinked Upconverting Nanocarriers Toward Selective Intracellular Drug Release, Small 9 (2013) 2937-2944.

[58] S. Sivakumar, F.C.J.M. van Veggel, M. Raudsepp, Bright White Light through Up-Conversion of a Single NIR Source from Sol−Gel-Derived Thin Film Made with Ln^{3+}-Doped LaF_3 Nanoparticles, J. Am. Chem. Soc. 127 (2005) 12464-12465.

[59] Z.Q. Li, X.D. Li, Q.Q. Liu, X.H. Chen, Z. Sun, C. Liu, X.J. Ye, S.M. Huang, Core/shell structured $NaYF_4$:Yb^{3+} /Er^{3+} /Gd^{3+} nanorods with Au nanoparticles or shells for flexible amorphous silicon solar cells, Nanotechnology 23 (2012) 025402.

[60] S. Obregón, A. Kubacka, M. Fernández-García, G. Colón, High-performance Er3+–TiO2 system: Dual up-conversion and electronic role of the lanthanide, J. Catal. 299 (2013) 298-306.

[61] P. Wu, J. Zhu, Z. Xu, Template-Assisted Synthesis of Mesoporous Magnetic Nanocomposite Particles, Adv. Funct. Mater. 14 (2004) 345-351.

[62] D.K. Yi, S.S. Lee, G.C. Papaefthymiou, J.Y. Ying, Nanoparticle Architectures Templated by SiO2/Fe2O3 Nanocomposites, Chem. Mater. 18 (2006) 614-619.

[63] J. Su, M. Cao, L. Ren, C. Hu, Fe_3O_4–Graphene Nanocomposites with Improved Lithium Storage and Magnetism Properties, J. Phys. Chem. C 115 (2011) 14469-14477.

[64] Y. Wu, Y. Wei, J. Wang, K. Jiang, S. Fan, Conformal Fe3O4 Sheath on Aligned Carbon Nanotube Scaffolds as High-Performance Anodes for Lithium Ion Batteries, Nano Lett. 13 (2013) 818-823.

[65] W.S. Seo, J.H. Lee, X. Sun, Y. Suzuki, D. Mann, Z. Liu, M. Terashima, P.C. Yang, M.V. McConnell, D.G. Nishimura, H. Dai, FeCo/graphitic-shell nanocrystals as advanced magnetic-resonance-imaging and near-infrared agents, Nat Mater 5 (2006) 971-976.

[66] P. Jiang, M.J. McFarland, Large-Scale Fabrication of Wafer-Size Colloidal Crystals, Macroporous Polymers and Nanocomposites by Spin-Coating, J. Am. Chem. Soc. 126 (2004) 13778-13786.

[67] J.-F. Chang, B. Sun, D.W. Breiby, M.M. Nielsen, T.I. Sölling, M. Giles, I. McCulloch, H. Sirringhaus, Enhanced Mobility of Poly(3-hexylthiophene) Transistors by Spin-Coating from High-Boiling-Point Solvents, Chem. Mater. 16 (2004) 4772-4776.

[68] G. Li, V. Shrotriya, J. Huang, Y. Yao, T. Moriarty, K. Emery, Y. Yang, High-efficiency solution processable polymer photovoltaic cells by self-organization of polymer blends, Nat Mater 4 (2005) 864-868.

[69] D.M. DeLongchamp, B.M. Vogel, Y. Jung, M.C. Gurau, C.A. Richter, O.A. Kirillov, J. Obrzut, D.A. Fischer, S. Sambasivan, L.J. Richter, E.K. Lin, Variations in Semiconducting Polymer Microstructure and Hole Mobility with Spin-Coating Speed, Chem. Mater. 17 (2005) 5610-5612.

[70] N. Sahu, B. Parija, S. Panigrahi, Fundamental understanding and modeling of spin coating process: A review, Indian Journal of Physics 83 (2009) 493-502.

[71] Z. Yue, X. Liu, P.J. Molino, G.G. Wallace, Bio-functionalisation of polydimethylsiloxane with hyaluronic acid and hyaluronic acid – Collagen conjugate for neural interfacing, Biomaterials 32 (2011) 4714-4724.

[72] Y. Lu, R. Ganguli, C.A. Drewien, M.T. Anderson, C.J. Brinker, W. Gong, Y. Guo, H. Soyez, B. Dunn, M.H. Huang, J.I. Zink, Continuous formation of supported cubic and hexagonal mesoporous films by sol-gel dip-coating, Nature 389 (1997) 364-368.

[73] D.D. Nguyen, N.-H. Tai, S.-B. Lee, W.-S. Kuo, Superhydrophobic and superoleophilic properties of graphene-based sponges fabricated using a facile dip coating method, Energy Environ. Sci. 5 (2012) 7908-7912.

[74] D.J. Kim, S.H. Hahn, S.H. Oh, E.J. Kim, Influence of calcination temperature on structural and optical properties of TiO2 thin films prepared by sol–gel dip coating, Mater. Lett. 57 (2002) 355-360.

[75] G.G. Valle, P. Hammer, S.H. Pulcinelli, C.V. Santilli, Transparent and conductive ZnO:Al thin films prepared by sol-gel dip-coating, J. Eur. Ceram. Soc. 24 (2004) 1009-1013.

[76] Y. Wang, X. Qian, X. Zhang, W. Xia, L. Zhong, Z. Sun, J. Xia, Plasma Surface Modification of Rigid Contact Lenses Decreases Bacterial Adhesion, Eye Contact Lens 39 (2013) 376-380.

[77] K.S. Kim, K.H. Lee, K. Cho, C.E. Park, Surface modification of polysulfone ultrafiltration membrane by oxygen plasma treatment, J. Membr. Sci. 199 (2002) 135-145.

[78] T. Ihara, M. Miyoshi, M. Ando, S. Sugihara, Y. Iriyama, Preparation of a visible-light-active TiO2 photocatalyst by RF plasma treatment, JMatS 36 (2001) 4201-4207.

[79] D. Hegemann, H. Brunner, C. Oehr, Plasma treatment of polymers for surface and adhesion improvement, Nuclear Instruments and Methods in Physics Research Section B: Beam Interactions with Materials and Atoms 208 (2003) 281-286.

[80] S.T. Dubas, P. Kumlangdudsana, P. Potiyaraj, Layer-by-layer deposition of antimicrobial silver nanoparticles on textile fibers, Colloids Surf. Physicochem. Eng. Aspects 289 (2006) 105-109.

[81] W. Zhao, J.-J. Xu, C.-G. Shi, H.-Y. Chen, Multilayer Membranes via Layer-by-Layer Deposition of Organic Polymer Protected Prussian Blue Nanoparticles and Glucose Oxidase for Glucose Biosensing, Langmuir 21 (2005) 9630-9634.

[82] M. Stamm, Polymer surfaces and interfaces, Polymer Surfaces and Interfaces: Characterization, Modification and Applications, ISBN 978-3-540-73864-0. Springer Berlin Heidelberg 1 (2008).

[83] T. Moro, Y. Takatori, K. Ishihara, T. Konno, Y. Takigawa, T. Matsushita, U.-i. Chung, K. Nakamura, H. Kawaguchi, Surface grafting of artificial joints with a biocompatible polymer for preventing periprosthetic osteolysis, Nat Mater 3 (2004) 829-836.

[84] M. Taniguchi, G. Belfort, Low protein fouling synthetic membranes by UV-assisted surface grafting modification: varying monomer type, J. Membr. Sci. 231 (2004) 147-157.

[85] K. Zhang, H. Chen, X. Chen, Z. Chen, Z. Cui, B. Yang, Monodisperse Silica-Polymer Core-Shell Microspheres via Surface Grafting and Emulsion Polymerization, Macromol Mater Eng 288 (2003) 380-385.

[86] X. Cao, Y. Habibi, L.A. Lucia, One-pot polymerization, surface grafting, and processing of waterborne polyurethane-cellulose nanocrystal nanocomposites, J. Mater. Chem. 19 (2009) 7137-7145.

[87] R. Yang, J. Xu, G. Ozaydin-Ince, S.Y. Wong, K.K. Gleason, Surface-Tethered Zwitterionic Ultrathin Antifouling Coatings on Reverse Osmosis Membranes by Initiated Chemical Vapor Deposition, Chem. Mater. 23 (2011) 1263-1272.

[88] H. Schmidt, S. Wang, L. Chu, M. Toh, R. Kumar, W. Zhao, A.H. Castro Neto, J. Martin, S. Adam, B. Özyilmaz, G. Eda, Transport Properties of Monolayer MoS_2 Grown by Chemical Vapor Deposition, Nano Lett. 14 (2014) 1909-1913.

[89] W. Liao, J.G. Ekerdt, Effect of CO on Ru Nucleation and Ultra-Smooth Thin Film Growth by Chemical Vapor Deposition at Low Temperature, Chem. Mater. 25 (2013) 1793-1799.

[90] N.P. Dasgupta, H.-B.-R. Lee, S.F. Bent, P.S. Weiss, Recent Advances in Atomic Layer Deposition, Chem. Mater. 28 (2016) 1943-1947.

[91] C.-H. Lin, S. Polisetty, L. O'Brien, A. Baruth, M.A. Hillmyer, C. Leighton, W.L. Gladfelter, Size-Tuned ZnO Nanocrucible Arrays for Magnetic Nanodot Synthesis via Atomic Layer Deposition-Assisted Block Polymer Lithography, ACS Nano 9 (2015) 1379-1387.

[92] M. Knez, A. Kadri, C. Wege, U. Gösele, H. Jeske, K. Nielsch, Atomic Layer Deposition on Biological Macromolecules: Metal Oxide Coating of Tobacco Mosaic Virus and Ferritin, Nano Lett. 6 (2006) 1172-1177.

[93] C.-Y. Chang, K.-T. Lee, W.-K. Huang, H.-Y. Siao, Y.-C. Chang, High-Performance, Air-Stable, Low-Temperature Processed Semitransparent Perovskite Solar Cells Enabled by Atomic Layer Deposition, Chem. Mater. 27 (2015) 5122-5130.

[94] J.M. Lackner, W. Waldhauser, T. Schöberl, Film growth phenomena in high-energetic room temperature pulsed laser deposition on polymer surfaces, Surf. Coat. Technol. 201 (2006) 4037-4039.

[95] A.P. Caricato, M. Fernández, Z. Frait, D. Fraitova, S. Luby, A. Luches, E. Majkova, G. Majni, R. Malych, P. Mengucci, Pulsed laser deposition of magnetic films by ablation of Co- and Fe-based amorphous alloys, Applied Physics A 79 (2004) 1251-1254.

[96] A.P. Caricato, G. Leggieri, A. Luches, F. Romano, G. Barucca, P. Mengucci, S.A. Mulenko, Morphological and structural characterizations of CrSi2 nanometric films deposited by laser ablation, Appl. Surf. Sci. 254 (2007) 1224-1227.
[97] A.P. Caricato, A. Luches, Applications of the matrix-assisted pulsed laser evaporation method for the deposition of organic, biological and nanoparticle thin films: a review, Applied Physics A 105 (2011) 565-582.
[98] A.P. Caricato, S. Capone, M. Epifani, M. Lomascolo, A. Luches, M. Martino, F. Romano, R. Rella, P. Siciliano, J. Spadavecchia, A. Taurino, T. Tunno, D. Valerini, Nanoparticle thin films deposited by MAPLE for sensor applications, in, 2008, pp. 69850H-69850H-69813.
[99] A.P. Caricato, A. Luches, G. Leggieri, M. Martino, R. Rella, Matrix-assisted pulsed laser deposition of polymer and nanoparticle films, Vacuum 86 (2012) 661-666.

Chapter 3

3 Experimental

In this chapter, the experiment details of this project are introduced: (1) the synthesis processes of graphene nanosheets, (2) the synthesis processes of FeCo nanoparticles, (3) the synthesis processes of up-conversion nanoparticles and modification of protein on up-conversion nanoparticles' surface, (4) deposition process of nanoparticles by MAPLE, (5) characterization methods.

3.1 Synthesis of graphite oxide

The preparation methods of graphene oxide (Figure 3.1) was based on this two references [1, 2]. In the first step, the graphite flakes were pre-oxidized by the oxidizing solution. The oxidizing solution was prepared by adding 10 g of phosphorus pentoxide and 10 g of potassium persulfate into 30 ml concentrated sulfuric acid (95 - 98 %). After this, 20 g of graphite flakes were added into the oxidizing solution. The oxidization process was continued under stirring at 80 °C for 6 hours. After the oxidization process finished, the mixture was diluted with water, filtered and washed until pH became neutral. The pre-oxidized graphite flakes were dried in air at room temperature.

The graphite oxide was treated according to the Hummers method [2]. 10 g of pre-oxidized graphite flakes were added into 230 mL cold concentrated sulfuric acid (95 - 98 %) in the ice-water bath. Then 30 g $KMnO_4$ was added gently with stirring. The ice-water bath was added to keep the temperature of the mixture below 20 °C. After this step, the mixture was stirred at 35 °C for 2 hours. The mixture was diluted with 1,500 mL water. To terminate the reaction, 25 mL H_2O_2 (30 wt. %) was added and the color of the mixture changed into bright yellow. Since the metal ions need to be removed, the graphite oxide was filtered and washed with 2,500 mL diluted HCl (3.7 %). The product which was got from this step was dried in air at room temperature. The graphite oxide was suspended in water to prepare a viscous, brown 2 wt. % dispersion and put to dialysis, for further removing of metal ions

and acids. For the using of following experiments, purified graphite oxide suspension was diluted into a 0.05 wt. % dispersion

3.2 Preparation of graphene nanosheets

Graphene nanosheets were prepared by this reference [3]. To prepare graphene oxide, the 0.05 wt. % graphite oxide dispersion was treated by ultra-sonication exfoliation for 30 minutes. To remove unexfoliated graphite oxide, the dispersion was centrifuged at 3,000 rpm for 30 minutes. The following procedures were used to achieve chemical conversion from graphene oxide to graphene nanosheets. 5 mL graphene oxide dispersion was mixed with 5 mL water in 20 ml glass vial. Then, 5 µL hydrazine solution (35 wt. %) and 35 µL ammonium hydroxide solution (28.0-30.0 wt. %) were added. To achieve mixing, the vial was shaken vigorously for 3 minutes. To protect the product, 2 mL paraffin oil was added gently to cover the liquid surface. The vial was put in the water bath of 95 °C for 1 hour. Dialysis was applied to remove excess impurities.

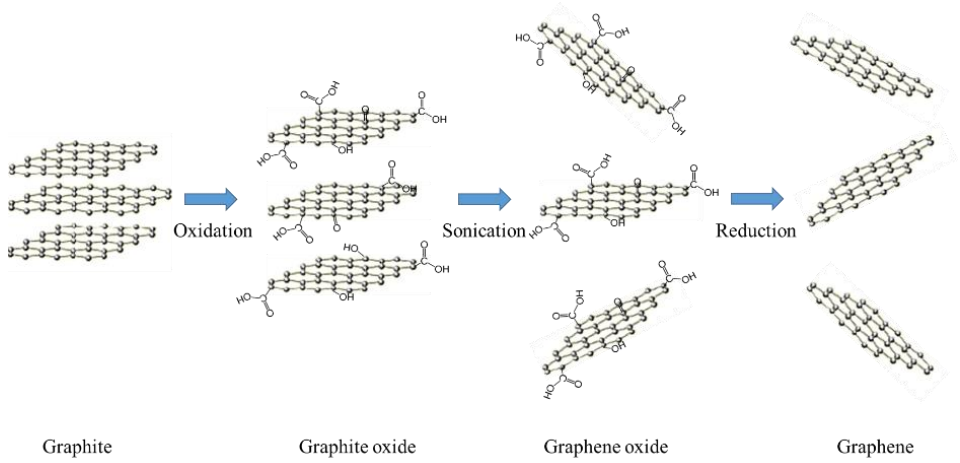

Figure 3.1 Schematic of graphene fabrication process

3.3 Synthesis of FeCo nanoparticles

The FeCo nanoparticles were synthesized base on this reference [4]. The metal ions were reduced through polyol process (Figure 3.2). Ferrous chloride tetrahydrate 0.0025 mol, cobaltous acetate tetrahydrate 0.0025 mol, and sodium hydroxide 0.2 mol was dissolved in 100 ml ethylene glycol. The dispersion was added to a 3-neck round bottom flask and

stirred for around 15 min to make the chemicals completely dissolve. Meanwhile, the nitrogen gas was added to remove the oxygen in the ethylene glycol. The solution was heated to 130 °C and refluxed for one hour at this temperature. To terminate the reaction, the system was cooled down to room temperature. The products were collected and washed with ethanol for three times. The FeCo nanoparticles powder was dried by freeze dryer.

$$2CH_2OH{-}CH_2OH \rightarrow 2CH_3CHO + 2H_2O$$

$$2CH_3CHO + M(OH)_2 \rightarrow CH_3COCOCH_3 + 2H_2O + M^0$$

M : Metal species (Fe, Co)

Figure 3.2 Schematic of polyol reduction process[5]

3.4 Synthesis of up-conversion nanoparticles

The synthesis of up-conversion nanoparticles was based on this reference [6]. 720 mg of gadolinium (III) nitrate hexahydrate, 170 mg of erbium (III) nitrate pentahydrate and 160 mg of ytterbium (III) nitrate pentahydrate were added in 20 ml ethylene glycol. The magnetic stirrer was applied to guarantee proper mixing of the solutes. 0.7 g of branched polyethyleneimine (PEI) was gently added to achieve proper dissolving.

336 mg sodium fluoride was dissolved in 10 ml ethylene glycol and added into dispersion dropwise. Then the dispersion was heated to 200 °C and refluxed for 6 hours. During the reaction process, nitrogen protection was applied. The products were collected by centrifugation and washed three times with ethanol and water. To collect dry powder of nanoparticles, the products were dissolved in 10 ml ethanol and placed in a 37 °C incubator for 12 hours.

3.5 Fabrication of protein modified up-conversion nanoparticles

The conjugation process was based on following reference [7]. 10 mg of up-conversion nanoparticles powder was dissolved in 5 ml distilled water. After this, 100 mg of Bovine serum albumin (BSA) was added to the dispersion. Then, 5 mg of 1-Ethyl-3-(3-dimethyl

aminopropyl) carbodiimide (EDC) was added into the solution. The solution was stirred vigorously at room temperature for 2 hours. Afterwards, another 5 mg of EDC was added to the solution. The solution was stirred for 6 hours at ambient temperature. The obtained BSA modified up-conversion nanoparticles were isolated by centrifugation. The products were re-dispersed in distilled water and stored at 4 °C.

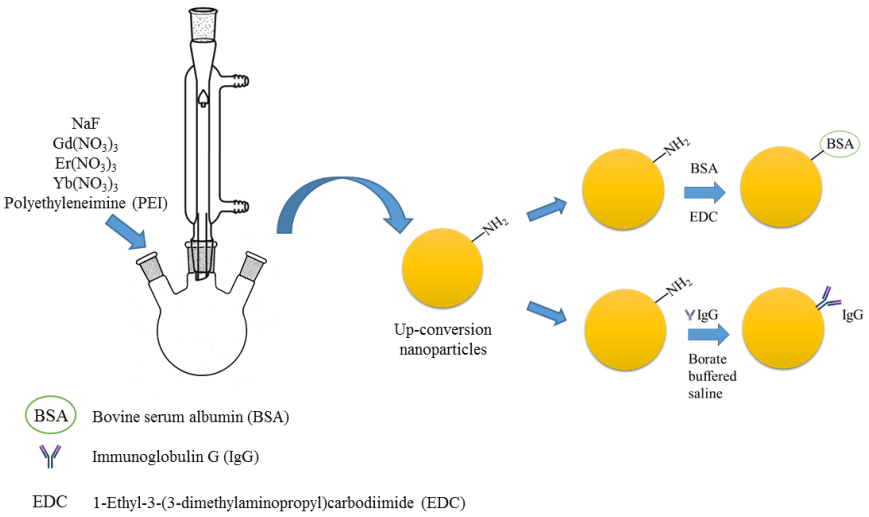

Figure 3.3 Schematic of fabrication and modification process of up-conversion nanoparticles

3.6 Deposition process of nanoparticles by MAPLE

The deposition process was finished by MAPLE equipment (PVD Products, Inc., USA). 2-propanol (isopropanol) was applied as the solvent for MAPLE deposition experiment. The solution was prepared by dispersing target nanoparticles in isopropanol with a concentration at 1 wt. %. The nanoparticles' solution was sonicated for around 5-10 minutes before deposition to achieve uniform dispersion. No other additional additives and surfactants were used or added in the target solution. Before the deposition process started, the target solution was added into the target holder and froze by the liquid nitrogen.

The laser source for these experiments was Nd:YAG laser (secondary harmonic, wavelength 532 nm). Laser frequency was 10 Hz and the $\tau_{fwhm} \cong 200$ μs. The laser spot area was around 0.63 cm^2. The laser fluence was different in three nanoparticle deposition experiments. Laser fluence of YBCO deposition was 150 mJ/cm^2. Laser fluence of FeCo

deposition was 300 mJ/cm^2. Laser fluence of up-conversion nanoparticles deposition was 150 mJ/cm^2.

The substrates of the MAPLE process was glass slip. In FeCo and YBCO experiments, the surface of the glass slip was covered graphene film which fabricated through drop casting. Then the glass slips were placed in the incubator for 5 min at 37 °C to immobilize the graphene on the surface of the substrate. The substrate glass slides were fixed on the substrate holder. The temperature of the substrate was around 25 °C during the deposition process.

The nanoparticle dispersion was immediately added to the target holder after the sonication treatment. Then it was frozen by the liquid nitrogen which flowed through the sidewall of the special target holder. Target dispersion was kept frozen during the deposition process. The experiment was conducted under 1×10^{-4} Torr background pressure. The distance of substrate to target is 4.5 cm (vertical configuration). The target and the substrate were rotating (target: 10 rpm, substrate: 25 rpm) during the laser irradiation period.

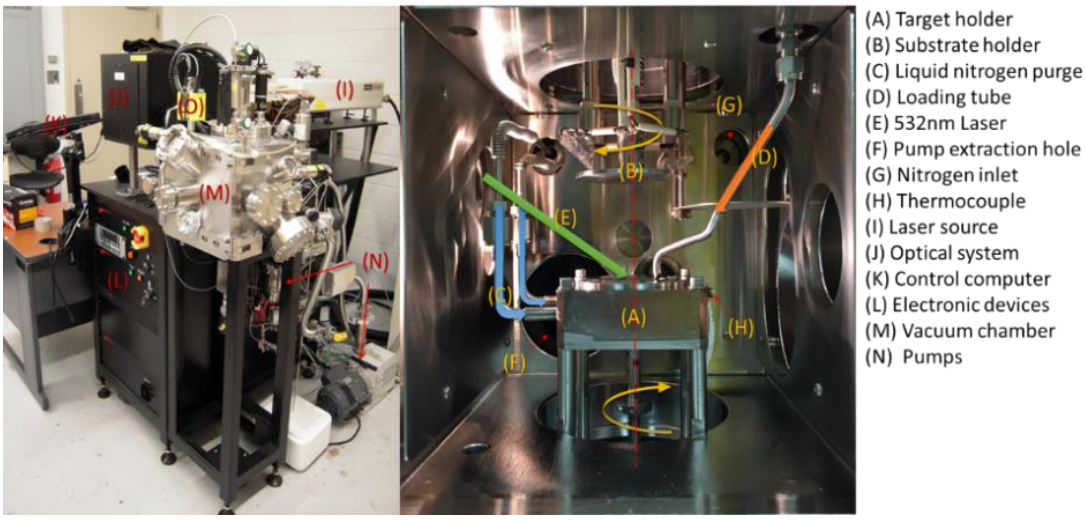

Figure 3.4 Illustration of MAPLE equipment and vacuum chamber

3.7 Characterization methods

The size and configuration nanoparticles before and after deposition were characterized by Transmission electron microscope (TEM, Philips CM10) and scanning electron microscopy (SEM, Hitachi 3400s). The deposition products were characterized by energy-

dispersive X-ray spectroscopy (SEM-EDS, Hitachi 3400s/TEM-EDS, Philips 420), vibrating sample magnetometer (VSM, LakeShore 7407, moment measure range: 10-7 to 103 emu; field accuracy: "±0.05%" full scale) and Fourier transform infrared spectroscopy (Bruker vector 22). The fabricated graphene nanosheets were observed by transmission electron microscope (TEM, Philips CM 10) and ultraviolet–visible spectroscopy (Cary 60 UV-Vis). The target solution and nanoparticles after ablation were characterized by Transmission electron microscope (TEM, Philips CM 10) and photoluminescence spectroscopy (PL, PTI QuantaMaster™ 40). The protein modified up-conversion nanoparticles were tested with human umbilical vein endothelial cells (HUVECs) and characterized with the confocal microscope (Zeiss LSM 5 Duo Vario Microscope). The TEM, SEM, TEM-EDS, SEM-EDS and confocal microscopy characterizations are performed with the help of biotron center at Western University.

3.7.1 Transmission electron microscopy

Transmission electron microscopy (TEM) is a microscopy technique which based on the electron beam. The beam of electron transmits through the sample while the electron beam interacts with the sample. The image is formed by collecting information produced by the interaction between electron beam and samples. Meanwhile, the picture of the sample is displayed by magnifying and focusing the image onto an imaging device. The TEM micrographs of FeCo particles, YBCO particles, up-conversion nanoparticles and protein modified up-conversion nanoparticles were collected by Phillips CM 10 TEM. The TEM samples were treated with MAPLE processes. The substrates of the samples were carbon coated copper grids (200 meshes) part of the grids were coated graphene films on its surface through the drop casting method. Some copper grids were fixed on the surface of the substrate holder and treated with MAPLE processes. The TEM samples which used to characterize nanoparticles were prepared by placing a drop of the sample solution on the surface of copper grids and were air-dried before the characterization.

3.7.2 Scanning electron microscopy

Scanning Electron Microscope (SEM) is a kind of microscope mainly based on the electron beam. The image of the target surface are generated through applying an electron beam to scan the surface of the sample. The electron beam interacts with the sample surface, the electrons are scattered and absorbed by the sample surface. The secondary electrons are produced through these processes and their intensifiers carry information of sample's surface topography and composition are collected by the detectors. The specimens are required to be electrically conductive for SEM characterization. Meanwhile, to prevent the accumulation of electrostatic charge, the samples require being electrically grounded. The non-conductive samples like organic samples need to be treated with metal coatings to grain conductivity. The conductive metal coatings could use platinum, gold, graphite, and tungsten as coating agents. In this study, FeCo/graphene samples were coated with gold on the surface of glass substrates by Hummer VI Sputter Coater. The micrographs and energy-dispersive X-ray spectroscopy (EDS) spectra were collected through SEM (Hitachi 3400s) at 30 kV.

3.7.3 Energy-dispersive X-ray spectroscopy

Energy-dispersive X-ray spectroscopy (EDS) is a technique which applied for elemental analysis and chemical characterization of the specimen. This technique is based on stimulation the emission of X-rays from the sample surface. This process would be achieved by the X-ray beam generated by the equipment interact with the sample surface. The high energy electron beam is focused on the specimen. This beam could excite the electrons in the inner shell of the atom, then another high energy electron would fill the shell hole and release a larger energy characteristic photon. The data which contains the information of unique structures of the sample atoms is collected by the special detector. The analyzer would identify the element type of the sample by analyzing the peaks on the emission spectrum. In this study, the energy-dispersive X-ray spectroscopy test of the deposition products was performed by Phillips 420 TEM-EDS and Hitachi 3400s SEM-EDS.

3.7.4 Fourier transform infrared spectroscopy

Fourier transform infrared spectroscopy (FT-IR) is a technique which is applied to characterize the functional groups of proteins and protein modified up-conversion nanoparticles. This technique generates an infrared spectrum absorption or emission of the liquid, gas and solid specimen. The mechanism of the FT-IR technique is that target molecules would vibrate when absorbing the energy from a monochromatic beam. In this study, FT-IR technique was used to characterize the up-conversion nanoparticles and protein modified up-conversion nanoparticles to identify the conjugation between proteins and nanoparticles. In addition, FT-IR was applied to verify the existence of the up-conversion nanoparticles and protein modified up-conversion nanoparticles on the surface of the substrate after MAPLE process. In this study, the FT-IR spectra of samples were characterized by Bruker Vector 22 FT-IR spectrometer. The scan range applied for the FT-IR was 600-4000 cm^{-1} and the scan resolution was 1 cm^{-1}. In this test, the air was used as background for the instrument.

3.7.5 Ultraviolet–Visible spectroscopy

Ultraviolet–visible spectroscopy (UV-Vis) is a technique which is based on the absorption and reflectance of the ultraviolet-visible spectral region. This technique is an important method of analytical chemistry. UV-Vis has been widely applied in physics, chemistry and life sciences. In nanotechnology, UV-Vis spectrum is applied to characterize the surface plasmon resonance (SPR) of Ag-PVP nanoparticles in solution and the size/shape of the Ag/PVP nanoparticles [8] and test the absorption properties of quantum dots [9] and carbon dots [10]. In addition, the UV-Vis spectrum is applied to test the *E.coli* concentration in the solution [8]. In this study, Agilent Cary 60 UV-Vis spectrophotometer was used to characterize the absorption spectrum of the graphene solution and graphene oxide solution.

3.7.6 Vibrating sample magnetometer

Vibrating sample magnetometer (VSM) is an equipment mainly used to measure magnetic properties. The test process of this instrument is that the specimen is placed in a uniform

magnetic field to magnetize the sample. The sample is placed in a quartz sample holder which is connected to a vibration motor. This motor would sinusoidally vibrate during the test process. The information is collected by the detector. Vibrating sample magnetometer has been applied in the test of various materials, such as magnetic powder, superconducting materials, magnetic films, anisotropic materials, magnetic recording materials and solid/liquid/ monocrystal magnetic materials, etc. In this study, the products of MAPLE process were collected and placed in the quartz sample holder. The magnetic properties were measured by LakeShore 7407 vibrating sample magnetometer (moment measure range: 10^{-7} to 10^{3} emu; field accuracy: "± 0.05 %" full scale).

3.7.7 Fluorescence spectroscopy

Fluorescence Spectroscopy is a technique which is applied to analyze fluorescence properties of the nanoparticles with optical properties. A beam of light was applied in this instrument to excite the electrons of sample molecule and the emission of the sample is collected by the sensors on the other end of the equipment. This data is collected by the detector and analyzed by the computer. In this study, the QuantaMaster™ 40 Spectrofluorometer (Photon Technology International Inc.) was applied to measure the fluorescence properties of up-conversion nanoparticles.

3.7.8 X-ray diffraction

X-ray crystallography is a method to characterize atomic structure/crystal structure of the material. This technique is based on the diffraction of the input x-ray into the specimen. The diffracted beam would be detected and collected by the sensors of the equipment. A graph is generated by the equipment which contains crystal structure information about the specimen materials. The information includes the position of the atom in the crystal lattice and the lattice structure of the materials. The YBCO particles crystal structures were studied by X-ray diffraction (XRD, Rigaku rotating-anode X-ray diffractometer with Co-Kα radiation).

3.7.9 Confocal microscopy

The confocal microscope is a microscope which based on adding spatial filters to increase the contrast of the micrograph. Compared with the normal optical microscope, this technique could rebuild the 3D structure of the samples by collecting information from different depth of the sample. The specimen is excited by the laser of the confocal microscope and the emission lights are detected by the sensors of the microscope. This technique is widely applied in biological fields, especially cell biology and microbiology. The deposited up-conversion nanoparticles samples and protein modified nanoparticles samples were tested by human umbilical vein endothelial cells (HUVECs) and imaged by the confocal microscope (Zeiss LSM 5 Duo Vario Microscope).

3.7.10 Cell viability test

The cells viability test is used to determine the cells and organs' ability of recover and maintain viability. This experiment is based on the chemical reaction process between the tetrazolium salt and the living cells. This technique has been applied to test the effect of the materials to the organisms. In this study, the deposited glass substrates were tested with the human umbilical vein endothelial cells (HUVECs) which cultured in MCDB media mixed with 10 % fetal bovine serum, 1 % penicillin and amphotericin B. The cells were incubated at 37 °C and 5 % CO_2 environment. The cells concentration were characterized by the hemocytometer, then the cells were added to the 8 wells plates. The plates were incubated for 24 hours for the cells to seed and grow. Then the MTT agent (3-(4, 5-dimethyl thiazolyl-2)-2, 5-diphenyl tetrazolium bromide) was added to the cell media to reacted with the cells and created purple formazan with intracellular shape and cells were incubated for 3 hours. The cell media was removed and DMSO was added to the well to dissolve the formazan. The liquid was transferred to the 96 well plates and analyzed with the bio-kinetic reader at 490 nm (Bio-Tek Instruments EL340I Microplate Reader).

3.8 Reference

[1] N.I. Kovtyukhova, P.J. Ollivier, B.R. Martin, T.E. Mallouk, S.A. Chizhik, E.V. Buzaneva, A.D. Gorchinskiy, Layer-by-Layer Assembly of Ultrathin Composite Films from Micron-Sized Graphite Oxide Sheets and Polycations, Chem. Mater. 11 (1999) 771-778.

[2] W.S. Hummers Jr, R.E. Offeman, Preparation of graphitic oxide, J. Am. Chem. Soc. 80 (1958) 1339-1339.

[3] D. Li, M.B. Muller, S. Gilje, R.B. Kaner, G.G. Wallace, Processable aqueous dispersions of graphene nanosheets, Nat Nano 3 (2008) 101-105.

[4] D. Kodama, K. Shinoda, K. Sato, Y. Konno, R.J. Joseyphus, K. Motomiya, H. Takahashi, T. Matsumoto, Y. Sato, K. Tohji, B. Jeyadevan, Chemical Synthesis of Sub-micrometer- to Nanometer-Sized Magnetic FeCo Dice, Adv. Mater. 18 (2006) 3154-3159.

[5] B. Jeyadevan, K. Shinoda, R.J. Justin, T. Matsumoto, K. Sato, H. Takahashi, Y. Sato, K. Tohji, Polyol Process for Fe-Based Hard(fct-FePt) and Soft(FeCo) Magnetic Nanoparticles, ITM 42 (2006) 3030-3035.

[6] H.-T. Wong, M.-K. Tsang, C.-F. Chan, K.-L. Wong, B. Fei, J. Hao, In vitro cell imaging using multifunctional small sized $KGdF_4:Yb^{3+},Er^{3+}$ upconverting nanoparticles synthesized by a one-pot solvothermal process, Nanoscale 5 (2013) 3465-3473.

[7] Q. Chen, C. Wang, L. Cheng, W. He, Z. Cheng, Z. Liu, Protein modified upconversion nanoparticles for imaging-guided combined photothermal and photodynamic therapy, Biomaterials 35 (2014) 2915-2923.

[8] G. Huang, Y. Chen, J. Zhang, Nanocomposited coatings produced by laser-assisted process to prevent silicone hydogels from protein fouling and bacterial contamination, Appl. Surf. Sci. 360, Part A (2016) 383-388.

[9] I.L. Medintz, H.T. Uyeda, E.R. Goldman, H. Mattoussi, Quantum dot bioconjugates for imaging, labelling and sensing, Nat Mater 4 (2005) 435-446.

[10] A. Jaiswal, S.S. Ghosh, A. Chattopadhyay, One step synthesis of C-dots by microwave mediated caramelization of poly(ethylene glycol), Chem. Commun. 48 (2012) 407-409.

Chapter 4

4 Fabrication of FeCo/graphene hybrid nanocomposites by MAPLE

In this chapter, FeCo nanoparticles were deposited on the surface of graphene sheets by MAPLE technique. The FeCo/graphene hybrid nanocomposites were fabricated through this process. The morphology and microstructures of the FeCo/graphene were characterized by TEM. The element composition and atomic ratio were characterized through TEM-EDS. The magnetic properties of FeCo nanoparticles and FeCo/graphene hybrid nanocomposites were collected and analyzed with VSM.

4.1 Introduction

Magnetic nanoparticles have drawn the great attention of the scientists in this decade. Various magnetic nanoparticles were developed with different methods. Different synthesis methods were developed to precisely control the size of the magnetic nanoparticles and fabricate monodisperse magnetic nanoparticles. The magnetic nanoparticles have been applied in different fields. These applications include contaminants/pollution removing [1, 2], computer memory devices [3], catalysts [4, 5], biotechnology [6] and Magnetic resonance imaging (MRI) [7, 8]. Due to the quantum confinement effect, the magnetic domain of the particles would reduce to one. The particles could achieve superparamagnetic behavior when the temperature above the blocking temperature and the size of the particles lower than a critical value. This type of magnetic nanoparticles has a fast response and giant paramagnetic behavior when outside environment magnetic fields are applied.

The magnetic nanoparticles are widely applied in various fields. One of the most common application is the separations process which is performed to recollect catalysts, wastes, bioproducts and cells in the liquid phase [9, 10]. Another application of magnetic nanoparticles in the catalyst fields is fabricating a new type of catalyst based on core-shell magnetic nanoparticles. The shell part of these nanoparticles could be the active layer of

the catalyst materials and the core parts with strong magnetic properties are applied as a crucial part of separation and recollection of the nano-catalysts [11, 12].

In biotechnology fields, the magnetic nanoparticles could be used to collect cells, biomolecules, and proteins. In most of the studies, the magnetic nanoparticles are modified by biomolecules, antibodies, and ligands to immobilize the target molecules on the surface [13]. Another application in biotechnology field is working as carriers for high-efficiency DNA and mRNA separation process [14]. The separation and collection of DNA, RNA and mRNA are extremely important for the investigation of disease diagnosis, gene library construction and gene expression process. The magnetic molecule carriers could increase the efficiency of these processes [15]. In addition, the magnetic nanoparticles could play a role as drug transporter for drug delivery process. By attaching the drugs on the surface of the magnetic nanoparticles and targeting the magnetic nanoparticles to the designated sites, drugs could be delivered to the lesions precisely and efficiently [6, 16]. Recently years, the hyperthermia treatment applications of the magnetic nanoparticles have drawn the interest of the scientists. The magnetic nanoparticles surgery method could be applied as an alternative way of cancer therapy. The mechanism of this method is to expose the magnetic nanoparticles in varying magnetic fields and the magnetic hysteresis losses would generate heat to treat the cancer cells [17, 18].

The FeCo nanoparticles are well-studied magnetic nanoparticles since these nanoparticles possess highest magnetic moments [19]. Furthermore, the FeCo alloy is one type of soft magnetic materials. Different with the superparamagnetic Fe_3O_4 nanoparticles which have negligible remanence and coercivity, the large size FeCo nanoparticles could be changed magnetic direction quickly when environment magnetic fields are reversed. These properties make FeCo nanoparticles extremely suitable for the applications which require high magnetic moments, such as recording tape and magnetic-resonance-imaging (MRI) agents [19]. However, the magnetic properties of the FeCo nanoparticles rely on the accurate manipulation of size and composition of the FeCo nanoparticles [20]. The researchers have developed various synthesis methods to overcome the challenges of controlling the composition and size of FeCo nanoparticles in the synthesis process. The normal chemical synthesis methods of FeCo nanoparticles include polyol method, thermal

decomposition method, and metal salt reduction method. An alternate method to synthesize small scales FeCo nanoparticles is chemical vapor deposition [19]. In this study, the FeCo nanoparticles were first synthesized through polyol method. Then the chemical synthesized FeCo nanoparticles were deposited and by Matrix Assisted Pulsed Laser Evaporation (MAPLE) technique. To fabricate FeCo/graphene hybrid nanocomposites, the graphene nanosheets were immobilized on the surface of the substrates. Then FeCo nanoparticles were deposited on the substrates by the MAPLE equipment.

4.2 Results

The FeCo nanoparticles were synthesized based on modified reference method [21]. The FeCo nanoparticles were synthesized through polyol process and rinsed by ethanol and water. To prepare the target solution for MAPLE process, as prepared FeCo nanoparticles were dispersed in isopropanol. The target solution was treated by MAPLE process. Meanwhile, FeCo/graphene hybrid nanocomposites were fabricated through this process. The influence of MAPLE process to the size, shape, and morphology of FeCo nanoparticles on the surface of the substrates was studied and characterized in this study. To investigate the effect of deposition time (*t*), the MAPLE deposition processes were performed in four different time periods: 0.5 h, 1 h, 1.5 h and 2 h. The magnetic properties and chemical composition of FeCo nanoparticles were characterized after the MAPLE deposition process.

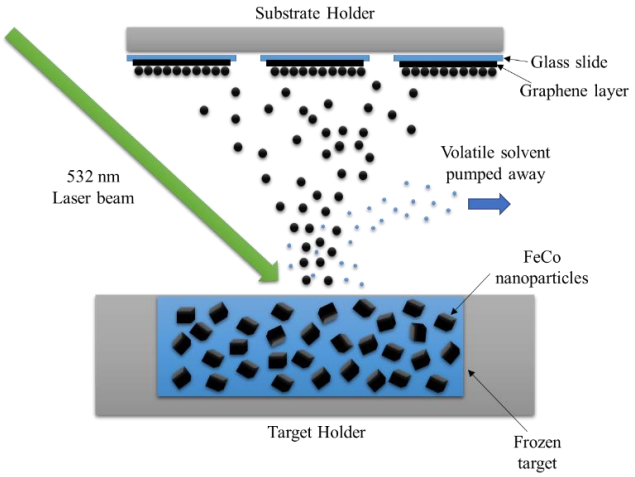

Figure 4.1 Schematic of MAPLE experiment and FeCo/graphene hybrid nanocomposites

4.2.1 Characterization of graphene nanosheets

The microstructures of graphene nanosheets which were prepared follow the reference [22]. The prepared graphene nanosheets were characterized by TEM. Figure 4.2 shows the TEM micrograph of the graphene nanosheets. The graphene nanosheets can be clearly observed, wrinkles or folds were observed which could be attributed to graphene's large aspect ratio.

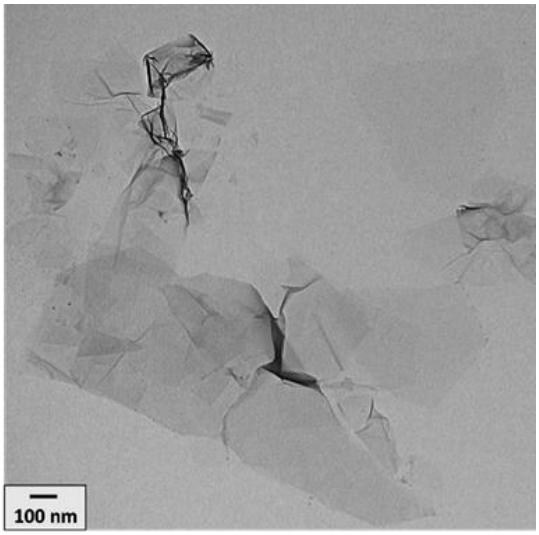

Figure 4.2 TEM image of graphene nanosheets

In addition, the UV-Vis spectra (Figure 4.3) of graphene oxide and graphene were collected to characterize the results of the reduction process. The graphene oxide solution has an absorbance peak at 231 nm. After hydrazine reduction, the absorbance peak red shifted to 270 nm, which suggested that the electronic conjugation within graphene basal plane was restored. Therefore graphene nanosheets were successfully prepared.

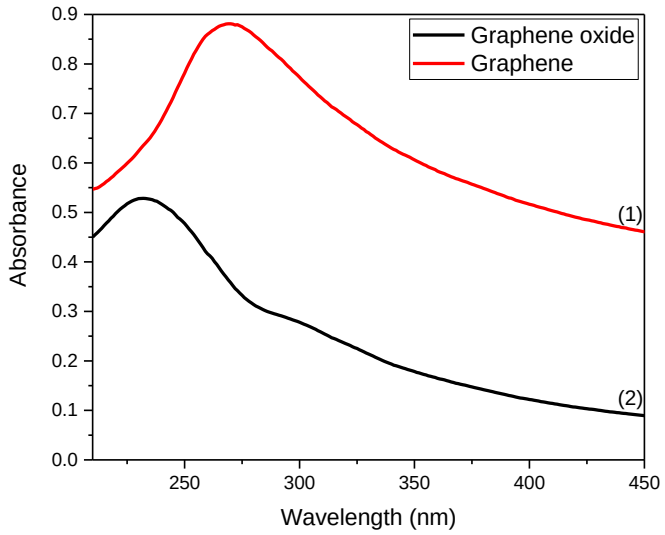

Figure 4.3 UV-Vis spectrum of (1) graphene and (2) graphene oxide. (The absorbance peak red-shifted from 231 nm of graphene oxide to 270 nm of graphene)

4.2.2 Characterization of FeCo nanoparticles

The chemical synthesized FeCo nanoparticles were characterized by transmission electron microscopy (TEM). The TEM micrographs were presented in Figure 4.4. The TEM micrographs indicate the average diameter of chemical synthesized FeCo nanoparticles is 300 ± 50 nm. Both cubic shape and sphere shape FeCo nanoparticles could be observed. The reason for this phenomenon could be the different Fe:Co ratio between the particles [21]. Most of chemical synthesis FeCo nanoparticles are cubic shape, part of the nanoparticles are sphere shape. The aggregation problems of nanoparticles present in the TEM micrographs. This problem is caused by the surfactant concentration and strong affinity between FeCo nanoparticles. The size of chemical synthesized FeCo nanoparticles was measured by software and the results were showed in the histogram. The results indicate the average size of chemical synthesized FeCo nanoparticles is 350 ± 50 nm.

The magnetic properties of chemical synthesized FeCo nanoparticles were measured by vibrating sample magnetometer (VSM) equipment. The room temperature magnetic hysteresis loop of FeCo nanoparticles was presented in Figure 4.5. The saturation magnetization (Ms) of the FeCo nanoparticles is highly related to the amount of the Fe element in the nanoparticles [21]. The saturation magnetization (Ms) of the FeCo

nanoparticles reached maximum (182 ± 2 emu/g) when the environment magnetic field at 11 ± 1 kOe. The FeCo nanoparticles show the ferromagnetic property at room temperature with a coercivity (Hc) around 0.13 ± 0.01 kOe. In addition, some references mention the size of the FeCo nanoparticle influence the magnetic moments and the magnetic properties of the nanoparticles [20]. The nanoparticles display ferromagnetic property since the particle size is large than 250 nm.

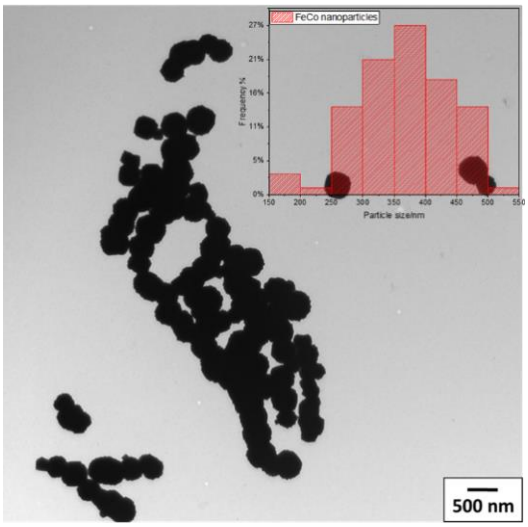

Figure 4.4 TEM micrograph of chemical synthesized FeCo nanoparticles and the size distribution histogram of FeCo nanoparticles

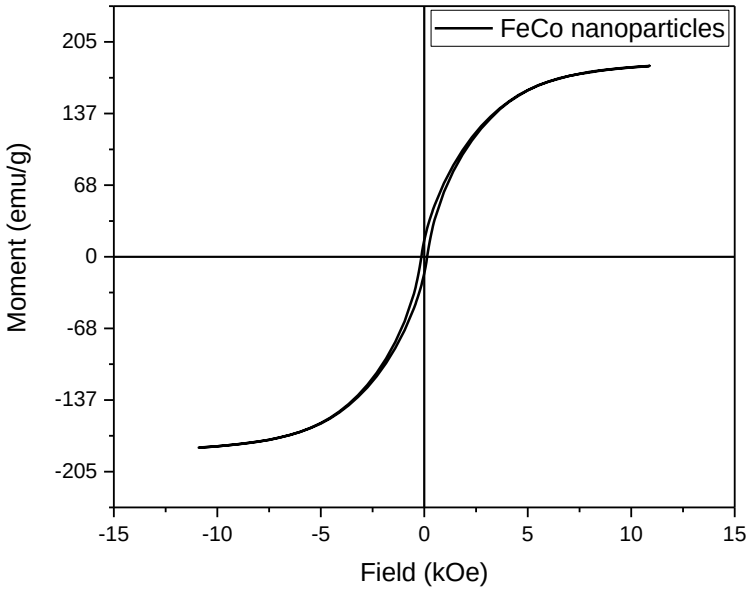

Figure 4.5 Magnetic hysteresis loop of FeCo nanoparticles at room temperature

4.2.3 Characterization of FeCo/graphene hybrid nanocomposites

The FeCo/graphene hybrid nanocomposites were characterized by the transmission electron microscopy (TEM). To prepared the TEM sample for the FeCo/graphene hybrid nanocomposites through MAPLE technique. The 200 mesh copper grids were fixed on the surface of the substrate holder, next to the glass slides which coated by graphene nanosheets. In Figure 4.6, the FeCo/graphene hybrid nanocomposites and small size FeCo nanoparticles could be observed. The graphene nanosheets were placed under the FeCo nanoparticles, this was shown by the TEM micrographs. In TEM micrographs, the wrinkles and folds of the graphene nanosheets could be observed and this shows that the structure of graphene nanosheets are preserved after the MAPLE deposition process. The TEM micrographs indicate that the size of the FeCo nanoparticles is extremely decreased from 300 ± 50 nm to 15 ± 10 nm. The shape of the FeCo nanoparticles is changed from cubic shape to sphere shape. This phenomenon indicates that the FeCo nanoparticles are influenced by the laser energy. The absorbance properties of the FeCo nanoparticles to the 532 nm Nd:YAG pulse laser could be the reason which causes this phenomenon[23].

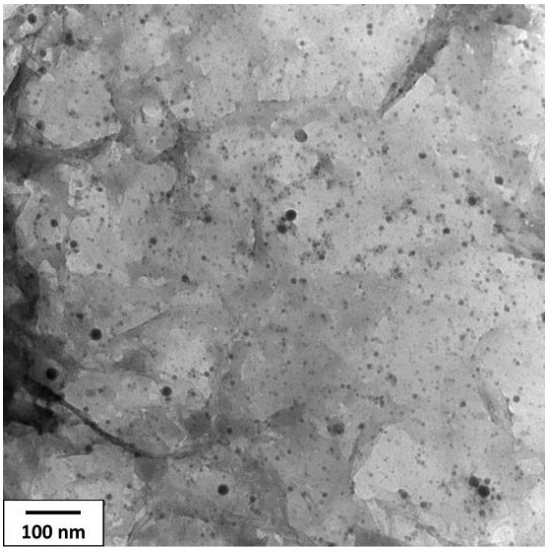

Figure 4.6 TEM micrograph of the FeCo/graphene hybrid nanocomposites

In addition, the chemical composition and element ratio of the FeCo hybrid nanocomposites after deposited by MAPLE technique was characterized through TEM-EDS. The results of TEM-EDS indicates the composition of the FeCo nanoparticles. The peak position in Figure 4.7 is same with reference [24]. The weight percentage and the atom percentage of different elements are presented in Figure 4.7. The results indicate that the molar ratio of Fe and Co is 1.79:1.92, close to 1:1. The TEM-EDS spectrum indicates that the chemical composition of the FeCo nanoparticles is not influenced by the pulse laser beam since the majority of laser energy is absorbed by the highly volatile solvent.

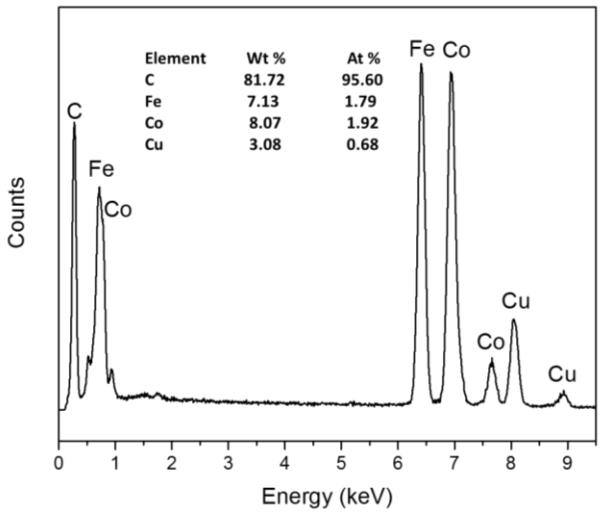

Figure 4.7 TEM-EDS result of the FeCo/graphene hybrid nanocomposites with *t* = 2 h

4.2.4 Relationship between surface morphology and deposition time (*t*)

In this study, the deposition time (*t*) was applied as a factor of the experiments. Among the experiment process, four deposition time periods were applied: 0.5 h, 1 h, 1.5 h and 2 h. The surface morphology of the substrates was investigated. The particle shape, particle size, and distribution of the FeCo nanoparticles on graphene surface were characterized by transmission electron microscopy (TEM).

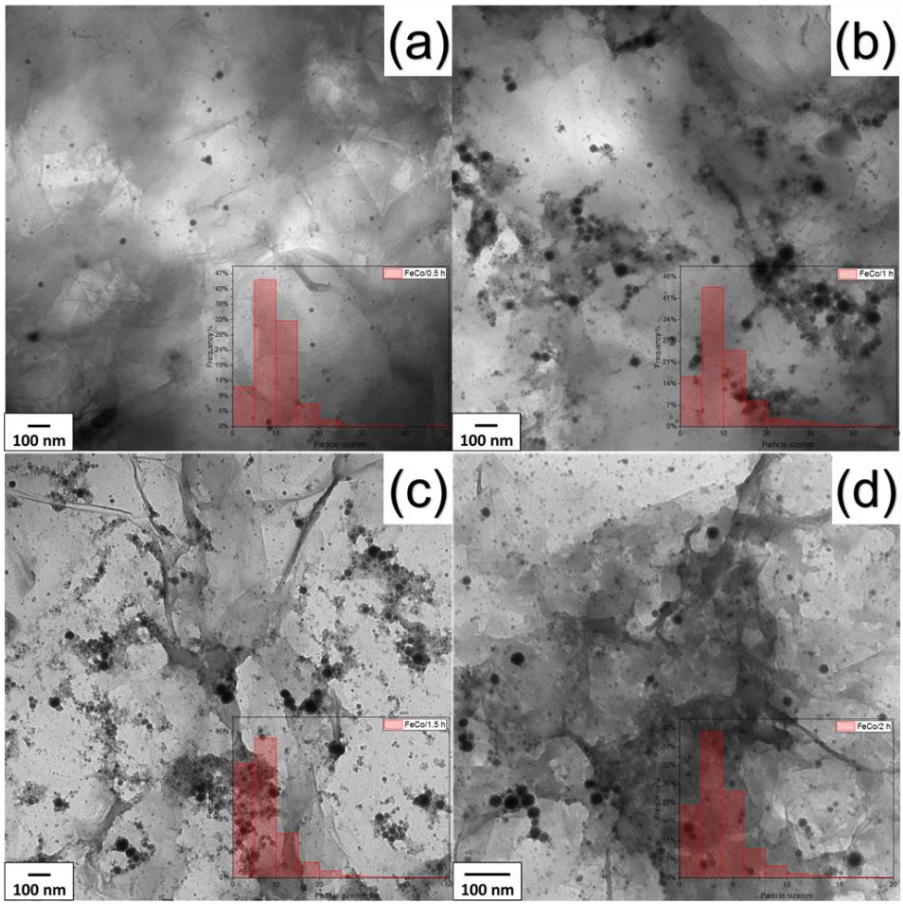

Figure 4.8 TEM micrographs and size distribution of the FeCo hybrid nanocomposites under different deposition time (a) *t* = 0.5 h (b) *t* = 1 h (c) *t* = 1.5 h (d) *t* = 2 h

In Figure 4.8, the size of the FeCo nanoparticles varied from 50 nm to 10 nm. The average particles size is remarkably reduced, compared with the as prepared chemical synthesized FeCo nanoparticles. After analyzing with the size measure software, the average particle size is 15 ± 5 nm when deposition time was 0.5 h (Figure 4.8 a) and 1 h (Figure 4.8 b). The average particles size of FeCo nanoparticles is not exceeding this range when deposition time reached 1.5 h (Figure 4.8 c) and 2 h (Figure 4.8 d). The maximum size of nanoparticles increases to 45 ± 10 nm when deposition time increased to 1 h and 1.5 h. Furthermore, most of the FeCo nanoparticles were sphere shape and part of the FeCo nanoparticles' shapes are irregular. These two factors indicate that the nanoparticles are influenced by the 532 nm laser. Base on the reference [23], the same phenomenon happened when researchers performed the TiO_2 nanorods deposition by the MAPLE technique. The reasons for this phenomenon could be the absorbance properties of the FeCo alloy and the

properties of the highly volatile solvent. In the addition, the amount of the FeCo nanoparticles on the surface of the graphene nanosheets are influenced by the MAPLE deposition time (*t*). It could be observed that the amount of the FeCo nanoparticles increased as the deposition time (*t*) changing from 0.5 h to 2 h. This could be concluded that more and more particles are deposited on the graphene surface as the deposition time accumulating.

4.2.5 The magnetic properties of the FeCo/graphene hybrid nanocomposites

The magnetic properties of FeCo/graphene hybrid nanocomposites were measured by the vibrating sample magnetometer (VSM, LakeShore 7407, moment measure range: 10^{-7} to 10^{3} emu; field accuracy: "± 0.05 %" full scale). The FeCo/graphene nanosheets samples were collected by using the solvent to dissolve the samples and centrifugation was applied to concentrate the samples. The solution of the samples was injected into the sample holder of VSM equipment and was dried before testing.

The magnetic hysteresis loop of the FeCo hybrid nanocomposites is presented in Figure 4.9. The maximum magnetization (Ms) of the hybrid nanocomposites with t = 0.5 h approaches to 0.4 ± 0.2 emu/g. The coercivity (Hc) of the FeCo/graphene nanosheets at the room temperature is around 0.02 ± 0.001 kOe. The FeCo/graphene hybrid nanocomposites displayed ferromagnetic property under the room temperature. These results indicate the magnetic FeCo/graphene hybrid nanocomposites could be fabricated through MAPLE technique. The saturation magnetization (Ms) and coercivity (Hc) of the magnetic hybrid nanocomposites are decreased compared with the chemical synthesis FeCo nanoparticles. Because samples were mainly made of graphene nanosheets and a small amount of FeCo nanoparticles were mixed inside of it. The magnetic properties of the samples could be improved by extending the deposition time (*t*). To achieve better results, the MAPLE system needs to be modified and improved to carry out long-time deposition. Another reason is the influence of the laser energy on the properties of the FeCo/graphene hybrid nanocomposites. The effects of laser energy need further investments and characterizations.

In Figure 4.9, the significate noise effects could be observed. This noise effects caused by the low amount of the FeCo nanoparticles and a lot of nonmagnetic graphene sheets. The deposited samples were tested by SEM-EDS to characterize the weight ratio/molar ratio of FeCo and carbon. The results indicate that the weight percentage of FeCo nanoparticles is 1.57 ± 0.2 %, that is, the mole percentage of FeCo nanoparticles is 0.034 ± 0.006 %. The low loading weight of FeCo nanoparticles results in the weak magnetic signal of the FeCo nanoparticles loaded graphene. The results would easily be influenced by the environmental vibration.

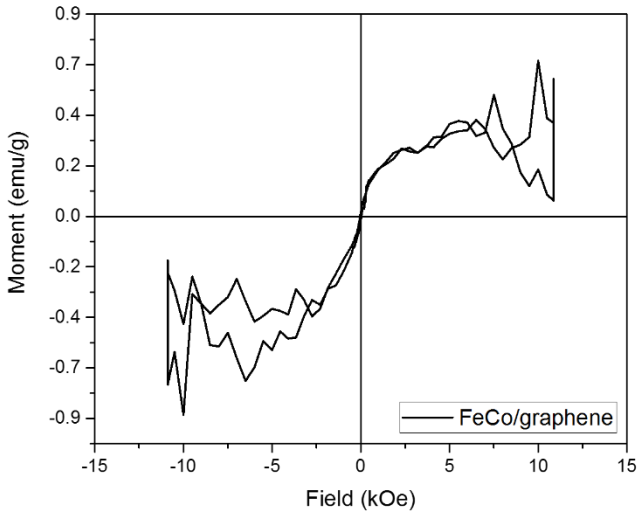

Figure 4.9 Magnetic hysteresis loop of FeCo/graphene hybrid nanocomposites at room temperature

4.3 Conclusion

In this study, the FeCo nanoparticles were synthesized through polyol process. the particles were further introduced in MAPLE system (532 nm laser/ fluence 300 mJ/cm^2) to fabricate FeCo/graphene hybrid nanocomposites. The particle size, particle shape and magnetic properties of FeCo nanoparticles were characterized by VSM and TEM. The results of TEM and TEM-EDS indicate the successful deposition of the FeCo nanoparticles on graphene nanosheets and chemical composition/atom ratio of the samples which are around 1.79:1.92 (Fe:Co). These results indicate that MAPLE technique could minimize the influence of laser on the chemical composition by introducing highly volatile solvent. The effect of time (*t*) on the size distribution and average particle size of the nanoparticles were investigated. The significant decrease of nanoparticle size is observed. The size of the FeCo

nanoparticles decreases dramatically from 350 ± 50 nm to 15 ± 10 nm after 0.5 h ablation by the laser. The amount of the FeCo nanoparticles on the graphene surface increases as the deposition time increases from 0.5 h to 2 h (0.5 h, 1 h, 1.5 h and 2 h). The magnetic properties of the FeCo/graphene hybrid nanocomposites were analyzed by the VSM. The decreasing of the maximum magnetic moment of FeCo/graphene hybrid nanocomposites were found compared with the chemical synthesized FeCo nanoparticles. The maximum magnetization (Ms) change from 182 ± 2 emu/g to 0.4 ± 0.2 emu/g and coercivity (Hc) change from 0.13 ± 0.01 kOe to 0.02 ± 0.001 kOe. The reason for this phenomenon could be caused by the composition of the hybrid nanocomposites. None-magnetic graphene nanosheets are the main component of the hybrid nanocomposites sample. This result indicates that magnetic graphene nanosheets can be achieved by depositing FeCo nanoparticles by MAPLE method. MAPLE technique is a suitable technique for the fabrication of the small size FeCo nanoparticles/hybrid nanocomposites. The influence of the 532 nm laser on the particle size, particle shape and magnetic properties of FeCo nanoparticles requires further investment. To further investigate the influence of laser and modify the MAPLE technique, more studies and experiments would be performed by our group.

4.4 Reference

[1] D.W. Elliott, W.-x. Zhang, Field Assessment of Nanoscale Bimetallic Particles for Groundwater Treatment, Environ. Sci. Technol. 35 (2001) 4922-4926.

[2] M. Takafuji, S. Ide, H. Ihara, Z. Xu, Preparation of Poly(1-vinylimidazole)-Grafted Magnetic Nanoparticles and Their Application for Removal of Metal Ions, Chem. Mater. 16 (2004) 1977-1983.

[3] T. Hyeon, Chemical synthesis of magnetic nanoparticles, Chem. Commun. (2003) 927-934.

[4] A.-H. Lu, W. Schmidt, N. Matoussevitch, H. Bönnemann, B. Spliethoff, B. Tesche, E. Bill, W. Kiefer, F. Schüth, Nanoengineering of a Magnetically Separable Hydrogenation Catalyst, Angew. Chem. 116 (2004) 4403-4406.

[5] S.C. Tsang, V. Caps, I. Paraskevas, D. Chadwick, D. Thompsett, Magnetically Separable, Carbon-Supported Nanocatalysts for the Manufacture of Fine Chemicals, Angew. Chem. 116 (2004) 5763-5767.

[6] A.K. Gupta, M. Gupta, Synthesis and surface engineering of iron oxide nanoparticles for biomedical applications, Biomaterials 26 (2005) 3995-4021.

[7] S. Mornet, S. Vasseur, F. Grasset, P. Veverka, G. Goglio, A. Demourgues, J. Portier, E. Pollert, E. Duguet, Magnetic nanoparticle design for medical applications, Prog. Solid State Chem. 34 (2006) 237-247.

[8] Z. Li, L. Wei, M.Y. Gao, H. Lei, One-Pot Reaction to Synthesize Biocompatible Magnetite Nanoparticles, Adv. Mater. 17 (2005) 1001-1005.

[9] S. Giri, B.G. Trewyn, M.P. Stellmaker, V.S.Y. Lin, Stimuli-Responsive Controlled-Release Delivery System Based on Mesoporous Silica Nanorods Capped with Magnetic Nanoparticles, Angew. Chem. Int. Ed. 44 (2005) 5038-5044.

[10] L. Nuñez, M.D. Kaminski, Transuranic separation using organophosphorus extractants adsorbed onto superparamagnetic carriers, J. Magn. Magn. Mater. 194 (1999) 102-107.

[11] J.-I. Park, J. Cheon, Synthesis of "Solid Solution" and "Core-Shell" Type Cobalt−Platinum Magnetic Nanoparticles via Transmetalation Reactions, J. Am. Chem. Soc. 123 (2001) 5743-5746.

[12] Y.-w. Jun, J.-s. Choi, J. Cheon, Heterostructured magnetic nanoparticles: their versatility and high performance capabilities, Chem. Commun. (2007) 1203-1214.

[13] L.X. Chen, T. Liu, M.C. Thurnauer, R. Csencsits, T. Rajh, Fe_2O_3 Nanoparticle Structures Investigated by X-ray Absorption Near-Edge Structure, Surface Modifications, and Model Calculations, J. Phys. Chem. B 106 (2002) 8539-8546.

[14] H. Gu, K. Xu, C. Xu, B. Xu, Biofunctional magnetic nanoparticles for protein separation and pathogen detection, Chem. Commun. (2006) 941-949.

[15] X. Zhao, R. Tapec-Dytioco, K. Wang, W. Tan, Collection of Trace Amounts of DNA/mRNA Molecules Using Genomagnetic Nanocapturers, Anal. Chem. 75 (2003) 3476-3483.

[16] T. Neuberger, B. Schöpf, H. Hofmann, M. Hofmann, B. von Rechenberg, Superparamagnetic nanoparticles for biomedical applications: Possibilities and limitations of a new drug delivery system, J. Magn. Magn. Mater. 293 (2005) 483-496.

[17] C.B. Catherine, S.G.C. Adam, Functionalisation of magnetic nanoparticles for applications in biomedicine, J. Phys. D: Appl. Phys. 36 (2003) R198.

[18] S. Mornet, S. Vasseur, F. Grasset, E. Duguet, Magnetic nanoparticle design for medical diagnosis and therapy, J. Mater. Chem. 14 (2004) 2161-2175.

[19] W.S. Seo, J.H. Lee, X. Sun, Y. Suzuki, D. Mann, Z. Liu, M. Terashima, P.C. Yang, M.V. McConnell, D.G. Nishimura, H. Dai, FeCo/graphitic-shell nanocrystals as advanced magnetic-resonance-imaging and near-infrared agents, Nat Mater 5 (2006) 971-976.

[20] G.S. Chaubey, C. Barcena, N. Poudyal, C. Rong, J. Gao, S. Sun, J.P. Liu, Synthesis and Stabilization of FeCo Nanoparticles, J. Am. Chem. Soc. 129 (2007) 7214-7215.

[21] D. Kodama, K. Shinoda, K. Sato, Y. Konno, R.J. Joseyphus, K. Motomiya, H. Takahashi, T. Matsumoto, Y. Sato, K. Tohji, B. Jeyadevan, Chemical Synthesis of Sub-micrometer- to Nanometer-Sized Magnetic FeCo Dice, Adv. Mater. 18 (2006) 3154-3159.

[22] D. Li, M.B. Muller, S. Gilje, R.B. Kaner, G.G. Wallace, Processable aqueous dispersions of graphene nanosheets, Nat Nano 3 (2008) 101-105.

[23] A.P. Caricato, V. Arima, M. Catalano, M. Cesaria, P.D. Cozzoli, M. Martino, A. Taurino, R. Rella, R. Scarfiello, T. Tunno, A. Zacheo, MAPLE deposition of nanomaterials, Appl. Surf. Sci. 302 (2014) 92-98.

[24] Y. Zhang, P. Wang, Y. Wang, L. Qiao, T. Wang, F. Li, Synthesis and excellent electromagnetic wave absorption properties of parallel aligned FeCo@C core-shell nanoflake composites, J. Mater. Chem. C 3 (2015) 10813-10818.

Chapter 5

5 Fabrication of YBCO/graphene hybrid nanocomposites by MAPLE

In this chapter, YBCO/graphene hybrid nanocomposites were prepared by depositing yttrium barium copper oxide (YBCO) superconductor particles onto graphene nanosheets via MAPLE process. The microstructures of YBCO nanoparticles deposited on graphene sheets by the MAPLE process are studied in terms of particle size and particle shape as a function of the deposition time (*t*). The surface morphology of YBCO/graphene hybrid nanocomposites samples (*t* = 0.5 h, 1 h, 1.5 h, 2.0 h) was characterized through TEM. The element composition of YBCO/graphene hybrid nanocomposites were characterized by TEM-EDS. The shape and size of YBCO particles before and after laser ablation were observed by TEM.

5.1 Introduction

Graphene is a typical two-dimensional carbon nanomaterial. It offers remarkable mechanical, electrical, thermal and optical properties. There are various applications of graphene sheets in energy-storage devices, polymer composite materials, mechanical resonators, sensors[1], etc. Graphene has a large surface area which can provide good catalytic properties and adsorption abilities. Many graphene nanocomposites were investigated and synthesized with enhanced performance and novel chemical, physical properties for supercapacitor [2], photovoltaic, electrodes, sensors [3], etc.

Yttrium barium copper oxide (YBCO) materials include different crystalline chemical compounds with the molecular formula: $YBa_2Cu_3O_7$. YBCO materials display superconductivity properties at the temperature around 77 K. High-temperature superconductivity has been utilized in magnetic resonance imaging (MRI), electrical devices, magnetic field sensors, etc. [4]. With the development of deposition technology, YBCO films coated on electrically conductive materials can overcome the low current

density and the grain boundary angle problems. Therefore, they could be used in different areas, including transformers and cables [5]. Conventional deposition processes (chemical vapor deposition [6] and physical vapor deposition [7]) could help YBCO materials overcome these drawbacks.

In this study, the YBCO/graphene hybrid nanocomposites were fabricated through MAPLE process. MAPLE is a contamination free surface modification system which could protect the structure of the target material. The target materials are dissolved or suspended in the solvent which is highly volatile. The solution is frozen by liquid nitrogen. The frozen solution (target) is irradiated by the high-energy pulsed laser beam. This whole process is performed under vacuum. Solvent molecules are pumped away by the pumps. The target molecules are deposited on the substrates.

5.2 Results

The as-purchased YBCO particles were properly dispersed in the isopropanol. By treating the target dispersion with MAPLE process, the YBCO nanoparticles were fabricated and deposited on the surface of graphene substrates. Meanwhile, the YBCO/graphene hybrid nanocomposites were produced through this process. To study the relationship between deposition time (t) and microstructure of the YBCO nanoparticles on the substrate, deposition time (t) was varied from 0.5 h, 1 h, 1.5 h and 2.0 h. The raw YBCO particles and YBCO/graphene hybrid nanocomposites were characterized to study the influence of the laser.

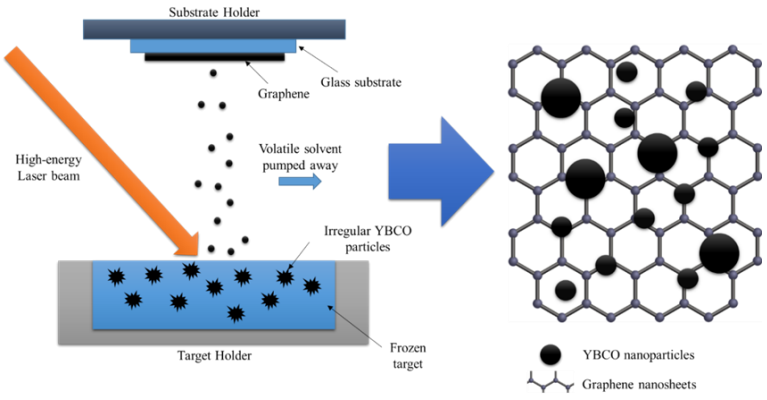

Figure 5.1 Schematic of MAPLE experiment and YBCO/graphene hybrid nanocomposites

5.2.1 Characterization of graphene nanosheets

In this study, the graphene nanosheets were prepared through the same method with the chapter 4 [8]. The graphene nanosheets were characterized by TEM and UV-Vis spectroscopy. The results were presented in chapter 4. Both of the TEM micrograph and UV-Vis spectra indicate that the graphene nanosheets were successfully synthesized.

5.2.2 Characterization of original YBCO particles

Figure 5.2 (a) shows the TEM micrographs of the original YBCO particles. The average size of these particles is around 3.5 ± 2 μm. These YBCO particles were applied as precursors in this study. The TEM micrographs indicate that the original YBCO particles possess irregular shape and rough surface which are caused by the mechanical fabrication processes. X-ray diffraction (XRD) test indicate that the XRD profile of as purchase original YBCO particles fits well with the structure of $Ba_{0.68}Y_{0.33}CuO_{3-x}$, of which the card number is PDF#41-0227 as shown in Figure 5.2 (b).

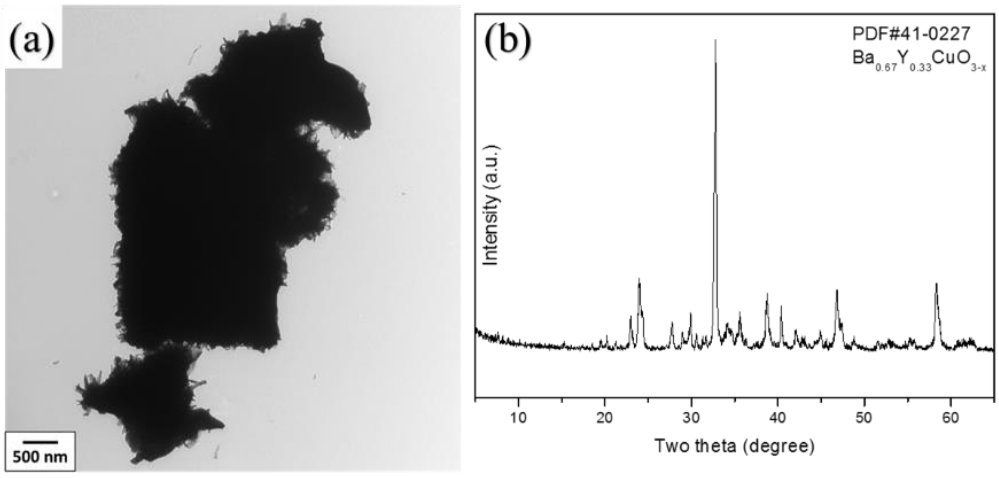

Figure 5.2 TEM micrograph (a) and XRD spectrum (b) of original YBCO particles

The original YBCO particles magnetic properties were characterized by VSM equipment. The hysteresis loops of YBCO were measured at 80 K and 300 K respectively, as shown in Figure 5.3. The YBCO particles show ferromagnetism at these temperatures. When temperature decreased from 300 K to 80 K, the saturation magnetization (Ms) at 10 kOe increases from 0.03 to 0.05 emu/g, while the coercivity (Hc) increases slightly from 120.6

to 123.0 Oe. As the particle size is much smaller than the bulk, the critical temperature of the YBCO powder may be even lower than 80 K.

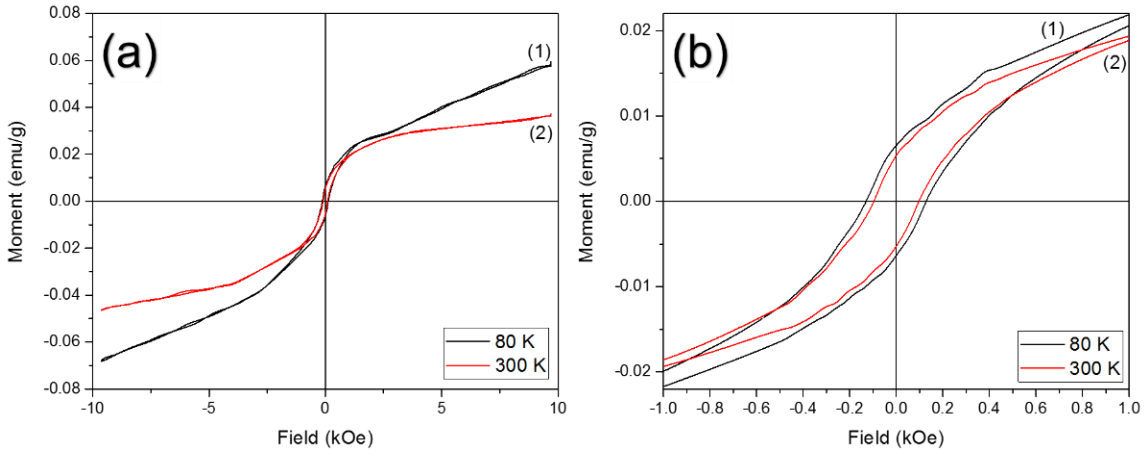

Figure 5.3 Magnetic properties of YBCO powder at (1) 80 K (2) 300 K, (a) full-scale magnetic hysteresis loops (b) magnetic hysteresis loops near axis origin.

5.2.3 Characterization of YBCO/graphene hybrid nanocomposites

The produced YBCO/graphene hybrid nanocomposites were characterized by TEM (Figure 5.4). To take TEM micrographs of YBCO/graphene hybrid nanocomposites, copper grids (200 meshes) were coated graphene on its surface and placed on the substrate holder. The polydisperse sphere shape YBCO nanoparticles could be observed in Figure 5.4. YBCO nanoparticle displayed darker color which contrasted with the color of graphene nanosheets. The size of YBCO nanoparticles was dramatically reduced ($d < 500$ nm), compared with the original YBCO particles (3.5 ± 2 μm). The graphene nanosheets could be observed in this micrograph and the wrinkles or folds remained. This shows that the structures of graphene nanosheets are preserved after interacted with YBCO nanoparticles fluxes which are generated by the MAPLE process.

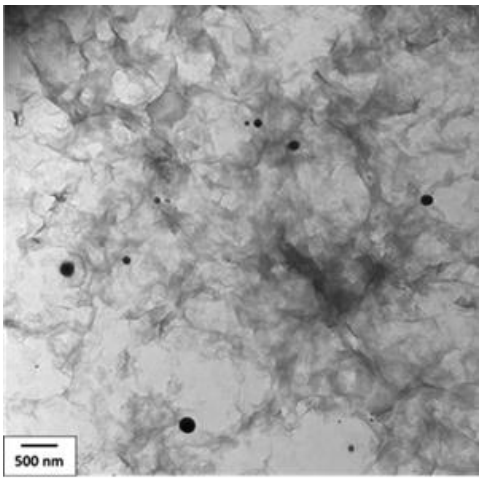

Figure 5.4 TEM micrograph of YBCO/graphene hybrid nanocomposites

In addition, the shape of YBCO nanoparticles which are deposited on the graphene surface becomes uniform (sphere). This phenomenon could be caused by the mechanism of MAPLE process. MAPLE process input high energy to the frozen target and there is a small part of the laser energy which is absorbed by the YBCO particle. To check the chemical composition of YBCO/graphene hybrid nanocomposites which are deposited on the graphene surface, the TEM-EDS was applied. The TEM-EDS spectrum is presented in Figure 5.5 and this spectrum is similar with the reference [9]. The results of element analysis indicate that the element composition and the atom ratio of YBCO are not changed after MAPLE deposition.

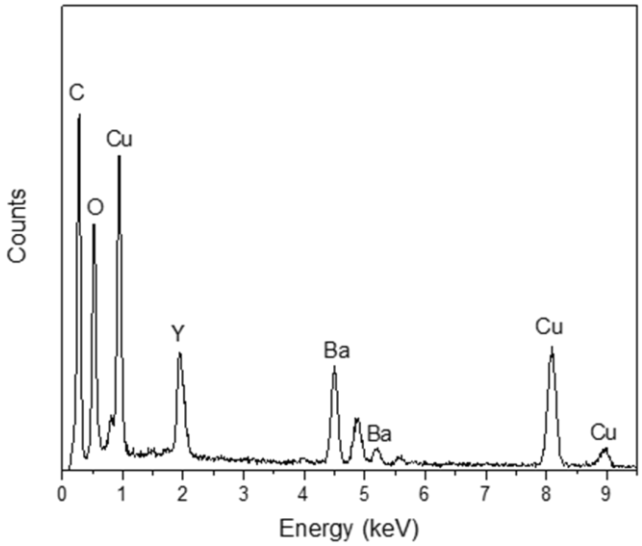

Figure 5.5 TEM-EDS spectrum of YBCO/graphene hybrid nanocomposites (*t* = 2 h)

5.2.4 Relationship between surface morphology and deposition time (*t*)

The microstructures and particle size distribution of the hybrid nanocomposites were characterized by TEM. The samples were deposited with different deposition time (*t* = 0.5 h, 1 h, 1.5 h and 2.0 h). The TEM micrograph (Figure 5.6) of the samples indicate that the particle size distribution, particle amount and surface morphology of the deposition YBCO particles are related to the deposition time (*t*). The YBCO nanoparticles with 100 ± 10 nm diameter could be observed when (*t*) = 0.5 h and 1.0 h (Figure 5.6 a and 5.6 b). When the deposition time (*t*) is increased to 1.5 h and 2.0 h (Figure 5.6 c and 5.6 d), the large YBCO nanoparticles (250 ± 50 nm) are presented in the micrographs.

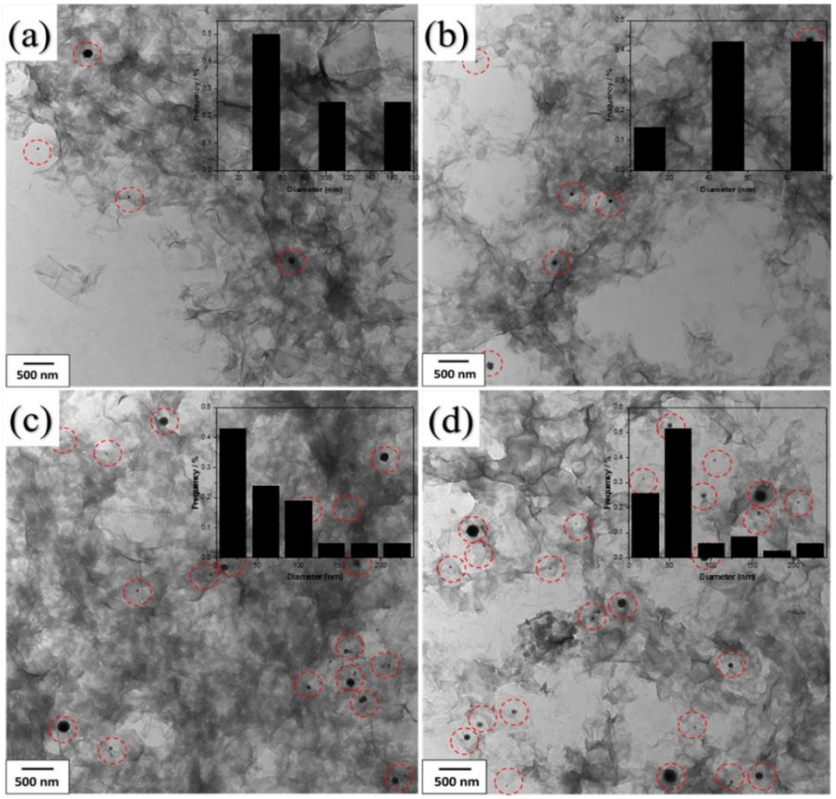

Figure 5.6 TEM micrographs of the YBCO particles on the surface of the substrate under different deposition time (a) *t* = 0.5 h (b) *t* = 1 h (c) *t* = 1.5 h (d) *t* = 2 h

After analysis with software, the results indicate that the average particle size of YBCO nanoparticles is 60 ± 20 nm. When the deposition time (*t*) is increased to 1.5 h and 2.0 h,

the large YBCO nanoparticles with 250 ± 50 nm diameter are presented. The particle amount is influenced by the deposition time. After analyzing the particle amount on the substrate surface, the results indicate that particle amount has a positive correlation with deposition time (*t*). The particle amount increases slightly when deposition time (*t*) was increased from 0.5 h to 1 h. However, the particle amount increases dramatically when the deposition time (*t*) was increased to 1.5 h. This result may indicate that 1 hour could be a threshold for the increase of the particle amount since the amount difference between 1.5 h sample and 2.0 h sample are not that obvious. As the (*t*) increasing, more YBCO nanoparticles would be carried out by the matrix molecules and the more YBCO nanoparticles are deposited on the substrates. The ablation phenomenon of nanoparticles could be observed in samples of various deposition time. This phenomenon is caused by the solvent absorbance of laser energy and the energy transfer between particles and solvent molecules. The same ablation phenomenon appeared when A.P. Caricato [10] and his co-workers operated the TiO_2 deposition experiments. This part needs further study to explain the mechanism of the YBCO deposition.

5.3 Conclusions

In this study, the YBCO/graphene hybrid nanocomposites were successfully fabricated through MAPLE equipment with 532 nm laser (150 mJ/cm^2). The deposition results were characterized by TEM and TEM-EDS. The XRD profiles and magnetic properties of as purchased YBCO particles were tested and collected by x-ray diffraction equipment and vibrating sample magnetometer. VSM results indicate the maximum magnetization (Ms) of original YBCO particles at 10 kOe increases from 0.03 to 0.05 emu/g, while the coercivity (Hc) increases slightly from 120.6 to 123.0 Oe when temperature decreased from 300 K to 80 K. The XRD profiles of the YBCO particles were found matching perfectly with the existing data of YBCO materials (PDF#41-0227). The TEM micrographs indicate the particle size distribution, particle amount and surface morphology of the deposited YBCO nanoparticles. The particles size of YBCO particles reduced dramatically after the MAPLE process. The average size of YBCO particles changes from 3.5 ± 2 μm to 60 ± 20 nm after MAPLE deposition process. The shape and morphology of YBCO particles before

and after MAPLE process was observed through TEM. The TEM-EDS spectrum shows the element composition and atomic ratio of YBCO nanoparticles was preserved after MAPLE deposition. Consequently, MAPLE is a proper method to produce YBCO/graphene hybrid nanocomposites and the YBCO/graphene hybrid nanocomposites can be applied as parts of conductor devices in the future.

5.4 References

[1] S. Park, R.S. Ruoff, Chemical methods for the production of graphenes, Nat Nano 4 (2009) 217-224.

[2] D. Wang, R. Kou, D. Choi, Z. Yang, Z. Nie, J. Li, L.V. Saraf, D. Hu, J. Zhang, G.L. Graff, J. Liu, M.A. Pope, I.A. Aksay, Ternary Self-Assembly of Ordered Metal Oxide−Graphene Nanocomposites for Electrochemical Energy Storage, ACS Nano 4 (2010) 1587-1595.

[3] X. Huang, Z. Yin, S. Wu, X. Qi, Q. He, Q. Zhang, Q. Yan, F. Boey, H. Zhang, Graphene-Based Materials: Synthesis, Characterization, Properties, and Applications, Small 7 (2011) 1876-1902.

[4] R. Hott, Application Fields of High-Temperature Superconductors, in: A.V. Narlikar (Ed.) High Temperature Superconductivity 2, Springer Berlin Heidelberg, Berlin, Heidelberg, 2004, pp. 35-48.

[5] V. Narayanan, I. Van Driessche, Aqueous chemical solution deposition of lanthanum zirconate and related lattice-matched single buffer layers suitable for YBCO coated conductors: A review, Prog. Solid State Chem. 40 (2012) 57-77.

[6] L. Montero, G. Gabriel, A. Guimerà, R. Villa, K.K. Gleason, S. Borrós, Increasing biosensor response through hydrogel thin film deposition: Influence of hydrogel thickness, Vacuum 86 (2012) 2102-2104.

[7] S. Foltyn, P. Tiwari, R. Dye, M. Le, X. Wu, Pulsed laser deposition of thick $YBa_2Cu_3O_{7-\delta}$ films with J $c \geq 1$ MA/cm^2, Appl. Phys. Lett. 63 (1993) 1848-1850.

[8] D. Li, M.B. Muller, S. Gilje, R.B. Kaner, G.G. Wallace, Processable aqueous dispersions of graphene nanosheets, Nat Nano 3 (2008) 101-105.

[9] C.S. Lim, L. Wang, C.K. Chua, Z. Sofer, O. Jankovsky, M. Pumera, High temperature superconducting materials as bi-functional catalysts for hydrogen evolution and oxygen reduction, J. Mater. Chem. A 3 (2015) 8346-8352.
[10] A.P. Caricato, V. Arima, M. Catalano, M. Cesaria, P.D. Cozzoli, M. Martino, A. Taurino, R. Rella, R. Scarfiello, T. Tunno, A. Zacheo, MAPLE deposition of nanomaterials, Appl. Surf. Sci. 302 (2014) 92-98.

Chapter 6

6 Deposition of protein modified up-conversion nanoparticles by MAPLE

In this chapter, protein modified up-conversion nanoparticles were deposited by Matrix Assisted Pulsed Laser Evaporation (MAPLE). Up-conversion nanoparticles ($NaGdF_4$: Yb^{3+}, Er^{3+}) were synthesized through chemical processes. The proteins (BSA and IgG) were modified on the nanoparticles surface by forming peptide bonds with amino groups on up-conversion nanoparticles surface. The up-conversion nanoparticles and protein modified up-conversion nanoparticles were deposited on the surface of glass substrates. The deposition results were characterized by transmission electron microscopy (TEM) and Fourier transform infrared spectroscopy (FT-IR). The human umbilical vein endothelial cells (HUVECs) were applied to test the biocompatibility of the deposited samples (IgG modified up-conversion nanoparticles). The results of this study demonstrate that MAPLE is a suitable process for depositing organic/biological nanoparticles. The up-conversion nanoparticles with/without protein modification could be deposited through MAPLE technique.

6.1 Introduction

The Lanthanide-doped up-conversion nanoparticles have been studied and invested by the researchers for decades. A noticeable feature of these nanomaterials is an optical phenomenon called up-conversing phenomenon (anti-Stokes emission). This phenomenon means that nanoparticles could absorb two or more low-energy photons and result in the emission of high-energy photons [1, 2]. The concept of the anti-Stokes emission was revealed by a physicist called Nicolaas Bloembergen in 1959 [3]. The studies of the up-conversion materials were accelerated in the mid-1960s. The first significance result of the up-converting phenomenon was found by François Auzel in 1966 [1]. In that study, the energy transfers happened between Yb^{3+} and Er^{3+}/Tm^{3+}. The Yb^{3+} was used to sensitize those two elements (Er^{3+}/Tm^{3+}) for the emission of high energy photons. Other researchers

soon found new element matches of different energy photons' emission. In 1966, Ovsyankin and Feoflov discovered the up-converting phenomenon which Yb^{3+}sensitize the other element [4]. After a short time, researchers found a new element couple Yb^{3+}-Ho^{3+} which could achieve the green light emission [5]. There are three mechanisms of the up-conversion process: energy transfer up-conversion (ETU), excited-state absorption (ESA) [6, 7] and photon avalanche (PA). The terminology "up-conversion" means transfer long wavelength radiation to the short wavelength radiation. An essential requirement for fabricating the up-conversion nanoparticles is the special stair-like arrangement of the energy levels which make the ions easily reach the emission energy level.

A large amount of the element couples were found by the researchers, for example, Re^{4+} [8, 9], Ni^{2+} [10], Ti^{2+} [11, 12] and Mo^{3+} [13, 14] doped solids [15, 16]. Various synthesis methods have been developed by the researchers for fabricating up-conversion nanoparticles. These up-conversion nanoparticles could be divided to two main types: up-conversion nanoparticles based on oxidic materials [17, 18] and up-conversion nanoparticles based on fluorides [19, 20]. Researchers use co-precipitation methods prepared $LuPO_4$ and $YbPO_4$ up-conversion nanoparticles [21]. Kong and his co-workers fabricated Er^{3+} doped YVO_4 nanoparticles through hydrothermal processes [22]. To re-disperse up-conversion nanoparticles in the water, the surface modified Y_2O_3 nanoparticles were synthesized by the researchers [23]. The fluorides type up-conversion nanoparticles hold a higher transfer efficiency compared with oxidic materials based up-conversion nanoparticles. In 2002, van Veggel and his co-workers fabricated LaF_3 nanoparticles which doped with rear earth ions [24]. After a period of times, the rear earth elements doped YF_3 and YbF_3 up-conversion nanoparticles were developed by the researchers. In 2005, Li and colleagues developed a method to fabricate rear earth elements doped YF_3 nanoparticles in 2 steps reaction [25]. The researchers tried to control the size distribution of the doped LaF_3 up-conversion nanoparticles [26]. Up-conversion particles with different shapes were developed by the researchers. $NaLuF_4$ microplates with doped with Yb^{3+}, Er^{3+} elements were produced by Li and his group member [27]. Hao et al. fabricated the $NaGdF_4$ doped Yb^{3+}, Er^{3+} with magnetic properties which could be applied in both MRI and imaging fields [28]. In 2004, the researchers from three groups fabricated ultra-small $NaYF_4$ up-

conversion nanoparticles which could form transparent colloidal solutions [29]. To control the size of the up-conversion nanoparticles, the Gd^{3+} ions were introduced to the synthesis processes. Wang and his group member doped Gd^{3+} into the $NaYF_4$:Yb^{3+}, Er^{3+} system to reduce the size of the up-conversion nanoparticles [30]. In 2009, Li and his group members synthesized 10 nm size up-conversion nanoparticles based on CaF_2: Yb^{3+}, Er^{3+} through hydrothermal processes [31]. More and more up-conversion nanoparticles with different shapes, sizes, compositions, and properties were developed by the researchers for different applications.

The up-conversion nanoparticles hold good fluorescence properties for imaging applications and part of them hold magnetic properties which could be applied in therapy treatments. In the biotechnology fields, the specific biological molecules were modified on the surface of the high-quality fluorescence up-conversion nanoparticles for the observation of the biological processes. The up-conversion nanoparticles could be widely applied in biological fields since they hold advantages such as good photo-stability, monodispersity, biocompatibility and high signal-to-noise ratio by NIR [32]. The penetration properties of the NIR radiation is high compared with other radiation sources. The applications of the up-conversion nanoparticles in the biological fields include: in vitro detection, in vivo detection, multimodal imaging, and cancer therapy. In medication detection fields, the up-conversion nanoparticles were connected with biotin and avidin for the in vitro detection [33]. A FRET biosensor based on modified up-conversion nanoparticles with gold nanoparticles were fabricated by the researchers [34]. For the in vivo detection, the up-conversion nanoparticles are introduced to the living organisms and the detection is based on the distribution of the nanoparticles. Since NIR radiation has better penetration properties, up-conversion nanoparticles could be detected under 10 mm depths [35]. Up-conversion nanoparticles could be applied to the RNA interference therapy to replace the fluorescence quantum dots which have drawbacks such as toxicity and auto-fluorescence [36]. The researchers connected the up-conversion nanoparticles with biomolecules and were used for tumor detection and drug delivery [37]. In these years, a new type of up-conversion nanoparticles which are doped with the gadolinium (Gd^{3+}) was fabricated and could be applied as the contrast agent for the MRI [38]. These up-conversion

nanoparticles could be used as magnetic and optical contrast agent for multimodal imaging [39]. Another application of the up-conversion nanoparticles is used as catalysts for the cancer treatment The up-conversion nanoparticles could activate photosensitizers which conjugated on their surface through resonance energy transfer and generate ROS or reacting O_2 to eliminate cancer cells [40, 41].

6.2 Results

In this study, the up-conversion nanoparticles ($NaGdF_4$: Yb^{3+}, Er^{3+}), Bovine serum albumin (BSA) modified up-conversion nanoparticles and Immunoglobulin G (IgG) modified up-conversion nanoparticles were fabricated through the chemical processes. Transmission electron microscopy (TEM) and Fourier transform infrared spectroscopy (FT-IR) were applied to characterize the modification results of the experiments. 1-Ethyl-3-(3-dimethyl aminopropyl) carbodiimide (EDC) and borate buffered saline (BBS) were applied to connect the up-conversion nanoparticles with the protein include IgG and BSA. The nanoparticles were collected after centrifugation. Then, nanoparticles were dissolved in the volatile solvent and frozen by the liquid nitrogen. Up-conversion nanoparticles, BSA modified up-conversion nanoparticles and IgG modified up-conversion nanoparticles were deposited through MAPLE technique. The deposition time (t) equal to 2 hours. The glass substrates with/without gelatin coating were fixed on the rotating substrate holder to achieve good morphology. The deposition results were characterized through TEM and FT-IR technique to investigate and characterize the deposition product. The human umbilical vein endothelial cells (HUVECs) were used to test the biocompatibility of the samples after the MAPLE treatment.

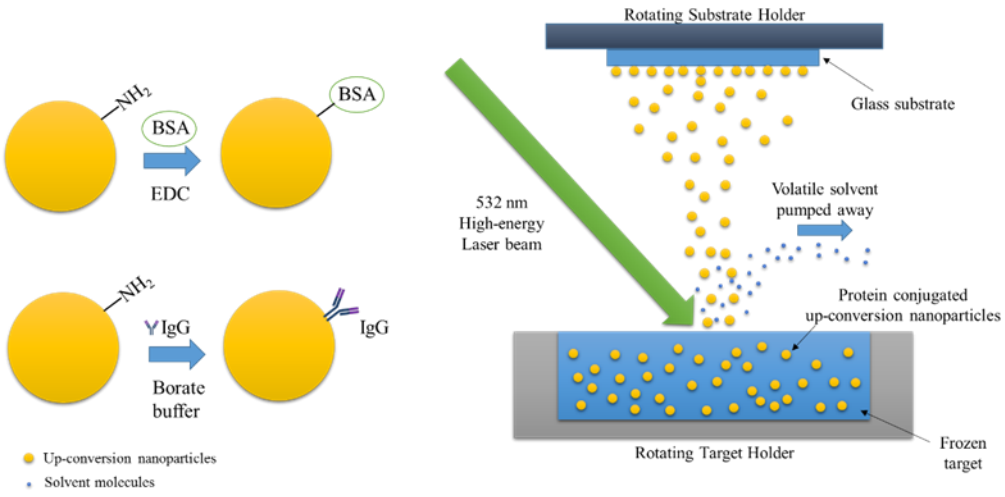

Figure 6.1 Schematic of the conjugation process (BSA and IgG with up-conversion nanoparticles) and MAPLE deposition process

6.2.1 Characterization of BSA modified up-conversion nanoparticles

The TEM micrographs of up-conversion nanoparticles and BSA modified up-conversion nanoparticles were presented in Figure 6.2. The TEM micrographs indicate that the up-conversion nanoparticles are mono-dispersed and the average diameter is 60 ± 10 nm with a cubic shape. The diameter of the up-conversion nanoparticles and BSA modified up-conversion nanoparticles were measured through the software. The results are presented in Figure 6.2. The results indicate the size of the up-conversion nanoparticles are around 60 ± 10 nm and the BSA modified up-conversion nanoparticles' average diameter is 65 ± 10 nm. Most of the up-conversion nanoparticles and BSA modified up-conversion nanoparticles' shapes are cubic shapes and some of them are sphere shapes. It could be observed that the surface of the original up-conversion nanoparticles are rough and can't observe coating on their surface. Compared with the original up-conversion nanoparticles, 5 - 6 nm BSA coatings on the nanoparticles' surface are clearly presented in the TEM micrographs. This indicates the BSA was successfully conjugated with the up-conversion nanoparticles. The fluorescence spectrum of the up-conversion nanoparticles was measured by the QuantaMaster™ 40 Spectrofluorometer (Photon Technology

International Inc.) and the spectrum is presented in Figure 6.2. Two peaks (550 nm and 650 nm) could be observed in the spectrum (λ_{ex} = 980 nm).

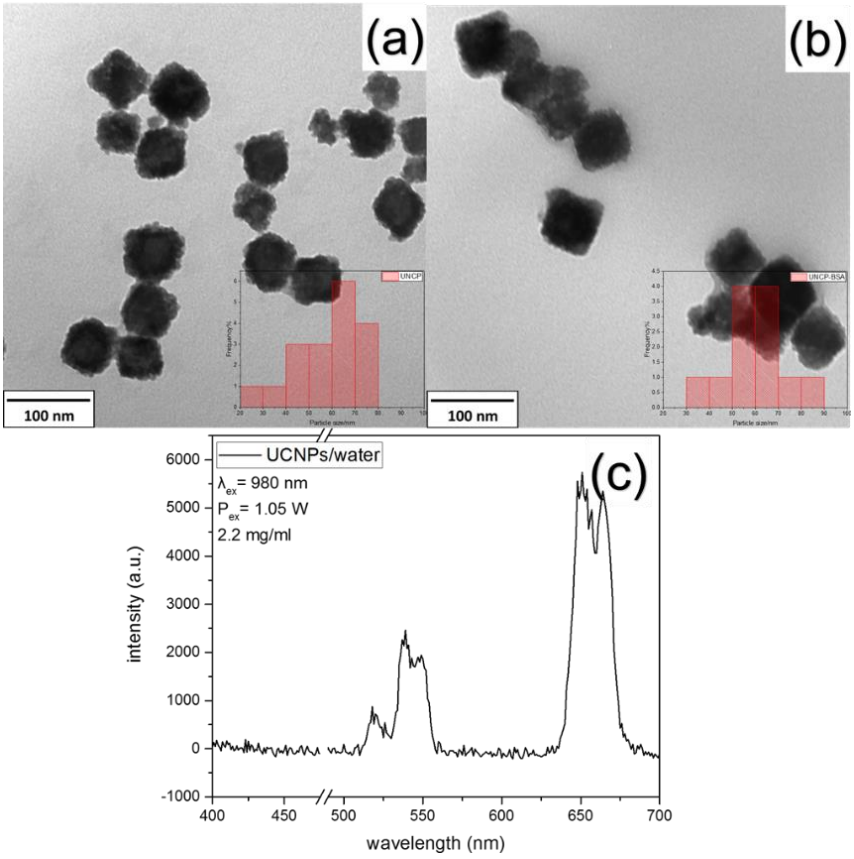

Figure 6.2 (a) TEM micrographs of up-conversion nanoparticles ($NaGdF_4$: Yb^{3+}, Er^{3+}) (b) TEM micrographs of BSA modified up-conversion nanoparticles (c) fluorescence spectrum of the up-conversion nanoparticles (excited by 980 nm laser, power 1.05 W)

To further study the modification results, Fourier-transform infrared spectroscopy (FT-IR) was applied (Figure 6.3). The FT-IR results indicate BSA and BSA modified up-conversion nanoparticles spectra have stretching vibration bands of the –OH groups at 3288 cm^{-1} and 3293 cm^{-1}. The –OH band of the up-conversion particles' spectrum is not obvious because up-conversion nanoparticles are covered with branched PEI. The stretching vibrations bands of the Carbonyl groups are found at 1644 cm^{-1} and 1646 cm^{-1} for BSA and BSA modified up-conversion nanoparticles which indicate the presence of the peptide bonds. In addition, the bending vibrations bands of $–NH_2$ was found at 1522 cm^{-1}, 1527 cm^{-1} and 1523 cm^{-1} in all 3 spectra because all these 3 nanoparticles contain

amino groups. Therefore, the successful modification was characterized by the FT-IR spectra.

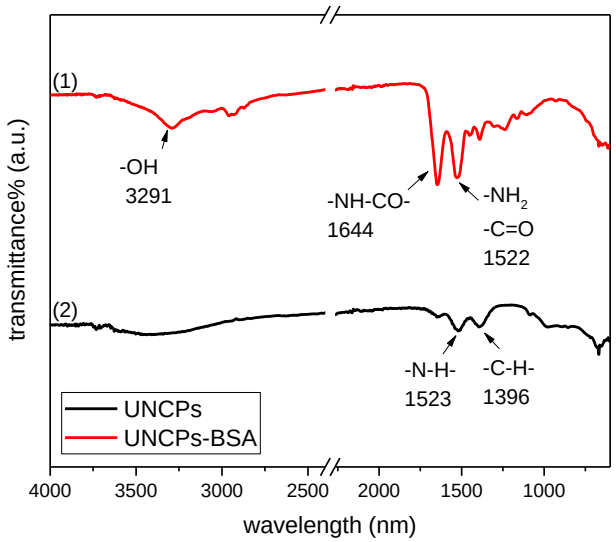

Figure 6.3 FT-IR spectra of (1) BSA modified up-conversion nanoparticles (2) up-conversion nanoparticles

6.2.2 Characterization of BSA modified up-conversion nanoparticles on the substrate after MAPLE process

The TEM micrographs of deposited up-conversion nanoparticles and BSA modified up-conversion nanoparticles are presented in Figure 6.4 (a) and Figure 6.4 (b). The TEM micrographs of the up-conversion nanoparticles on the substrate indicate the average size is 60 ± 10 nm. However, the shape of the up-conversion nanoparticles was influenced by the laser and changed from cubic shape to sphere shape. The same phenomenon was found by Caricato, A. P and his group member, this phenomenon is the effect of the laser or the volatile solvent on the target materials [42]. Figure 6.4 (b) is the TEM micrograph of the up-conversion nanoparticles which were deposited on the substrate. The BSA coatings on the surface of the nanoparticles are obvious in this micrograph. The average size of the nanoparticles is 50 ± 10 nm and nanoparticles are sphere shape and cubic shape. These results indicate the successful deposition of the up-conversion particles and BSA modified up-conversion nanoparticles on the glass substrates through the MAPLE technique. In addition, these results indicate that the laser effects were minimized by the volatile solvent. The FT-IR characterization (Figure 6.4 c) was applied to further study the deposition

results of the up-conversion nanoparticles and BSA modified up-conversion nanoparticles. The stretching vibration band of –OH groups is found at 3667 cm^{-1}, This result indicates the existence of carboxyl groups on the substrate which come from the BSA modified up-conversion nanoparticles on substrates surface. The bending vibration band of amino groups is found at 1577 cm^{-1} and this is caused by the amino groups which were fixed on the surface of up-conversion nanoparticles. The stretching vibration bands of methylene could be found in both two spectra and indicate the existence of BSA and branched PEI. Therefore, the FT-IR spectra indicate the successful deposition of both up-conversion nanoparticles and BSA modified up-conversion nanoparticles.

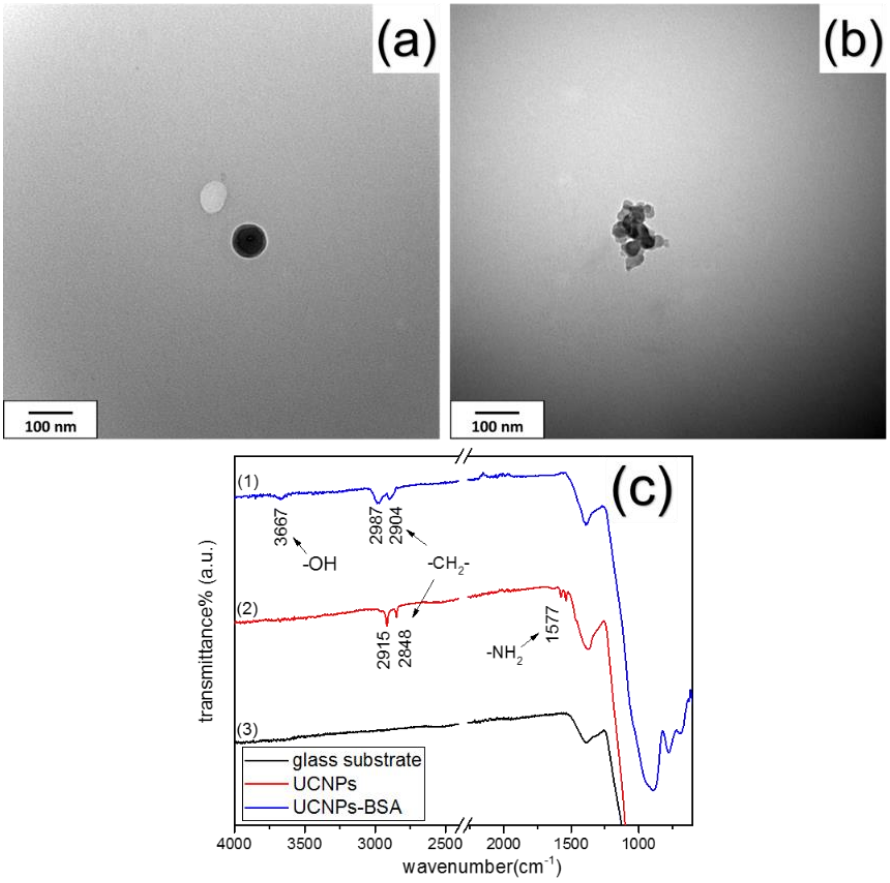

Figure 6.4 TEM micrographs of (a) up-conversion nanoparticles (b) BSA modified up-conversion nanoparticles on the substrate after MAPLE deposition (c) FT-IR spectra of (1) BSA modified up-conversion nanoparticles deposited on glass substrate (2) up-conversion nanoparticles deposited glass substrate (3) glass substrate

6.2.3 Characterization of IgG modified up-conversion nanoparticles before and after MAPLE process

The IgG-conjugated up-conversion nanoparticles were characterized through FT-IR and TEM. The FT-IR spectra are presented in Figure 6.6 (b). In Figure 6.6 (b), the stretching vibration bands of –OH groups could be observed at 3673 cm^{-1}, 3372 cm^{-1}, and 3382 cm^{-1} at both two spectra. The –OH groups are found by FT-IR which indicate that IgG antibodies are conjugated on the surface of the up-conversion nanoparticles. The stretching vibration bands of methylene are found at 2987 cm^{-1} and 2900 cm^{-1}. These two peaks are obvious at the spectrum of IgG modified up-conversion nanoparticles. These peaks indicate the presence IgG modified up-conversion nanoparticle on the deposited substrates' surface. The bending vibration bands of amino groups were found at 1515 cm^{-1} and 1511 cm^{-1} for both two spectra. Both PEI (polyethylenimine) and IgG antibodies which are fixed on the surface of the up-conversion nanoparticles possess amino groups. The stretching vibration bands of carboxyl groups could be found at 1249 cm^{-1} in IgG modified up-conversion nanoparticles spectrum. The stretching vibration bands of peptide bands is found at 1650 cm^{-1}. These results indicate the successful conjugation between IgG antibodies and up-conversion nanoparticles.

In addition, the TEM micrographs indicate the successful conjugation between the up-conversion nanoparticles and IgG antibodies. The TEM micrographs of the IgG modified up-conversion nanoparticles are presented in Figure 6.5. The IgG antibodies are found in these pictures (mark with red circle). The size of the IgG antibodies in the TEM micrographs are 20 ± 5 nm [43]. The structure of the IgG is presented clearly in these micrographs. This is another proof for the successful fabrication of the IgG modified up-conversion nanoparticles.

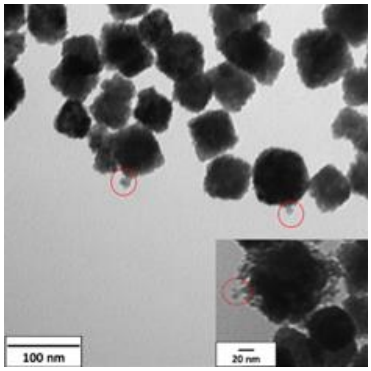

Figure 6.5 TEM micrographs of the IgG modified up-conversion nanoparticles (IgG marked with red circles)

Then the IgG modified up-conversion nanoparticles were deposited on the glass slide. Samples were tested with FT-IR after MAPLE deposition process treatments (Figure 6.6 a). The results indicate that the stretching vibration bands of –OH groups could be observed at 3648 cm^{-1}. -OH groups come from the IgG antibodies which are conjugated on the surface of the up-conversion nanoparticles. The existence of methylene groups could be indicated by the stretching vibration bands at 2985 cm^{-1} and 2900 cm^{-1}. The existence of amino groups could be observed by the bending vibration band at 1575 cm^{-1} which were found at the spectrum of the up-conversion nanoparticles. These functional groups are parts of the branched PEI which are fixed on the surface of the up-conversion nanoparticles. Compared with the spectra of the up-conversion nanoparticles and glass substrate, these results could indicate the existence of IgG modified up-conversion nanoparticles on the surface of substrates after MAPLE deposition.

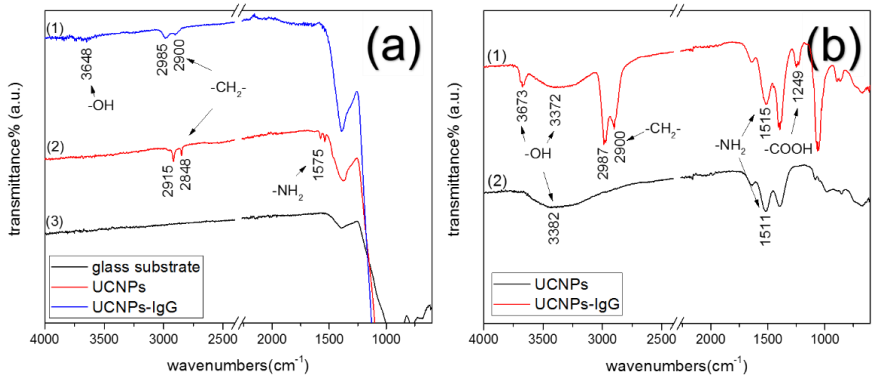

Figure 6.6 (a) FT-IR spectra of (1) IgG modified up-conversion nanoparticles deposited on glass substrate (2) up-conversion nanoparticles deposited glass substrate (3) glass substrate (b) FT-IR spectra of (1) IgG modified up-conversion nanoparticles (2) up-conversion nanoparticles

6.2.4 Biocompatibility test of the deposited samples

In this test, the glass substrates were coated with gelatin for cells seeding. Among the deposition process, different substrates were applied to investigate the difference between the control group samples and deposition treated samples. The biocompatibilities of three different types samples were tested by this experiment: control group samples, up-conversion nanoparticles deposited samples and IgG modified up-conversion nanoparticles deposited samples. Figure 6.7 presents the confocal microscope micrographs of three different samples. Compared with the control samples, the cells which grow on the other two samples' surface hold higher amounts and better connections with each other. These results indicate the successful deposition of two nanoparticles (UCNPs and UCNPs-IgG) and the biocompatibility of these nanoparticles. The results indicate the IgG modified up-conversion nanoparticles were successfully deposited by the MAPLE technique and hold good biocompatibility.

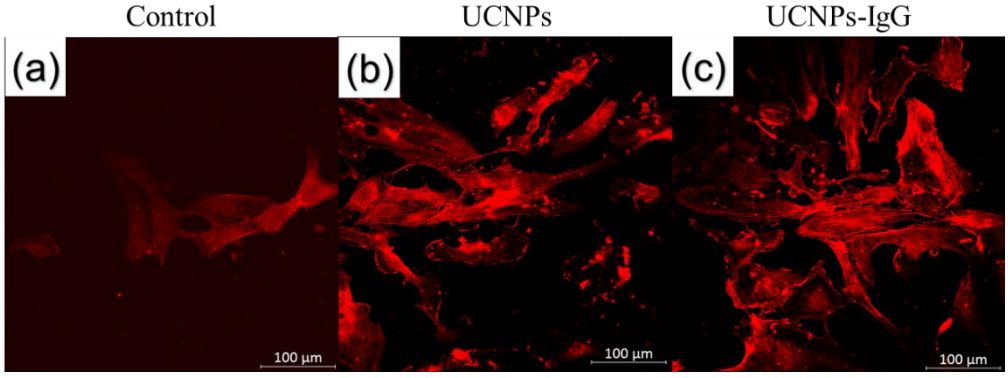

Figure 6.7 Confocal micrographs of HUVECs on the surface of (a) control sample, (b) up-conversion nanoparticles samples, (c) IgG modified up-conversion nanoparticles samples

The length of cells, the length of connections, area of the cells and cells number were investigated through the ImageJ software (Figure 6.8). The lengths of the cells are defined as the largest length value which could be measured in this cell. The length of the connection is defined as the distance between the edge of the cells tips and the cell nuclei. The former three factors are indicated the better growth status of the HUVECs on the surface of up-conversion/IgG modified up-conversion nanoparticles, compared with the control samples. The cells number on the surface of up-conversion nanoparticles sample is higher than other two groups and the cells number of IgG modified up-conversion

nanoparticles sample is similar to the control groups' result. Most of the references show the up-conversion nanoparticles have a good biocompatibility compared with other nanoparticles [44, 45]. The results of the investigation by ImageJ software indicate that both up-conversion nanoparticles and IgG modified up-conversion nanoparticles possess good biocompatibility. The influence of IgG modified up-conversion nanoparticles on the cells is not obvious compared with the up-conversion nanoparticles. Because the IgG is one kind of antibodies, its effect on the growth of the cells is not obvious compared with other biomolecules.

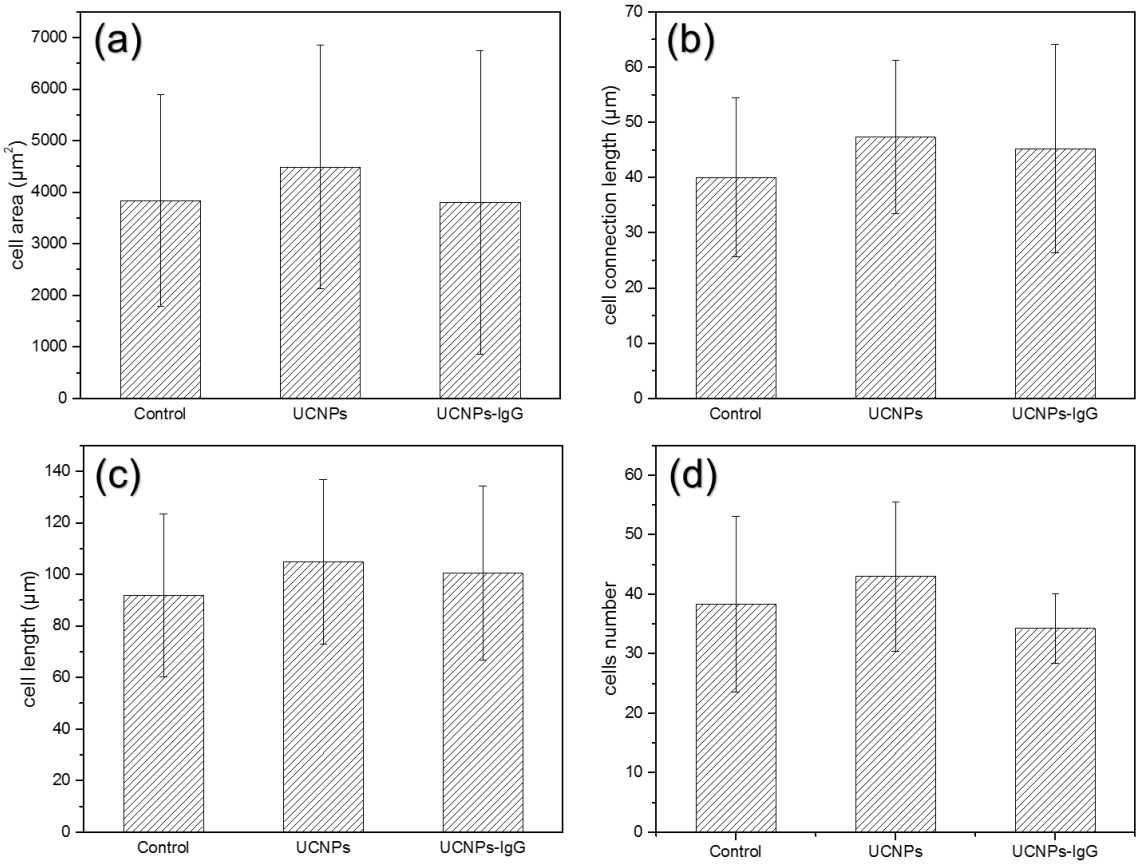

Figure 6.8 Investigation results of HUVECs for control sample/UCNPs/UCNPs-IgG: (a) cell area, (b) cell connection length (c) cell length (d) cells number

6.2.5 Cell viability test of the deposited samples

The tests were carried out by testing the cell concentration on the surface of the deposited samples. The HUVECs were grown on the surface of the deposited samples for 24 hours. The results of this test could indicate the cells' response to the up-conversion nanoparticles and IgG modified up-conversion nanoparticles. Three types of samples were tested: control samples, up-conversion nanoparticles deposited on glass substrates and IgG modified up-conversion nanoparticles deposited on glass substrate. These samples were soaked in the cell culture medium for 24 hours at 37 °C in the incubator. Then the MTT test was carried out after 24 hours. Figure 6.9 indicates the results of MTT test. The results show that the cell concentration of the glass substrates, up-conversion nanoparticles samples and IgG modified up-conversion nanoparticles samples were 103.96 %, 105.44 % and 103.96 % individually (Figure 6.9). The results could indicate that up-conversion nanoparticles and protein modified up-conversion nanoparticles have no toxic effects on the cells and these particles could be considered as biocompatible materials.

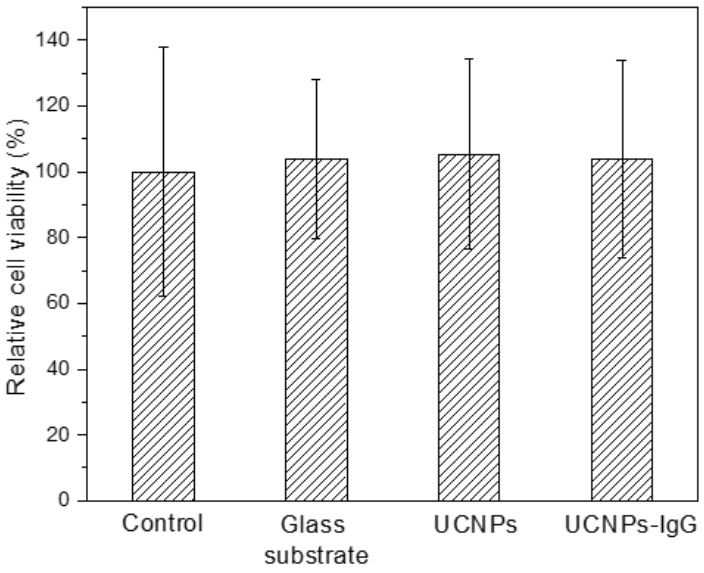

Figure 6.9 Cell viability of control sample, glass substrate, UCNPs, and IgG modified UCNPs

6.3 Conclusions

In this study, the up-conversion nanoparticles, BSA modified up-conversion nanoparticles, and IgG modified nanoparticles were successfully deposited on the surface of the glass substrate with or without gelatin coating. The TEM and FT-IR results indicate the

immobilization of these nanoparticles on substrates' surface which was achieved by the MAPLE equipment with a pulsed Nd:YAG laser at 532 nm (150 mJ/cm^2). The up-conversion nanoparticles were characterized by the fluorometer and peaks at 550 nm/650 nm were observed under 980 nm continuous laser excitation. The size of the up-conversion nanoparticles was 60 ± 10 nm and 5-6 nm BSA coatings were observed by the TEM. The deposited samples were characterized by TEM. The average size of BSA modified up-conversion nanoparticles is 50 ± 10 nm and the BSA coatings were observed after MAPLE deposition process. To verify the deposition results, deposited samples were characterized by FT-IR. The presences of functional groups (-OH/-NH_2/-COOH) indicate successful deposition of protein modified up-conversion nanoparticles. The influence of laser on the particle shape and particle size are minimized. The proteins (BSA and IgG) are protected by the volatile solvents and deposited on the substrate surface along with the up-conversion nanoparticles. These products could be used to fabricate the new biological devices which are based on the up-conversion nanoparticles. Our group is currently working on developing biomaterial devices based on protein modified up-conversion nanoparticles which are deposited through MAPLE technique. The further investigation of the interactions between the deposited nanoparticles with primary umbilical vein endothelial cells (HUVECs) would be carried out in the future studies.

6.4 Reference

[1] F. Auzel, Upconversion and Anti-Stokes Processes with f and d Ions in Solids, Chem. Rev. 104 (2004) 139-174.

[2] M. Haase, H. Schäfer, Upconverting Nanoparticles, Angew. Chem. Int. Ed. 50 (2011) 5808-5829.

[3] N. Bloembergen, Solid State Infrared Quantum Counters, Phys. Rev. Lett. 2 (1959) 84-85.

[4] B. Zhou, B. Shi, D. Jin, X. Liu, Controlling upconversion nanocrystals for emerging applications, Nat Nano 10 (2015) 924-936.

[5] Enhancement in a Ho^{3+}–Yb^{3+} quantum counter by energy transfer, Appl. Phys. Lett. 10 (1967) 126-127.

[6] F.E. Auzel, Materials and devices using double-pumped-phosphors with energy transfer, Proc. IEEE 61 (1973) 758-786.

[7] R. Kopelman, Topics in Applied Physics, Vol. 15, edited by FK Fong, in, Heidelberg: Springer-Verlag, 1976.

[8] D.R. Gamelin, H.U. Güdel, Spectroscopy and Dynamics of Re^{4+} Near-IR-to-Visible Luminescence Upconversion, Inorg. Chem. 38 (1999) 5154-5164.

[9] W. Markus, U.G. Hans, Luminescence spectroscopy and NIR to VIS upconversion of Cs_2 GeF_6 : 2% Re^{4+}, J. Phys.: Condens. Matter 13 (2001) 9583.

[10] O.S. Wenger, H.U. Güdel, Photon Upconversion Properties of Ni^{2+} in Magnetic and Nonmagnetic Chloride Host Lattices, Inorg. Chem. 40 (2001) 157-164.

[11] O.S. Wenger, H.U. Güdel, Chemical Tuning of the Photon Upconversion Properties in Ti^{2+}-Doped Chloride Host Lattices, Inorg. Chem. 40 (2001) 5747-5753.

[12] S.M. Jacobsen, H.U. Güdel, Higher excited state luminescence in Ti2+:MgCl2 Dynamics of radiative and nonradiative processes, J. Lumin. 43 (1989) 125-137.

[13] D.R. Gamelin, H.U. Güdel, Two-photon spectroscopy of d^3 transition metals: near-IR-to-visible upconversion luminescence by Re^{4+} and Mo^{3+}, J. Am. Chem. Soc. 120 (1998) 12143-12144.

[14] D.R. Gamelin, H.U. Güdel, Excited-State Dynamics and Sequential Two-Photon Upconversion Excitation of Mo^{3+}-Doped Chloro- and Bromo-elpasolites, J. Phys. Chem. B 104 (2000) 10222-10234.

[15] M. Wermuth, H.U. Güdel, Photon Avalanche in Cs_2ZrBr_6:Os^{4+}, J. Am. Chem. Soc. 121 (1999) 10102-10111.

[16] Photon avalanche in Cs_2ZrCl_6: Os^{4+}, J Chem Phys 114 (2001) 1393-1404.

[17] J.F. Suyver, A. Aebischer, D. Biner, P. Gerner, J. Grimm, S. Heer, K.W. Krämer, C. Reinhard, H.U. Güdel, Novel materials doped with trivalent lanthanides and transition metal ions showing near-infrared to visible photon upconversion, Opt. Mater. 27 (2005) 1111-1130.

[18] S. Polizzi, S. Bucella, A. Speghini, F. Vetrone, R. Naccache, J.C. Boyer, J.A. Capobianco, Nanostructured Lanthanide-Doped Lu_2O_3 Obtained by Propellant Synthesis, Chem. Mater. 16 (2004) 1330-1335.

[19] M. Pollnau, D.R. Gamelin, S. Lüthi, H. Güdel, M. Hehlen, Power dependence of upconversion luminescence in lanthanide and transition-metal-ion systems, Phys. Rev. B 61 (2000) 3337.

[20] G. Yi, B. Sun, F. Yang, D. Chen, Y. Zhou, J. Cheng, Synthesis and characterization of high-efficiency nanocrystal up-conversion phosphors: ytterbium and erbium codoped lanthanum molybdate, Chem. Mater. 14 (2002) 2910-2914.

[21] K. Kömpe, H. Borchert, J. Storz, A. Lobo, S. Adam, T. Möller, M. Haase, Mit einer Quantenausbeute von 70 % grün lumineszierende $CePO_4$:Tb-Nanopartikel mit einer Schale aus $LaPO_4$, Angew. Chem. 115 (2003) 5672-5675.

[22] Y. Sun, H. Liu, X. Wang, X. Kong, H. Zhang, Optical Spectroscopy and Visible Upconversion Studies of YVO_4:Er^{3+} Nanocrystals Synthesized by a Hydrothermal Process, Chem. Mater. 18 (2006) 2726-2732.

[23] S.A. Hilderbrand, F. Shao, C. Salthouse, U. Mahmood, R. Weissleder, Upconverting luminescent nanomaterials: application to in vivo bioimaging, Chem. Commun. (2009) 4188-4190.

[24] J.W. Stouwdam, F.C.J.M. van Veggel, Near-infrared Emission of Redispersible Er^{3+}, Nd^{3+}, and Ho^{3+} Doped LaF_3 Nanoparticles, Nano Lett. 2 (2002) 733-737.

[25] R.X. Yan, Y.D. Li, Down/Up Conversion in Ln^{3+}-Doped YF_3 Nanocrystals, Adv. Funct. Mater. 15 (2005) 763-770.

[26] G.-S. Yi, G.-M. Chow, Colloidal LaF_3:Yb,Er, LaF_3:Yb,Ho and LaF_3:Yb,Tm nanocrystals with multicolor upconversion fluorescence, J. Mater. Chem. 15 (2005) 4460-4464.

[27] C. Li, J. Yang, P. Yang, X. Zhang, H. Lian, J. Lin, Two-Dimensional β-NaLuF4 Hexagonal Microplates, Crystal Growth & Design 8 (2008) 923-929.

[28] Z.-L. Wang, J.H. Hao, H.L.W. Chan, Down- and up-conversion photoluminescence, cathodoluminescence and paramagnetic properties of $NaGdF_4$: Yb^{3+},Er^{3+} submicron disks assembled from primary nanocrystals, J. Mater. Chem. 20 (2010) 3178-3185.

[29] S. Heer, K. Kömpe, H.U. Güdel, M. Haase, Highly Efficient Multicolour Upconversion Emission in Transparent Colloids of Lanthanide-Doped $NaYF_4$ Nanocrystals, Adv. Mater. 16 (2004) 2102-2105.

[30] F. Wang, Y. Han, C.S. Lim, Y. Lu, J. Wang, J. Xu, H. Chen, C. Zhang, M. Hong, X. Liu, Simultaneous phase and size control of upconversion nanocrystals through lanthanide doping, Nature 463 (2010) 1061-1065.

[31] G. Wang, Q. Peng, Y. Li, Upconversion Luminescence of Monodisperse CaF2:Yb3+/Er3+ Nanocrystals, J. Am. Chem. Soc. 131 (2009) 14200-14201.

[32] F. Wang, D. Banerjee, Y. Liu, X. Chen, X. Liu, Upconversion nanoparticles in biological labeling, imaging, and therapy, Analyst 135 (2010) 1839-1854.

[33] S. Sivakumar, P.R. Diamente, F.C.J.M. van Veggel, Silica-Coated Ln3+-Doped LaF3 Nanoparticles as Robust Down- and Upconverting Biolabels, Chem. Eur. J. 12 (2006) 5878-5884.

[34] L. Wang, R. Yan, Z. Huo, L. Wang, J. Zeng, J. Bao, X. Wang, Q. Peng, Y. Li, Fluorescence Resonant Energy Transfer Biosensor Based on Upconversion-Luminescent Nanoparticles, Angew. Chem. Int. Ed. 44 (2005) 6054-6057.

[35] D.K. Chatterjee, A.J. Rufaihah, Y. Zhang, Upconversion fluorescence imaging of cells and small animals using lanthanide doped nanocrystals, Biomaterials 29 (2008) 937-943.

[36] S. Jiang, Y. Zhang, Upconversion Nanoparticle-Based FRET System for Study of siRNA in Live Cells, Langmuir 26 (2010) 6689-6694.

[37] L. Xiong, Z. Chen, Q. Tian, T. Cao, C. Xu, F. Li, High Contrast Upconversion Luminescence Targeted Imaging in Vivo Using Peptide-Labeled Nanophosphors, Anal. Chem. 81 (2009) 8687-8694.

[38] R. Kumar, M. Nyk, T.Y. Ohulchanskyy, C.A. Flask, P.N. Prasad, Combined Optical and MR Bioimaging Using Rare Earth Ion Doped $NaYF_4$ Nanocrystals, Adv. Funct. Mater. 19 (2009) 853-859.

[39] Y.I. Park, J.H. Kim, K.T. Lee, K.-S. Jeon, H.B. Na, J.H. Yu, H.M. Kim, N. Lee, S.H. Choi, S.-I. Baik, H. Kim, S.P. Park, B.-J. Park, Y.W. Kim, S.H. Lee, S.-Y. Yoon, I.C. Song, W.K. Moon, Y.D. Suh, T. Hyeon, Nonblinking and Nonbleaching Upconverting Nanoparticles as an Optical Imaging Nanoprobe and T_1 Magnetic Resonance Imaging Contrast Agent, Adv. Mater. 21 (2009) 4467-4471.

[40] J. Zhou, Z. Liu, F. Li, Upconversion nanophosphors for small-animal imaging, Chem. Soc. Rev. 41 (2012) 1323-1349.

[41] K. Liu, X. Liu, Q. Zeng, Y. Zhang, L. Tu, T. Liu, X. Kong, Y. Wang, F. Cao, S.A. Lambrechts, Covalently assembled NIR nanoplatform for simultaneous fluorescence imaging and photodynamic therapy of cancer cells, ACS nano 6 (2012) 4054-4062.
[42] A.P. Caricato, V. Arima, M. Catalano, M. Cesaria, P.D. Cozzoli, M. Martino, A. Taurino, R. Rella, R. Scarfiello, T. Tunno, A. Zacheo, MAPLE deposition of nanomaterials, Appl. Surf. Sci. 302 (2014) 92-98.
[43] J. Yang, M. Mayer, J.K. Kriebel, P. Garstecki, G.M. Whitesides, Self-Assembled Aggregates of IgGs as Templates for the Growth of Clusters of Gold Nanoparticles, Angew. Chem. Int. Ed. 43 (2004) 1555-1558.

Chapter 7

7 Summary and future work

7.1 Summary

The deposition methods of nanocomposites include dip coating, spin coating, chemical vapor deposition, physical vapor deposition, etc. Among these deposition techniques, Matrix Assisted Pulsed Laser Evaporation (MAPLE) method overcomes the drawbacks of the conventional physical vapor deposition methods such as target material degradation, thickness controlling and polymer/biomaterial deposition. This technique is applied in the deposition of polymers, biomolecules, proteins, and nanoparticles. To solve the biofouling problems of the silicone hydrogel, our group developed anti-biofouling coating by depositing ZnO/PEG nanoparticles and Ag/PVP nanoparticles through MAPLE technique. In this study, three different magnetic nanocomposites were deposited by using the MAPLE technique.

In Chapter 4, the major objective is fabricating FeCo/graphene magnetic hybrid nanocomposites with magnetic properties through the MAPLE technique. FeCo nanoparticles were deposited on the graphene sheets by the MAPLE technique (532 nm laser/fluence 300 mJ/cm^2). The microstructures and properties of the FeCo/graphene hybrid nanocomposites were characterized. The TEM micrographs indicate the morphology of the FeCo nanoparticles on the graphene surface with increasing deposition time (*t*). The chemical composition and atomic ratio of the FeCo nanoparticles were investigated by the TEM-EDS. The atomic ratio of the deposited FeCo nanoparticles (Fe:Co) is around 1.79:1.92. Our results indicate that the chemical composition of FeCo is preserved after the MAPLE deposition. The particle size and shape of the FeCo nanoparticles were studied when the deposition time (*t*) increases from 0.5 h to 2 h (0.5 h, 1 h, 1.5 h and 2 h). The relationships between *t* and size distribution of the FeCo nanoparticles were analyzed. The size of the FeCo nanoparticles decreases dramatically from 350 ± 50 nm to 15 ± 10 nm after 0.5 h ablation by the laser. The number of the FeCo

nanoparticles on the surface of the graphene substrate increases as *t* increasing. The maximum magnetization of the chemical synthesized FeCo nanoparticles is 182 ± 2 emu/g, while the maximum magnetization of the FeCo/graphene hybrid nanocomposites (*t* = 0.5 h) is 0.4 ± 0.2 emu/g. The decreased Ms of the FeCo/graphene hybrid nanocomposites as compared to the Ms of the FeCo nanoparticles before the deposition could be related to the very small amount of FeCo nanoparticles were deposited on the graphene sheets when *t* = 0.5 h. With *t* increasing, it is expected that the Ms of the FeCo/graphene hybrid nanocomposites could increase. Consequently, magnetic graphene nanosheets can be achieved by depositing FeCo nanoparticles onto graphene sheets' surface. MAPLE technique offers a way to control the magnetic properties of magnetic graphene sheets by adjusting the deposition time.

In Chapter 5, the main objective of this session is depositing YBCO nanoparticles onto the surface of graphene nanosheets through the MAPLE technique. The YBCO nanoparticles were deposited on the surface of the graphene nanosheets to fabricate YBCO/graphene hybrid nanocomposites by MAPLE system (150 mJ/cm^2). Transmission electron microscopy (TEM) micrographs demonstrate the successful deposition of the YBCO nanoparticles. The chemical composition of the YBCO/graphene hybrid nanocomposites were characterized by the TEM-EDS. The results of the TEM-EDS indicates the chemical composition of the YBCO nanoparticles was preserved after the MAPLE treatment. The effects of the deposition time (*t*) which was changed from 0.5 h to 2 h (0.5, 1, 1.5 and 2 h) on microstructures (particle size/shape) of nanoparticles were studied. The TEM micrographs show the particles size and shape of the YBCO nanoparticles on the surface of the graphene nanosheets are different before and after deposition. The average particle size changes from 3.5 ± 2 μm to 60 ± 20 nm and the particle shape changes from irregular shape to sphere shape after the MAPLE deposition. The amount of the YBCO nanoparticles increases as the deposition time (*t*) increasing.

In Chapter 6, the main objective of this session is verifying the possibilities of depositing up-conversion nanoparticles and protein modified up-conversion nanoparticles through MAPLE system. Up-conversion nanoparticles and protein modified up-conversion nanoparticles were deposited on the surface of the glass substrates. The laser fluence of

this project is 150 mJ/cm^2. The protein-modified up-conversion nanoparticles were characterized by TEM and FT-IR. The TEM micrographs show that the average size of the up-conversion nanoparticles is 60 ± 10 nm. The BSA coated on nanoparticles can be observed in TEM micrographs. The bending of amide functional groups and stretch of carboxyl groups at 1644 cm^{-1} and 1249 cm^{-1} after proteins are modified onto nanoparticles can be observed in FT-IR spectra. These results indicate the successful modification. The samples were characterized by the TEM/FT-IR after MAPLE deposition. The FT-IR spectra indicate that both up-conversion nanoparticles and protein modified up-conversion nanoparticles are deposited by the MAPLE process with the presence of the peaks of -OH/-NH_2 groups at 3367 cm^{-1}/3648 cm^{-1} and 1575 cm^{-1}/1577 cm^{-1}. The TEM micrographs of the deposited up-conversion nanoparticles and BSA modified up-conversion nanoparticles indicate that the average particles size of the nanoparticles is around 50 ± 10 nm, and the BSA coatings' thickness is 5 - 6 nm. In addition, TEM micrographs clearly demonstrate that IgG antibodies were modified onto the up-conversion nanoparticles. Human umbilical vein endothelial cells (HUVECs) were applied to study the interactions between cells and the deposited samples. As compared to the control samples, cell length, cell connection length, cell area and cells number of HUVECs which grew on the surface of the up-conversion nanoparticles are increasing. The results indicate that up-conversion nanoparticles may enhance the adhesion of the cell, and improve the cell growth. The MTT test shows the up-conversion nanoparticles and IgG modified up-conversion nanoparticles do not cause the toxic effect on cells.

The results of this study indicate the good versatility of MAPLE deposition system for depositing different kinds of nanoparticles and preserve their chemical composition/microstructure.

7.2 Future works

In this study, MAPLE process was applied in all three projects. One disadvantage of the MAPLE deposition technique is the production rate, especially for the deposition of YBCO and FeCo nanocomposites. The structural changes of the equipment or the modifications of the deposition processes could be developed to improve the production rate of the

deposition products. More experiments and characterizations would be applied to study the mechanism of the deposition processes.

The effects of the laser on the target materials are found in the MAPLE deposition processes of all three nanocomposites. These effects could be minimized by changing the wavelength of the laser and high volatile solvent. The effect of the laser wavelength, laser fluence and volatile solvent type on target materials would be investigated in the future.

Curriculum Vitae

Name: Songlin Yang

Post-secondary Education and Degrees:

Tianjin University

Tianjin, China

2011-2015 B.Eng

The University of Western Ontario

London, Ontario, Canada

2015-2017 M.E.S.c

Related Work Experience:

Teaching Assistant

The University of Western Ontario

2016-2017

Publications:

Songlin Yang and Jin Zhang, Matrix-Assisted Pulsed Laser Evaporation (MAPLE) Technique for Deposition of Hybrid nanocomposites, Front Nanosci Nanotech. 3 (2017) 1-9. (DOI: 10.15761/FNN.1000146), published.

Songlin Yang and Jin Zhang, Deposited BSA/IgG conjugated up-conversion nanoparticles by the matrix-assisted pulsed laser evaporation (MAPLE), accepted, proceeding of TANN' 17.

Songlin Yang, Longyi Chen and Jin Zhang, Graphene/YBCO Hybrid Nanocomposites Prepared by Matrix Assisted Pulsed Laser Evaporation, in preparation.